Delft University of Technology

Civil Engineering and Geosciences

MSc. Applied Earth Sciences - Geo-Engineering

Screw and Screw-Injection Piles:

Classification of the load-settlement response and improving the design process

Author:
Friso Bote ter Steege
4452089

Thesis committee:
Prof. dr. ir. K. G. Gavin
Prof. dr. ir. F. Pisanò
Ir. K. J. Duffy

April 5, 2022

Preface

This thesis is written to obtain the MSc. degree of Applied Earth Sciences with track Geo-Engineering, at the faculty of Civil Engineering and Geosciences of TU Delft.

I would like to thank Ken and Kevin for their supervision, and Federico for helping out the committee in such short notice. The help offered by Dirk is also not forgotten. After having weekly meetings with Kevin for such a period of time, it feels somewhat strange knowing that these will not happen in the future.

With graduation in sight, it seems fitting to thank Jan-Kees, Pascal and Dominique for their trust and support in 2016. This thesis would not be possible without their help to obtain a postponement of the BSA. I would like to extend special gratitude to Dominique, who I have enjoyed learning from and working with throughout the master programme.

Finally, I would like to close with a fitting quote, which Erica suggested is an absolute must in the preface:

"Good judgement comes from experience, experience comes from bad judgement."

F. B. ter Steege
Delft, March 2022

Abstract

The Dutch pile design method, NEN9997-1, classifies screw and screw-injection piles as fully displacing. For these pile types, the design code prescribes a base factor α_p 0.63 and shaft factor α_s in sand of 0.009. However, an ongoing TU Delft research programme on these pile types has indicated findings conflicting with NEN9997-1. This thesis investigates whether screw and screw-injection piles should be classified as fully displacing piles and how the design process can be improved, through the interpretation of existing load tests.
The thesis compares measurements of pile load tests to the load-settlement behaviour of fully displacing and (partly) soil replacing piles, including the effect of limiting q_c to a maximum of 15 MPa for shaft friction. From appropriately instrumented tests, α_p and α_s factors are determined and compared to the prescribed factors. Additionally, a shear box test is performed in order to investigate debonding between the grout body and steel tube of a screw-injection pile.
Interpretation of the load tests strongly signify that the load-settlement behaviour of screw and screw-injection piles does not resemble that of fully displacing piles, but rather (partly) soil replacing piles. Determined values of α_p range from 0.23 to 0.35, while values for α_s in sand range from 0.011 to 0.012. Limiting q_c along the shaft is shown to produce less realistic capacity and behaviour predictions when compared to measured test data. The shear box experiments indicate that in dense soils with high q_c values, debonding between the grout and steel tube of a screw-injection pile under high load can occur.

Summary

In 2017, the pile base factor α_p has been reduced by 30%. This has prompted a research programme at TU Delft, where different pile types are studied and tested on their capacity and load-settlement behaviour. This thesis focuses on screw and screw injection piles. These pile types present a vibration free solution to problems with driven piles in city centres, reducing noise disturbance and damage to pre-existing foundations. However, due to their lesser occurrence, screw piles and their installation effects are less well understood. Currently, the α_p for these pile types is set to a reduced value of 0.63. In the Dutch design code, NEN9997-1, screw and screw-injection piles are classified as fully displacing piles. According to NEN9997-1, the load-settlement behaviour of screw and screw-injection piles is similar to that seen in driven piles. However, findings of the TU Delft research programme into screw and screw-injection piles have shown results conflicting with this claim.

Existing pile load tests are analysed using a database driven approach. Pile test reports have been selected with a preference for static load tests, strain measurement data, and additional investigations such as differently shaped pile tips and excavation of the piles after testing. Data required for pile capacity calculation has been digitalised, such as the pile dimensions and CPT profile. For each pile test, the soil profile has been extensively analysed and each soil layer given a classification according to NEN9997-1. For piles with strain data or separate pile tip load measurements, the pile base factor α_p and shaft factor α_s has been determined prior to capacity calculations.
Using a program written in Python, the pile shaft and base capacity are calculated according to the method described in NEN9997-1. Based on the calculated maximum shaft and base capacity of the pile, the load-settlement response of the pile is then predicted, utilising the characteristic load-settlements curves as prescribed in NEN9997-1. Different combinations of load-settlement curves are applied, to determine if the pile response better represents fully displacing piles, or (partly) soil replacing piles, respectively. The results are compared to the recorded pile load test data, and adjusted and refined in order to increase the accuracy of the prediction. This is mainly achieved by varying factors α_p, α_s and switching between load-settlement curve 1 or 2. In addition, calculations are performed with and without limiting the cone resistance q_c, as performed in NEN9997-1, in order to quantify the effect of limiting on the overall predictions on pile capacity and load response.

The findings of the thesis show:

- The load-settlement behaviour of screw and screw-injection piles resembles more closely the behaviour seen in (partly) soil replacing piles. Sand content between 20 and 40% in outcoming grout samples further indicate that screw-injection piles are not fully displacing.
- Values found for α_p range from 0.23 to 0.35 for the instrumented tests. The application of α_p 0.35 on uninstrumented tests provides realistic capacity and load-settlement predictions. The range of α_p found in the thesis of 0.23-0.35 is significantly lower than the currently prescribed 0.63.
- Instrumented tests indicate an α_s in sand between 0.011 and 0.012. The application of 0.011 on instrumented tests provides realistic capacity and load response predictions. The range of α_s 0.011-0.012 found in the thesis is significantly higher than the currently prescribed 0.009.

- The currently prescribed α_s factors in clay, between 0.02-0.03, provide accurate predictions for soft clays encountered in the Netherlands. In the case of a pile test in stiff, overconsolidated clay, these factors underestimate the capacity of the pile. Application of a multiplication factor 1.25×, increasing these values to between 0.025-0.0375, provides more realistic capacity and load-settlement predictions in stiff, overconsolidated clay.

- Load-settlement predictions without limiting q_c along the shaft approach the measured test data more closely than those made with the use of limiting q_c along the shaft to a maximum of 15 MPa, as prescribed by NEN9997-1.

- A laboratory experiment indicates that in dense soils with high q_c values, debonding between the grout body and steel tube of a screw-injection pile under high load can occur. This is suggested as an explanation for sudden strain softening measured in one of the pile tests discussed in this thesis.

- Test data does not indicate a difference in pile capacity or load-settlement behaviour between flat, conical or pyramid shaped pile tips.

- The commonly used assumption for screw-injection piles of using the base diameter to approximate the diameter of the grout body does not accurately predict the true diameter of the shaft. However, applying this assumption in pile capacity and load-settlement calculations provides results close to measured test data.

- The screwing motion of screw piles during installation can reduce the adhesive force of clays, and may cause overexcavation of the soil immediately surround the pile. This reduces the radial stress on the shaft of the pile. Additionally, lateral soil transport and grain crushing at the pile tip can cause a reduction in stiffness of the base resistance. These effects of screwing likely contribute to the softer load-settlement response seen in screw and screw-injection piles, when compared to driven piles. The effects of overexcavation have been shown in one of the pile tests, where this causes large local increases of the pile diameter, which require a severe increase in concrete consumption to fill. Additionally, inadequate concrete fluidity has been shown to cause structural failure long before the designed capacity of a pile.

The main findings from the thesis suggest that the load-settlement behaviour of screw and screw-injection piles resembles that of (partly) soil replacing piles, prescribed in NEN9997-1 as load-settlement curve 2. The analysis of pile tests indicates an α_p between 0.23 and 0.35, and an α_s in sand between 0.011 and 0.012. Compared to calculations without limits applied, the limiting of cone resistance q_c along the shaft to a maximum of 15 MPa produces less accurate results, when compared to measured test data. Shear box tests indicate that in dense soils with high q_c values, debonding between the grout body and steel tube of a screw-injection pile under high load can occur. A summary of the pile test database is given in Table 1.

Pile test	**Maasvlakte 2**	**Beemster Scale**	**Rosmalen**	**Limelette**	**Sonate**
Test type	Static	Static	Static	Static	Rapid
No. of piles	4	4	5	10	3
Pile type(s), Brand name	Type 3, Terr-Econ	Type 1, unspecified	Type 3, unspecified	Type 1+2, Fundex, Atlas, Olivier, De Waal, Omega	Type 3, HEKbuispaal
Screw or screw-injection	Screw-injection	Screw	Screw-injection	Screw	Screw-injection
Soil along shaft	Sand	Sand	Sand	Clay	Sand
Soil around base	Sand	Sand	Sand	Sand	Sand
Shaft/base load splitting	Yes	Yes	Yes	No	No
Method load splitting	Fibre optic	Fibre optic	Separate load cell for pile tip	-	-
Strain gauge method(s)	FBG, BOFDA	FBG	-	-	-
Investigation on pile tips	-	Yes, flat and conical	Yes, flat and pyramid	-	-
Piles excavated?	No	Yes	Yes	Yes	No
Shaft diameter [m]	0.61	0.12	0.4	0.36-0.41	0.71
Measured shaft diameter [m]	-	0.12	0.44-0.54	0.39-0.55	-
Base diameter [m]	0.85	0.15	0.4	0.41-0.55	0.85
Load-settlement curve best fit	2	2	2	2	2
Determined α_p	0.35	0.27	0.23	-	-
Determined α_s, sand	0.011	0.012	0.011	-	-
Fitted α_p	0.35	0.27	0.23	0.35	0.35
Fitted α_s, sand	0.011	0.011	0.011	0.011	0.011
Fitted α_s, clay	0.02-0.03	-	-	0.025-0.0375	0.02-0.03
Difference between pile tip shapes?	-	No	No	-	-
q_c limiting along shaft?	No, limiting produces less accurate results	No, limiting produces less accurate results	No, limiting produces less accurate results	No, limiting produces less accurate results	No, limiting produces less accurate results
q_b limited to 15 MPa?	Not affected with stated pile factors	Not affected with stated pile factors	Not affected with stated pile factors	Not affected with stated pile factors	Not affected with stated pile factors

Table 1: Overview of pile test database results.

Contents

Chapter 1

Introduction

1.1 Screw and screw-injection piles: their increased importance in a crammed country

Building in an old city centre is risky. In an increasingly crammed town with monumental buildings, the existing foundations and buildings are often susceptible to vibrations transferred through the subsurface. Driven piles, which are commonly used, are essentially hammered into the ground, propagating strong vibrations over a significant area. These vibrations can easily damage the pre-existing - old and worn - foundations, causing settlements and major damage to the buildings we wish to preserve for coming generations.

Screw and screw-injection piles present an excellent solution to this modern problem. Whilst driven piles are like hammering a nail, screw piles can be compared to screwing a screw. As a consequence, these piles can be installed almost completely vibration free, meaning that the pre-existing foundations of historic buildings will not be damaged. Additionally, nearby inhabitants will not be bothered by noise disturbance.

During installation, a water-cement mixture, called grout, can be injected near the pile tip. This has two advantages: first, the grout acts like a lubricant, reducing friction along the shaft and tip during installation. Second, when the grout cures after pile installation, it forms a significant cement-like shell around the pile, enlarging the diameter and therefore increasing the bearing capacity. Screw piles which inject grout during installation are referred to as screw-injection piles.

Screw piles have additional benefits: they can generally be founded to greater depths than driven piles, and are more equipped to penetrate dense, tough soil layers. However, because screw and screw-injection piles are relatively new technologies, the general understanding of these pile types and their behaviour is lacking when compared to more common options, such as the driven pile.

1.2 Research question

In 2017, the pile base factor α_p for piles has been reduced by the NPR by 30%. The α_p for screw and screw-injection piles has been reduced to 0.63 as of now. This has prompted a research programme at TU Delft, where different types of piles are studied and tested on their behaviour and bearing capacities, to investigate the α_p factor and other aspects such as installation effects. Findings of the TU Delft research programme suggest that the load-settlement response of these pile types does not match with the behaviour prescribed in the design code. Additionally, instrumented pile tests indicate values of α_p even lower than the current value of 0.63. It is believed the evaluation of existing pile load tests will provide additional knowledge on the topic of screw and screw-injection piles.

Therefore, the aim of this thesis is to answer the following research question: **Should screw and screw-injection piles be classified as fully displacing piles, and how can the design process be improved through the interpretation of existing load tests?**

The main research question is supported by the following sub-questions:

- How do the measurements of screw and screw-injection pile load tests compare to the load-settlement behaviour of fully displacing and (partly) soil replacing piles?
- Does limiting the cone resistance values q_c and maximum tip resistance q_b as prescribed in NEN9997-1 provide realistic estimates of the pile capacity?
- How do the currently prescribed α_p and α_s factors in NEN9997-1 compare to real pile tests?
- What influence do the installation effects of screw and screw-injection piles have on the load-settlement behaviour?

Chapter 2

Literature review on screw and screw-injection piles

2.1 Introduction to screw and screw-injection piles

Numerous types of pile foundations exist. Different pile types suit varying ground conditions, and each have distinct advantages and disadvantages. Piles can be end bearing, where the tip of the pile provides support; friction piles, where the shaft friction provides support; or a combination of both. Different installation techniques exist, like impact driven piles and screwed piles. Pre-cast piles may be hammered into the ground, or piles can be cast in-situ after a borehole is drilled (Holeyman 2001). Furthermore, according to Rajapakse (2016) all piles can be categorised as displacement piles and nondisplacement piles. Displacement piles move soil radially as the pile shaft enters the ground, while nondisplacement piles form a void by boring or excavation of the soil (Rajapakse 2016). Examples of displacement piles are driven piles and vibro piles, while Continuous Flight Auger and anchor piles are examples of nondisplacement piles. Essentially, this means that displacement piles generally have higher bearing capacities than nondisplacement piles due to the increase of lateral ground stress caused by soil rearrangement (Transportation Research Board 1977).

The term 'screw pile' describes a collection of different pile techniques which all have in common the screwing action during the installation phase. The main differentiating factor is whether the pile is nondisplacing or displacing. Though, importantly, a pile can also be partially soil replacing. Simply put, a nondisplacement screw pile works like a drill bit: material is transported out of the hole, while a displacement screw pile works like a screw: soil material is pushed aside due to the angle and rotation of the screw flanges. This is illustrated in Figure 2.1.

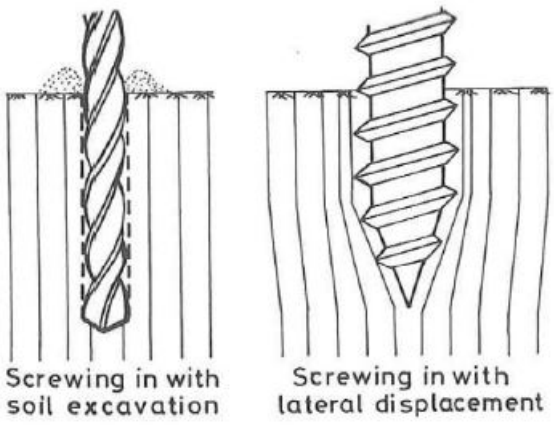

Figure 2.1: Analogy between non-displacement piles and displacement piles. From Van Impe (1988).

A screw pile may be installed with or without the injection of grout (a water-cement mix). Whether this is done depends on the required capacity of the pile and the soil conditions. Grout is usually injected from the drill tip, or slightly above it (Duffy et al. 2021; Geerling et al. 1992). This is illustrated in the top right panel of Figure 2.2. The main advantage of using grout during the installation of a pile is to increase its bearing capacity by increasing the pile diameter (Krasinski and Wisniewski 2018). Additionally, injecting cement grout during installation causes a temporary a reduction in driving resistance. In essence, the cement grout acts like a lubricant during the installation of the pile, while increasing the total bearing capacity after completion of the pile (Funderingstechniek.com 2021, May 15).

This thesis focuses on screw and screw-injection (SI) piles. The definition for screw-injection piles in this report is considered as: *screwed, (partly) replacing piles using grout injection.* Typical features of piles that fall under this definition are:

- Screwing action during drilling phase.
- Utilisation of steel casing tube that may be extracted, or left in situ after pouring concrete.
- Drill tip either fixed to, or separate from the casing. Separate drill tip remains underground after removal of casing.
- Grout injection applied during installation.
- Cast in situ or steel tube remains in place.

This thesis distinguishes 3 types of pile installation methods which fall under the above written definition of 'screw injection pile'. These are as follows:

1. Screw pile with smooth shaft
2. Screw pile with helical shaft
3. Screw pile with permanent steel casing

Further details are given in the sections below.

2.1.1 Type 1: Screw pile with smooth shaft

The most common type of screw-injection pile employs a temporary cylindrical steel drill tube. A drilling tube with separate drill tip is placed at the surface. The casing is then screwed to target depth using axial pressure and torque, whilst simultaneously cement grout may be injected. After reaching the final depth, there are two methods for concreting: the first method is to pour concrete, and then extract the drilling tube using a rotary and oscillatory motion, as shown in Figure 2.2. The second method is to extract the casing whilst simultaneously pumping concrete under pressure into the borehole through the pile tip, as shown in Figure 2.3a. In either case, rebar may be inserted before or after concreting, after which the installation process is completed (Van 't Hek 2021, April 5; Vroom 2021a, April 5). Examples of this type of pile are Fundex, Omega and HEKPILE (Franki Foundations 2021b, April 5; Fundex 2021a, April 5; Van 't Hek 2021, April 5; Vroom 2021a, April 5).

Figure 2.2: Figure showing installation of SI pile using temporary tube: temporary tube and drill tip placed at surface (1), tube screwed to depth while injecting grout (2), rebar and pouring of concrete (3), drilling tube removed (4). Edited from Vroom 2021a, April 5.

2.1.2 Type 2: Screw pile with helical shaft

The main discerning aspect of the second type is the shape of the pile shaft, which is helical, in contrast to the smooth shaft of Type 1. The aim of the screw-shaped shaft is to increase the contact area of the shaft with the soil and thereby increasing the shaft friction. The installation process of this method is identical to type 1 up until the final drilling depth is reached. The helical shape can only be produced using the second concreting method, as they are formed during extraction of the auger by rotation of the flanges whilst simultaneously injecting concrete (Franki Foundations 2021a, April 5; Olivier Industrie 2021, April 5). The screw shaped shaft (Figure 2.3b) results in increased skin friction, leading to a higher bearing capacity (Larisch 2014). The thickness of the flanges is influenced by the auger geometry, but can depend on penetration and extraction rates. Larisch (2014) has shown that higher extraction rates create bigger concrete flanges and pitches in the pile. Examples of this type of pile are Atlas and Olivier (Franki Foundations 2021a, April 5; Olivier Industrie 2021, April 5).

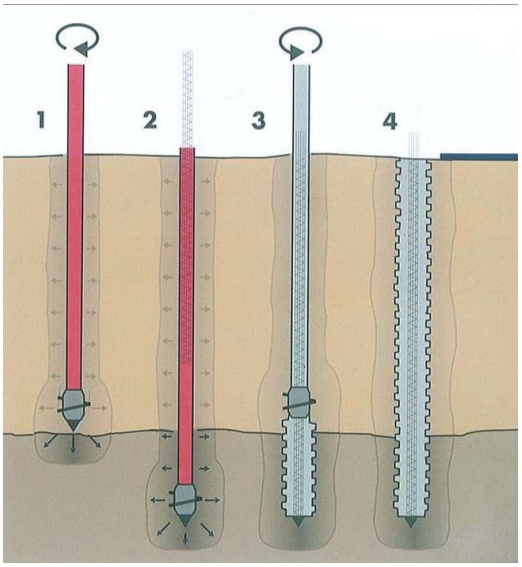

(a) Type 2 pile installation method: clockwise drilling (1), required depth reached (2), reverse screwing while filling space with concrete (3), finished pile (4). (Olivier Industrie 2021, April 5).

(b) Screw shaped (helical) shaft of pile Olivier Industrie (2021, April 5).

Figure 2.3: Helical shaped SI piles

2.1.3 Type 3: Screw pile with permanent steel casing

This variation of SI pile differs from first type in that the steel drilling tube is not extracted and remains permanently underground. Therefore, there is an additional interface created: the grout-steel interface. The pile installation process is similar to type 1, as illustrated in Figure 2.4. When the target depth for the pile is reached, rebar is inserted and concrete is poured. The steel tube is then cut at the top, while the rest of the casing remains in in situ underground (Fundex 2021b, April 5; Vroom 2021b, April 5). The main advantage of a SI pile with a permanent casing is that it does not need to be extracted, although this does come at increased material costs. This allows for installation depths significantly larger than installation methods that extract the drilling tube (Fundex 2021b, April 5). Examples of this type of pile are Tubex (by the Fundex company) and steel casing screw piles produced by Vroom (Fundex 2021b, April 5; Vroom 2021b, April 5).

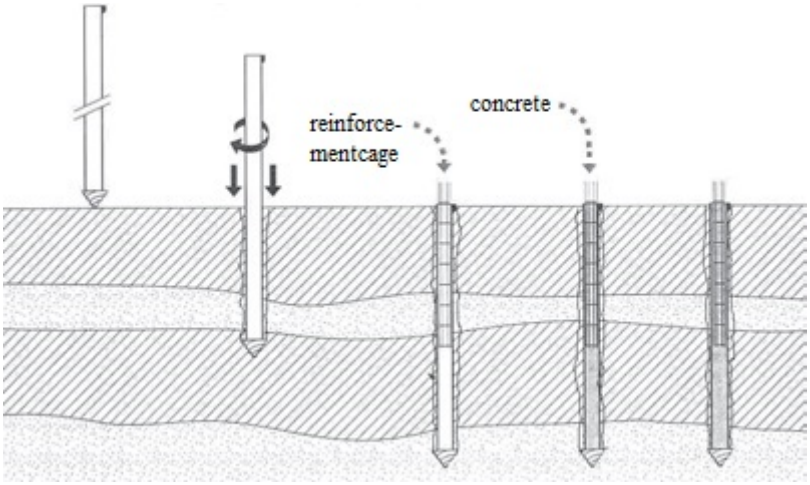

Figure 2.4: Figure showing installation of SI pile using permanent tube: drilling tube with welded drill tip placed at surface (1), tube screwed to depth while injecting grout (2), rebar inserted (3), concrete poured (4), finished pile (5) From Fundex 2021b, April 5.

2.2 Installation Effects

Multiple processes during the installation of a pile affect the soil surrounding the pile. Some of these effects are always present due to the nature of a soil-displacing pile, but several installation effects may vary by pile technique and differing installation parameters. Therefore, a distinction can be made between the inherent installation effects of (partly) soil displacing piles and the installation effects variable by design and operator choices. The installation effects discussed in the following sections mainly consider piles founded in sand.

2.2.1 General installation effects

Cavity expansion Soil is pushed outwards when pile installation occurs. Along the shaft, a cylindrical expansion occurs, while a spherical cavity is formed at the pile tip (de Boorder 2019). This process is known as cavity expansion and leads to compression of the soil and excess pore pressures close to the pile (Randolph 2003). A reduction in the effective horizontal stress occurs and the shear force during installation instantly lowers (de Boorder 2019). This process is illustrated in Figure 2.5. However, the normal stresses caused by cavity expansion are reduced in SI piles. Torsional forces and vertical shearing have a large impact and lower approximately 50% of the normal stress on the pile shaft that would be predicted by cavity expansion alone (Basu and Prezzi 2009).

Dilation, compaction and grain crushing The forces occurring during installation may cause the surrounding soil to dilate or compact, and can even crush grains. This occurs mainly under the pile base, where the pressures are highest. Dilation and compaction significantly affect the bearing capacity of the pile. Whether dilation or compaction occurs is dependent on the relative density of the soil, and the confining stress (Bolton 1987). Generally, dilation leads to higher shear strength while compaction produces a decrease in shear strengths. At the pile tip, the high stresses caused by the axial forces exerted during installation mostly cause compaction and grain crushing. According to Basu and Prezzi (2009), soil within a range of 1.3-3.6D undergoes dilation due to the pile installation. Soil beyond this zone is undergoes contractive behaviour. After a radius of approximately 12D no volumetric change is seen in the soil (Basu and Prezzi 2009).

Friction fatigue The soil directly adjacent to the pile shaft is deformed severely (Randolph 2003). This effect is more pronounced in soil closer to the pile head, as these parts are impacted most by

displacement and contraction/expansion caused by the installation of the pile. As the soil keeps undergoing forces causes by screwing and erosion during installation, strain softening occurs (See Figure 2.5). This process is called friction fatigue, and causes the horizontal stress acting on the pile shaft to decrease as the distance to the base of the pile increases (de Boorder 2019). Gavin and O'Kelly (2007) found that for piles in dense sand, high-intensity cyclic loading causes the largest reduction in horizontal effective stress on the pile shaft. Due to the screwing motion during installation, this mechanism is very different in screw piles. Additionally, when grout injection is used, the soil surrounding the pile is severely affected and the effect of friction fatigue negligible.

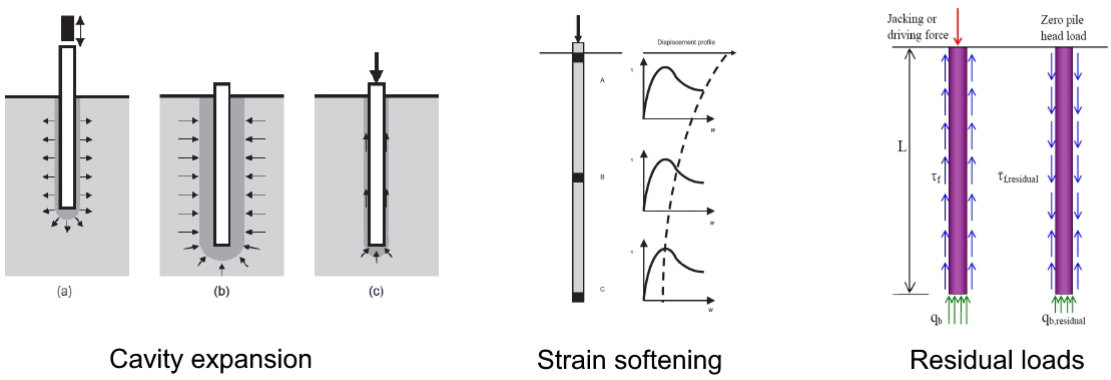

Figure 2.5: Figure illustrating inherent installation effects, edited after de Boorder (2019).

Residual loads Due to the pressures exerted during installation of the pile, residual loads start to form. These residual loads develop after the axial force is removed when the final pile depth is reached. When this force is eliminated, residual compressive stresses remain at the bottom of the pile (pointing in the upwards direction). These are balanced by negative skin friction on the upper part of the pile shaft (pointing in downwards direction), as shown in Figure 2.5. Fellenius (2015) shows the influence of residual loads on a static load test performed on an Omega screw pile. Test data indicates that residual loads were present in the pile before the start of the test. Figure 2.6 clearly indicates the discrepancy between the test data (green) and true distribution (red). One can see the underestimated toe resistance and overestimated shaft resistance. Fellenius (2015) notes that if the effect of a residual load in not included when analysing test results, the following will occur:

- the shaft resistance along the upper portion of the pile will be overestimated
- the shaft resistance along the lower portion will be underestimated
- the total shaft resistance will be correspondingly underestimated

Fellenius (2015) further concludes that the presence of residual loads is not a trivial part of a pile response analysis, as it can significantly influence the interpretation of a load test. If it is not recognised, the results can be considerably off-target. Moreover, the existence of a residual load will cause a stiffer load-movement response on a pile, when compared to a pile without residual loads. Finally, the results of a pile test affected by residual loads can easily mislead to the belief that the pile has developed an ultimate toe resistance, while in reality, this is not the case. However, the case presented by Fellenius is exceptional. Residual loads are difficult to measure, and are not considered in this thesis due to their unavailability in the test data. Even if residual loads develop due to the soil-displacing action of a screw pile, the liquid grout body allows these stresses to dissipate.

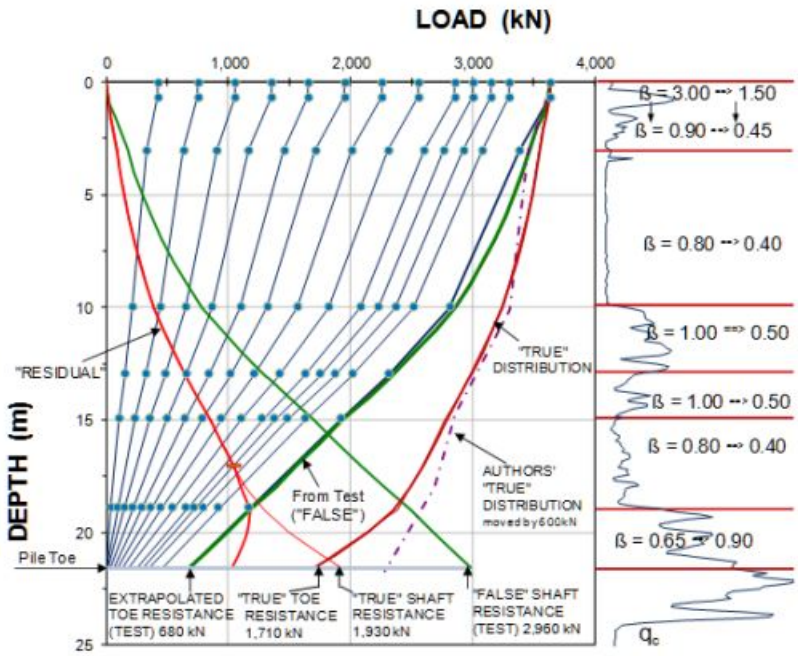

Figure 2.6: Load distributions from Omega pile test (Fellenius 2015).

2.2.2 Screw pile specific installation effects

Because screw injection piles have so many different parameters that vary, it is important to understand what these parameters are, why they vary and how they might influence the final pile capacity. However, due to the large variation in pile types, soil conditions and design requirements it can be difficult to ascertain the actual effect of a specific installation parameter. For example, adding extra cement to the grout mix makes it stronger, but due to the higher viscosity it might not penetrate as deep in the soil, possibly reducing the total pile capacity relative to the original grout mixture. The installation effects are all interrelated, which makes it difficult to analyse their effects or suggest a guideline. For example, if the penetration rate is increased, the flow of grout must be increased to ensure a full shell develops around the tube.

Pile tip shape The shape of the pile tip can influence how the soil at the tip is transported, which may affect the final stress states that dictate the pile capacity. Research by van der Geest et al. (2019) and Geerling et al. (1992) have different conclusions: whereas results from van der Geest et al. (2019), seem to indicate that a conical pile tip produces a higher base capacity, findings from Geerling et al. (1992) do not indicate a difference between a flat or conical pile tip. However, van der Geest et al. (2019) do note that their findings on pile tip shapes contain a significant amount of uncertainty. Generally, there is no clear consensus on the effect of pile tip shape.

Auger shape Holeyman (2001) notes that the angle of the screw flange, variability of the flange angle and increasing diameter of the auger head have a positive effect on the penetrability and screw pile installation (see Figure 2.7). Holeyman proposes an example of two different types of Atlas screw piles (type 2 piles), the original and a modified version with 'a small intersection for opening the flange over a few centimetres' (Holeyman 2001). Compared to the original, the modified version nearly doubled the installation velocity efficiency. The required torque was much lower than for the original auger. This is shown in Figure 2.7. Furthermore, Holeyman (2001) explains the principle of the Omega auger, which provides much better lateral soil displacement and penetrability. On the other hand, Larisch (2014) declares that the auger shape does not seem to have a major influence on the capacity of piles in stiff or hard clay. He suggests that maintaining a constant penetration rate

and auger rotations during installation provide more favourable pile capacities. Though these findings seem contradictory, both Holeyman (2001) and Larisch (2014) seem to underline the importance on the penetration rate of the pile. However, in contrast to Larisch, Holeyman suggests that the auger shape itself affects the penetration velocity.

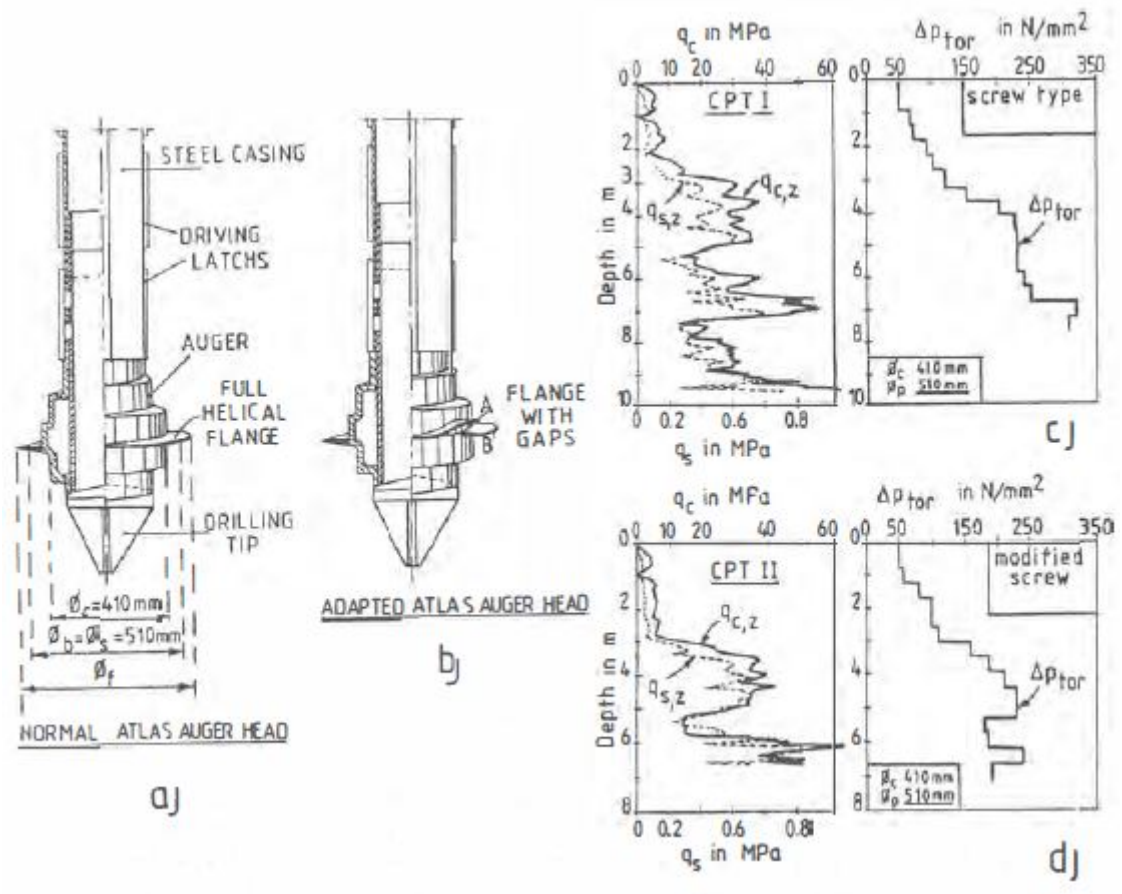

Figure 2.7: Example of the influence of auger head shape (Holeyman 2001, p. 136).

Penetration rate The penetration rate, also called vertical speed, drilling speed and penetrability, is the vertical distance the screw pile travels per time unit. Holeyman (2001) suggests that more attention should be paid to details relating to the total installation energy of screw piles. The drilling speed is governed by the torque and pull-down forces. If either of those is not sufficient, the penetration rate will decrease. With a constant penetration rate, a constant flow of soil is transported via the auger flights to the borehole wall. If the penetration rate falls, with no change in the auger rotation, more soil will be pushed into the borehole wall. This causes overstressing at the borehole wall, resulting in a failure and subsequent collapse of soil into the excavation. The sheared and collapsed soil then goes through the process again, but cannot reattain its original strength (Larisch 2014). NeSmith (2003) suggests a method where the penetration rate and torque are combined to develop an index that relates to the subsurface conditions and pile capacity, further indicating the direct influence the vertical speed has on the final pile capacity.

Pull-down force The pull-down force is one of the forces governed by the installation crew that dictate the penetration rate. It is the force exerted in the vertical direction in order to push the auger down into the soil, like pushing against a screw when driving it into a plank. However, because of the torsional force and the self-weight of the drilling tube, the pull-down force is used mainly for when the aforementioned factors are not enough (Larisch 2014). Maintaining a constant penetration rate above a minimum value increases the final bearing capacity of a pile (Larisch 2014). As such, the axial

force in itself does not directly influence the total pile resistance, but a lack of pull-down force may significantly reduce the penetration rate and is thus an important aspect of the whole process.

Torque A more important force than the pull-down force, the torque is the primary force needed to generate a sufficient penetration rate. The torque is a rotational force, like the twisting of the wrist when driving a screw. The torsional force is converted by the auger head into a vertical component, driving the auger head to larger depths. Holeyman (2001) has shown that depending on flange types and different auger shapes, the required torque varies drastically. Furthermore, torque is the main force that influences the number of rotations of the auger, which in turn affects the amount of soil displaced in the excavation.

Rotational speed The number of rotations (usually measured in rotations per minute) made by the auger affects penetration rate but also the soil displacement. In a cohesive soil, such as a clay, one wants to maintain a constant penetration rate and rotations per minute. This provides a steady soil transport and displacement rate into the borehole wall. That way, clay is compacted instead of sheared off and then re-compacted or transported towards the surface (Larisch 2014). This sheared soil will not be able to reattain the original strength and will therefore lead to lower pile capacities. At depths close to the surface, the re-moulded soil can be transported towards the surface, causing heave in addition to lower capacities along the shaft.

Grout injection rate Grout injection provides several advantages for SI piles. The main advantage is an increase of bearing capacity due to the forming of a grout body around the excavation, essentially increasing the pile diameter and shaft friction. This is attained due to grout permeating into surrounding soil, creating a sand-grout interface (Kaddouri 2020). Second, the grout acts as a lubricant during the excavation, reducing friction between the auger and surrounding soil and therefore reducing the energy required for pile installation. Third, the injection of the grout into the soil can fluidise the soil directly beneath the drilling tip, making it easier to screw the deeper into the soil. This is similar to the process using in driven piles to locally liquefy the soil at the pile tip to ease pile driving (Korff 2020). The grout injection rate is the amount of grout injected per unit time. It should be sufficiently high so that the grout is able to penetrate into the soil, but over-injection of grout will transport grout out of the excavation, taking with it soil particles. A too low injection rate may increase the friction of the auger with the soil and grout might not sufficiently penetrate the surrounding soil, lowering the overall capacity. The grout injection rate is dependent on the drilling speed, soil properties and water/cement ratio.

Grouting pressure The grouting pressure affects the ability of the grout to fluidise the soil underneath the drill tip and, more importantly, to penetrate into the surrounding soil. Research by Hossain and Yin (2004) has shown that a higher grouting pressure results in higher shear strengths. If grout is injected under higher pressures, it is able to penetrate further into the soil, which in turn enlarges the sand-grout interface and increases the pile capacity. However, the pressure cannot always simply be increased, as too high pressures can break down the soil and transport particles away, reducing stresses and thus the overall pile capacity.

Grout water/cement ratio Grout for SI piles must be flowable in order to be used for injection. At the same time, grout should provide the required properties to withstand high radial stresses. This can be influenced by the ratio at which water and cement are used. The water-cement ratio may be seen as an indication of the distance between cement particles before hydration occurs (Kaddouri 2020). A higher water/cement ratio means that the distance between the cement particles is larger and the mixture more flowable, but the bonds between the particles must grow over a larger distance. To the contrary, a lower water/cement ratio indicates lower distances between the cement particles and a more viscous fluid, but the short distance for the bonds to grow increases the strength of the

grout (Kaddouri 2020). In short, a higher water/cement ratio indicates less cement particles, a less viscous fluid and lower strengths. A trade-off must be made between ability to inject and the strength parameters of the grout. Research on the water/cement ratio by Li et al. (2020) clearly shows the relationship between these factors, shown in Figure 2.8.

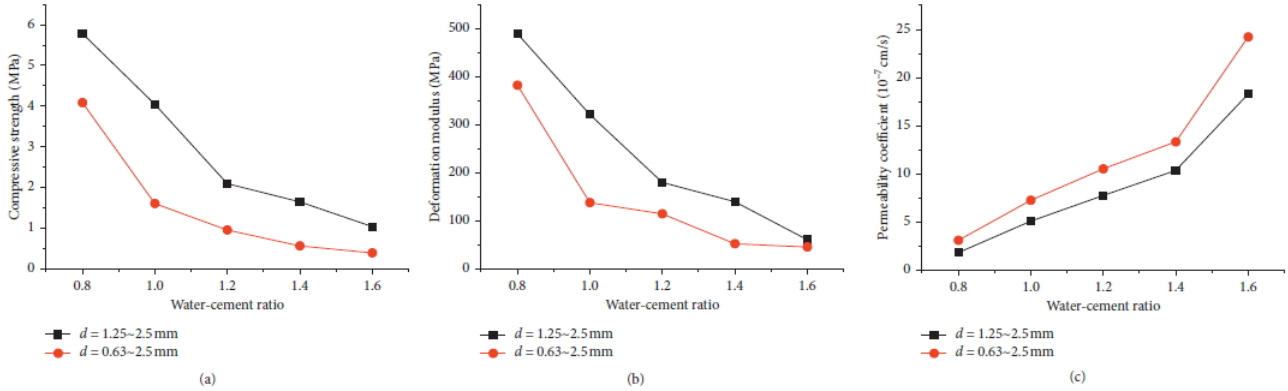

Figure 2.8: Compressive strength vs water/cement ratio (a), Deformation modulus vs water/cement ratio (b) and permeability coefficient vs water/cement ratio (c). After Li et al. (2020).

Grout injection location The location of the grout outlet for screw-injection piles differs from pile to pile. Most designs include grout injection at the pile tip and sides (Fundex 2021a, April 5; Vroom 2021a, April 5)). Not only the location of the grout outlet can differ, the direction at which it directs grout may also vary, from directly downwards to the side. The effects of the injection location and direction are not well understood. Figures 2.9a and 2.9b illustrate two possible injection methods used. Figure 2.9a shows the location of the grout outlet on a screw-injection pile used at the Maasvlakte 2 pile test. The grout injection direction for the piles at this test is horizontal, with a tooth in front of the outlet to disperse the grout. The main aim here is mixing with the ground, with soil fluidisation as a secondary benefit. Figure 2.9b shows a cross section of another SI pile, where the grout outlet is located higher up and injects around a 45° angle rather than horizontally.

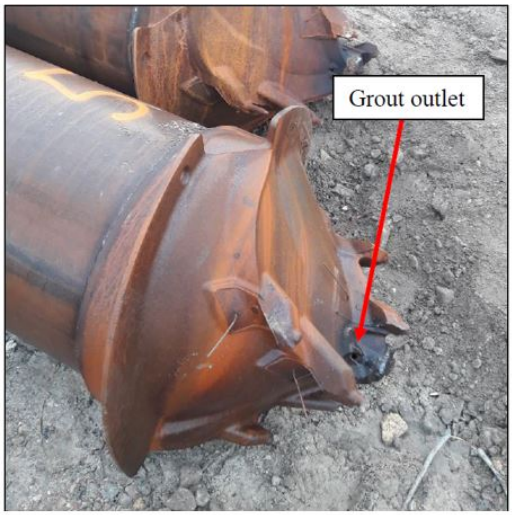

(a) Grout outlet in SI piles at Maasvlakte 2 pile test (Duffy et al. 2021).

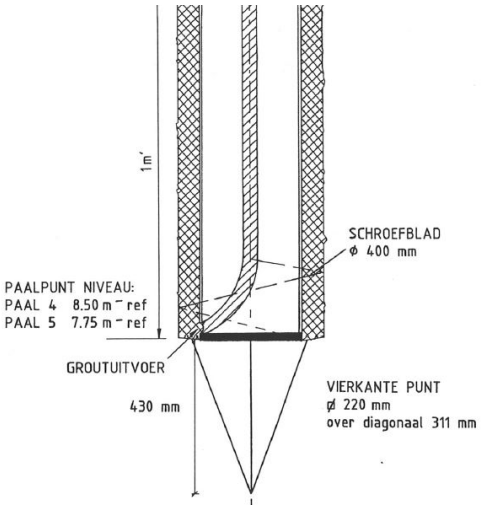

(b) Cross section of test pile showing grout outlet, labelled *'Groutuitvoer'* (Geerling et al. 1992).

Figure 2.9: Figures indicating variance in grout outlet location and direction.

Buoyancy of tube A risk during installation of Type 3 piles (such as Tubex) is once the installation depth is reached, the tube could become buoyant in the (still fluid) grout body. This may result is the loss of stresses built up underneath the pile tip, and therefore decrease α_p. However, whether buoyancy truly affects the value of α_p is not yet known. Once concrete is poured in the pile, upwards buoyancy is prevented by the downward load of the concrete.

Concrete pouring method Generally, there are 2 methods of pouring concrete. The first method is simply pouring concrete in the drilling tube, then extracting the casing using oscillatory motion, as shown in Section 2.1.1. This process occurs under atmospheric pressure. This first method is influenced mainly by the type of concrete poured, as no other factors play a role.

The second method, which occurs in piles like Atlas and Omega (Franki Foundations 2021a, April 5; Franki Foundations 2021b, April 5), pumps concrete into the excavation under pressure as the auger and drilling tube are extracted while rotating in reverse direction. As the second method is influenced more heavily by variables such as concrete viscosity and pressure, installation effects regarding concrete pouring mainly relate to this method. A positive concrete pressure must be maintained at the pile tip, as this indicates that the auger is embedded in fresh concrete and that the concrete pressures inside the tube are equal to the horizontal stresses at the borehole wall (Larisch 2014). A negative concrete pressure may indicate that the auger tip is not embedded in concrete and likely, a cavity between the top of the concrete column and the auger tip has formed. This can lead to collapse of the borehole wall into to cavity, and generates a defective pile (Larisch 2014). According to Larisch (2014), tests have indicated that soil decompression at the auger base can be countered by installing concrete under high pressure. Furthermore, these tests showed that high concrete installation pressures can increase pile capacities in general for Omega piles. However, it is noted that installing rebar becomes more difficult when using high concrete pressures (Larisch 2014).

The main difference is that the first method pours concrete first, then extracts the drilling tube, while the second method does both at the same time. Additionally, the second method pumps concrete under pressure as opposed to pouring under atmospheric pressure. The advantage of the second method is that concrete can be inserted under higher pressures during auger extraction, allowing for the formation of helical flanges like those on the Atlas pile (Figure 2.3b, and increasing the overall capacity in general. The disadvantage of this method is that it is more sensitive to mistakes; if a cavity forms due to an interruption in the concrete supply or insufficient concrete pressure, defective piles may form.

In summary, it is clear that overall there are numerous factors that influence the overall capacity of screw injection piles. Generally, the literature has a focus on small scale, site specific pile tests. This makes it difficult to translate findings to a bigger picture. While the effects of installation parameters are generally known, the interaction between them and the specific influence on the final pile capacity are not well understood. This presents an opportunity for more research into the installation effects of screw injection piles. Figure 2.10 shows a simplified graphic overview of the installation parameters and their supposed interactions.

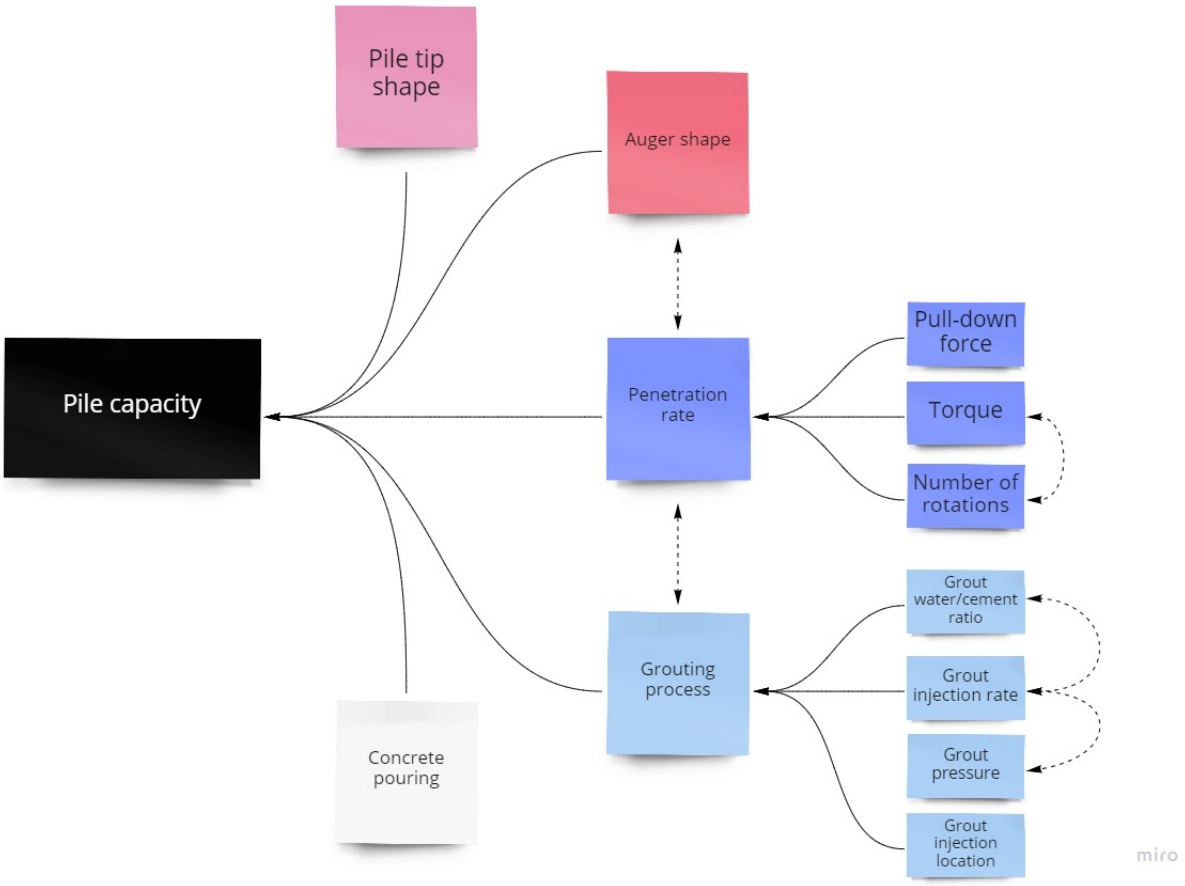

Figure 2.10: Graphic representation of installation parameters.

2.3 Pile Testing

The capacity of a pile can be determined by performing a load test on the pile. There are 3 types of pile tests: static, dynamic and rapid. Generally speaking, a static load test is the most reliable. However, a static test also takes the longest amount of time to perform and is more expensive than the alternatives.

2.3.1 Static Load Test

The static load test (SLT) is the most accurate and reliable method to determine the bearing capacity of the pile tip, the shaft friction and the deformation behaviour of a pile (APTS 2021b, May 13). An assembly is placed over the pile, consisting of concrete or steel blocks, although alternative methods can also be employed, such as grout anchors. The load is transferred to the pile using a hydraulic jack, using the blocks or anchors as a reaction force. The load at the pile head is measured using a load cell, and may be crosschecked with the pressure readings in the jack. Load steps are applied until the predetermined failure load is reached. During the test, strain and displacement can be measured throughout the pile depending on the sensors used.

(a) Static load test setup (APTS 2021b, May 13).

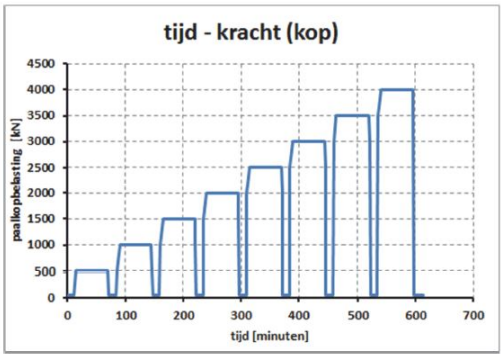

(b) Example of A1 test load steps with unloading/reloading cycles (NPR 2017).

Figure 2.11: Example of SLT setup and time-force diagram

The procedure for a load test is described in NPR 7201 (NPR 2017). The Dutch load step procedure for compressive tests with class A1, A2 and B is summarised as follows:

1. The load at the pile head should be applied evenly to the value of the first load step F_1, in at least 5 minutes.
2. The force of step F_1 should be kept constant for at least 1 hour, with an accepted divergence of at most 1%. If in the last 20 min a settlement occurs larger or equal than 0.1 mm, the load step must be extended until the settlement in the last 20 min is smaller than 0.1 mm, or until a period of 4 hours has passed. After each load step the load must be reduced to the '0 force', which is maintained for 15 min, after which the next load step may be applied.
3. The planned load steps may be applied, repeating the procedure mentioned above.
4. If the force on the pile cannot be increased further because 1) the load frame cannot deliver a larger force or 2) the pile has failed, the test must be stopped. The pile base settlement must reach more than 10% D_{eq} for soil displacing piles and 20% D_{eq} for soil replacing piles.
5. After the final load step, the force on the pile head must be reduced stepwise to the '0 force' in a time period of at least 10 min. This '0 force' must be kept constant for 30 min.

It is important to note that different countries may follow a different programme, prescribed by their respective standards. Furthermore, an article by Gavin et al. (2021) has indicated that the load step programme, especially unload/reload cycles with respect to pile creep, can affect the pile capacity. This adds difficulty when comparing tests using a different load scheme.

2.3.2 Dynamic Load Test

Dynamic load testing (DLT) is a faster though effective alternative to static load testing. During a dynamic test, a load is suddenly applied to the pile by either an impact hammer or drop weight (APTS 2021a, May 13). A stress wave is generated, which travels down to the bottom of the pile before returning to the pile head. Near the top of the pile, the stress waves are captured by measuring the strain and acceleration. CAPWAP analysis, an iterative curve-fitting technique, is then performed, that matches a curve to the measured response of the pile, which then determines the pile capacity (Fellenius 1990). The measured acceleration is used as input to the pile model with accompanying estimates of soil resistance, quake and dampening parameters. The calculated force-time signal at the pile head is compared to the measured force-time signal. During the process, the soil resistance, quake and dampening parameters are adjusted until agreement is reached between the calculated and

measured signal (Federal Highway Administration 2021, May 14). An example is shown in Figure 2.12b.

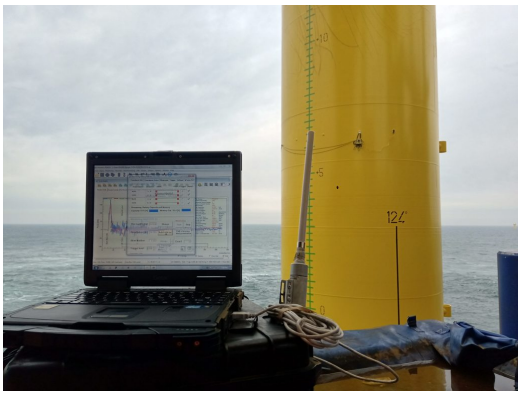

(a) Dynamic load test setup (APTS 2021a, May 13).

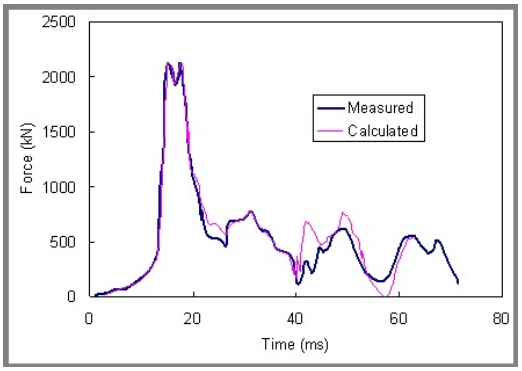

(b) Example of CAPWAP signal matching (Federal Highway Administration 2021, May 14).

Figure 2.12: Example of DLT setup and force-time signal

Although the results of a dynamic load test are mostly in agreement with a static load test, Fellenius (1990) indicates a lower reliability and more importantly, a higher difficulty in differentiating the resistance from shaft friction and pile tip capacity. The ability to differentiate shaft and base resistance is especially important in pile tests with the aim of determining α_p and α_s.

2.3.3 Rapid Load Test

The rapid load test (RLT) combines the advantages of the static and dynamic load test. The rapid load test loads the pile during a short moment. It is much faster than a static load test, although the load duration is much longer than during a dynamic load test. At the pile top, load is measured using one or more load cells, displacements with a reflector system on the pile and acceleration with an accelerometer (Allnamics 2021, May 13). Because the load duration is relatively long, between 10 and 1000 times the pile length divided by the wave propagation speed in the pile (NPR 2017), no stress wave phenomena are involved (Allnamics 2021, May 13). This makes the rapid load test a quasi-static test, which produces simplified graphs which help to interpret the results (Figure 2.13b), removing the need for signal analysis. Therefore, the results of rapid load tests are more accurate, reliable and man-independent when compared to a dynamic load test. Because of this, the NPR allows rapid load tests to be used for category A2 and lower pile tests (NPR 2017). There are two major test methods: launching a reaction mass, or dropping the reaction mass from a height. These are called 'StatNamic' and 'StatRapid', respectively, by Allnamics.

Launched reaction mass / 'StatNamic' StatNamic has been developed in the 1980s and was the first available RLT option. The method is based on launching a mass from the pile top. Due to the reaction of the launch, a gentle push is given on top of the pile, long enough to avoid stress wave phenomena (Allnamics 2021, May 13).

Dropped reaction mass / 'StatRapid' StatRapid is a newer method and the most commonly used RLT technique. It is a semi-static, high strain test method. The StatRapid method drops a weight onto a specially designed cushion located at the top of the pile. The kinetic energy of the drop weight is transferred into a relatively long push on top of the pile, avoiding stress wave phenomena. An example of a StatRapid setup is shown in Figure 2.13a

(a) Rapid load test (StatRapid) setup (Allnamics 2021, May 13).

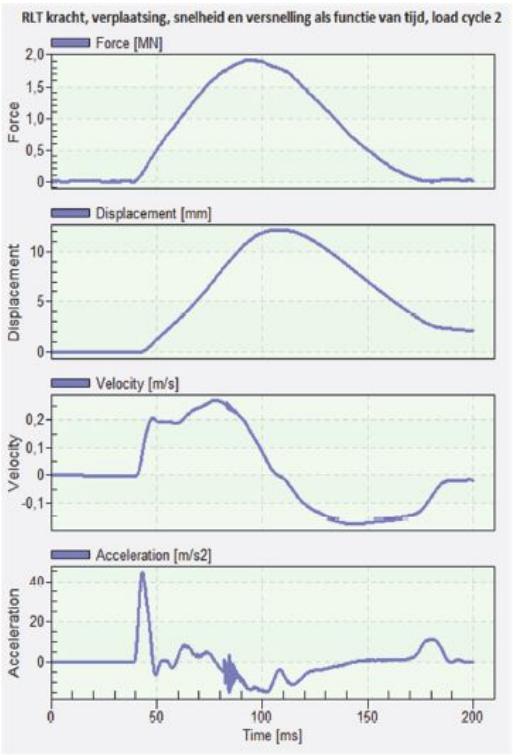

(b) Example of RLT diagrams (NPR 2017).

Figure 2.13: Example of RLT setup and time graphs for one load cycle

2.4 Uncertainties with load testing

2.4.1 Geometrical data

Holeyman (2001) lists geometrical data as one of the uncertainties present when assessing SI piles. Due to the grout injection and extraction of the drilling tube, the actual size of the pile is influenced. Depending on local variations in the soil and the grout properties, the grout body that forms around the pile is irregular and not precisely predictable. Additionally, as stresses in the ground find equilibrium after the tube is extracted, bulges may form, further influencing the shape of the pile. Figure 2.14 shows irregularities in pile diameter along the shaft of screw-injection piles. As the average circumference of the pile shaft and pile diameter are important variables in calculating the expected bearing capacity, uncertainties in these calculations due to the unpredictable shape of the pile are expected and must be taken into account.

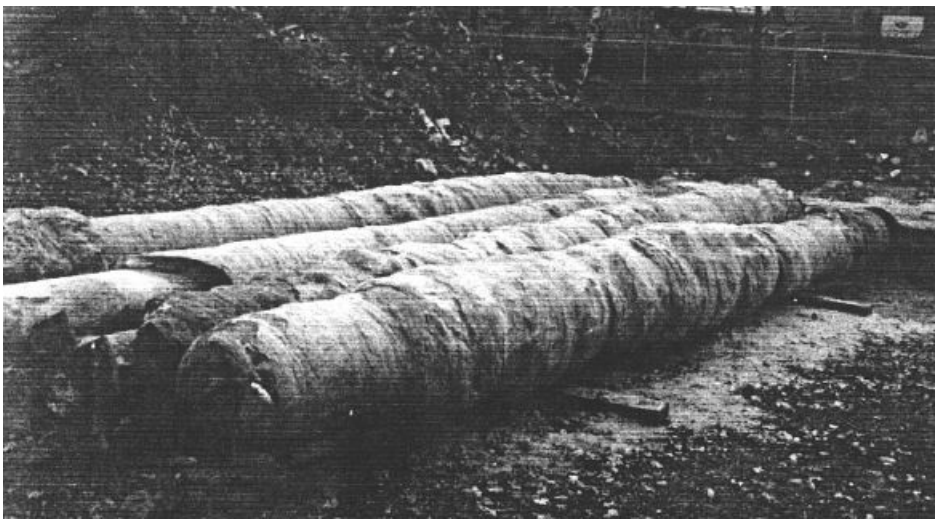

Figure 2.14: Picture illustrating variable pile diameter of SI piles (Geerling et al. 1992).

2.4.2 Prediction methods

Predictions for the final pile bearing capacity are made using design methods such as the NEN described in Section 2.5. Heidarie Golofzani et al. (2020) define the Dutch pile design method as a CPT based alpha method. Findings by Heidarie Golofzani et al. (2020) indicate that compared methods used outside of the Netherlands, the alpha based method is the most reliable for predicting pile capacities.
However, these alpha based methods contain theoretical imperfections. Figure 2.17a assesses the Dutch method based on criteria defined by Heidarie Golofzani et al. (2020). According to Doherty and Gavin (2011), the soil behaviour governed by effective stress and the changes in stress-strain relationships caused by pile installation cannot be completely described by the initial undrained strength profile. Doherty and Gavin (2011) also mention that the friction along the soil-shaft interface at the failure surface where the shear resistance develops, is not considered. Design methods also involve empiricisms, in which factors are calibrated against load test data (Tang and Phoon 2018). However, when designs fall out of the scope of the calibrated data, additional uncertainty is introduced. For example, the NEN9997-1 method is designed for use in the Netherlands, where lots of soft soils are found. This method could therefore lose accuracy in soils not commonly encountered in the Netherlands, such as stiff, heavily overconsolidated clays.

2.4.3 Variability of soil throughout tests site

The subsurface is often generalised as several defined homogeneous layers. In reality, this is not the case. Soils are heterogeneous and spatial variability is an intrinsic feature of a site profile (Tang and Phoon 2018). The selection of soil parameters, such as the friction angle ϕ, to define these layers are subjective. Therefore, even within the same design model, different pile resistances can be obtained (Karlsrud 2014). The NEN method bases much of its prediction on a CPT profile, which itself contains several uncertainties. Because CPT tests do not record data continuously, but rather in a range of centimetres, it is possible that thin layers are missed. Consequently, the spatial variability of the soil may be underestimated.

2.4.4 Effects of pile installation

As described more extensively in Section 2.2, it is clear that the different installation effects influence the pile geometry, final bearing capacity and influence readings during pile installation and pile tests. Figure 2.10 shows a graphic overview of the varying parameters and their influence.

2.4.5 Measurement devices

There are a lot of interpretations and assumptions made during the whole pile design and testing process. As described previously, human interpretation and bias occurs in the early stages of the process. Empirical relations used in the Dutch design method, chosen values for soil properties and interpretation of the CPT data all translate into uncertainties as the process continues. However, human interpretation is also likely to occur during the analysis of recorded data. For example, vibrations recorded by the LVDTs due to nearby roadworks must be filtered out for accurate results. Though, if this occurrence is not noted during the test, it might simply be misinterpreted or overlooked as noise. A very important source of information used in this thesis are the measurements from strain gauges. An introduction to the relevant systems encountered in the thesis is given in the followings paragraphs.

Pile instrumentation types According to a state of the art review by Flynn and McCabe (2021), the typical types of instrumentation used in concrete piles are, ranked from old to new:

- electrical resistance strain gauges (ERSGs)
- vibrating wire strain gauges (VWSGs)
- fibre optic strain sensors (FOSSs)

All strain gauges in concrete piles operate under the assumption that the strain measured by the gauge is equal to the strain in the surrounding concrete. This is valid when no cracking occurs in the pile at the level of the gauge (Flynn and McCabe 2021).

ERSGs are the simplest and least expensive method to determine strain in piles. The gauges are usually 5-15 mm long and are attached directly on the surface of a structural member. When contraction or expansion of the structural member occurs, this results in a proportional change in electrical resistance of the ERSG. This can be calibrated against known applied strains, which allows the strain to be quantified from the measurements.

VWSGs are, as of now, the most popular choice of gauge according to the article. A steel wire is tensioned between two mounting blocks. This is then housed in a protective casing and sleeve, which in its entirety is welded to steel bars or metal flanges at each end. A magnetic field is generated by coils in the casing, which oscillates the steel wire at its resonant frequency. This process generates an AC current, of which the frequency is recorded by a datalogger. A change of load within the pile causes a proportional change in length, and thus the frequency of the vibrations. From the change in frequency, the strain can be derived.

FOSSs are generally subdivided in two categories:

- discrete types, where the primary role of the fibre optic cable is to transfer light to and from a discrete sensor.
- distributed fibre optic sensing (DFOS), where the fibre optic cable itself acts and the strain sensor throughout the length of the cable.

Examples of optical fibre are shown in Figure 2.15a. Fibre Bragg Grating sensors (FBGs), depicted in Figure 2.15b, are a variant of discrete types. These are made of a prefab grating within the core on an optical fibre in the sensor, which induces a periodic variation in refractive index to reflect light around the Bragg wavelength. When the sensor experiences a change in strain, the Bragg wavelength undergoes a corresponding change which can then be correlated to strain.

DFOS can be subdivided in:

- optical frequency-domain reflectometry
- Brillouin optic time-domain analysis (BOTDA)
- Brillouin optic time-domain reflectometry (BOTDR)
- Brillouin optic frequency-domain analysis (BOFDA)

The main advantage of DFOS over other instrumentation types is the ability to provide continuous measurements of strain along the full length of the cable, however, the accuracy or measurement frequency can be worse. BOTDA, BOTDR and BOFDA are based on Brillouin scattering of light within an optical fibre. The interaction between incident light and the density of propagating waves or acoustic photons results in the scattering of light at a shifted frequency (Flynn and McCabe 2021). This shifted frequency is referred to as the Brillouin frequency shift, and varies proportionally to a change in length of the cable due to strain. A BOTDA sensor is shown in Figure 2.15c.

Strain gauges may be placed in different arrangements. The main advantage of placing sensors away from the centre of the pile is that the effect of pile inclination can be measured, although to accurately measure this in each direction of the pile, at least three locations (at 120°) are needed, increasing costs. An overview of different optical fibres, FBG and BOTDA gauges and typical strain gauge arrangements are shown in Figure 2.15d.

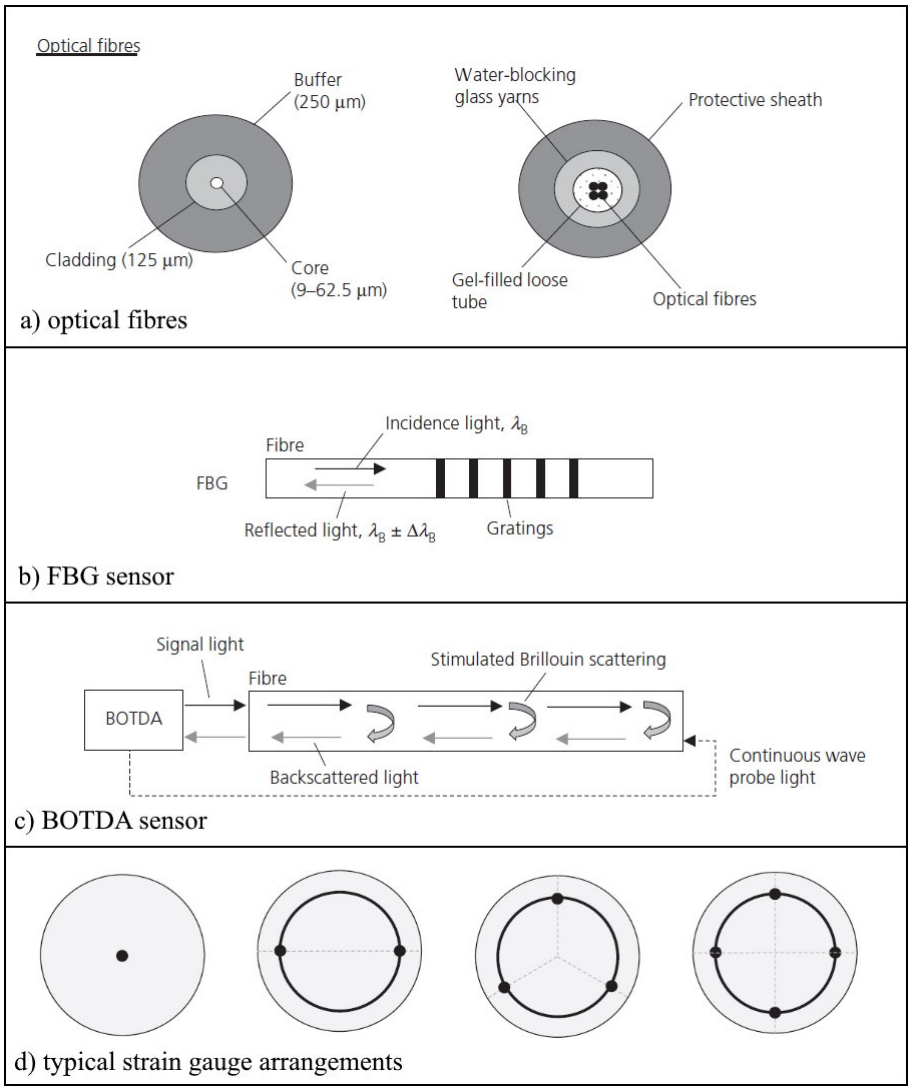

Figure 2.15: Overview of fibres, sensors and gauge arrangements. Edited from Flynn and McCabe (2021).

As shown in Figure 2.17b, the difference between the two fibre optic techniques is more noticeable at shallower depths. This may be caused by slippage of the fibre optic cable inside the BOFDA sensor. It is up to humans to investigate this effect and to decide how to use the recorded data. Furthermore, data manipulation such as smoothing or extrapolation can be applied. Regarding Figure 2.17b, the BOFDA curve is continuous yet noisy; although smoothing it could make sense, it might also reduce the accuracy of the data. The FBG data points could be extrapolated but will then show data that has not actually been measured.

The biggest source of uncertainty during the data analysis is the conversion from data readings to a usable format, such as converting from strain to load. Selecting variables for the conversion process is done by humans and has a severe impact on how the data is used to procure final results. Research on the determination of the elastic modulus of a concrete pile by Lam and Jefferis (2014) demonstrated the impact of the human factor as it was found that the theoretically correct equation used to find the elastic modulus of a pile performed worse than all other compared methods. Lam and Jefferis (2014) point out that curing concrete in the ground is affected by in situ conditions, such as the weight of overlying concrete and water in the soil, which differs significantly from a lab environment. Their review and analysis of 10 different methods concluded that the secant modulus method was the most satisfactory, with the tangent modulus method also proving to be a valuable option. However, Lam and Jefferis (2014) end their paper with the notion that stress determination in concrete depends 'most importantly on the knowledge and experience of the engineers'. Therefore, understanding the pros and cons of each method is required to make informed decisions, further underlying the unmistakable impact of the human factor and its associated uncertainties. An illustration of this is shown in Figure 2.16.

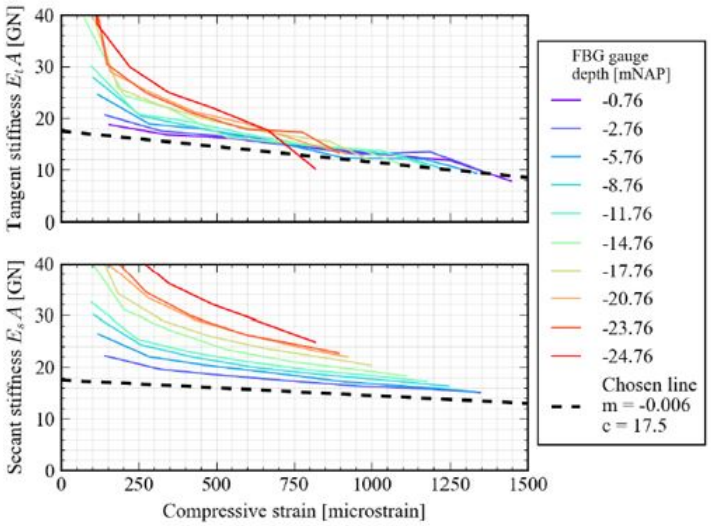

Figure 2.16: Fellenius tangent and secant stiffness methods (Duffy et al. 2021).

2.4.6 Measurement uncertainties

The methods used to record data during pile tests provide uncertainties. Linear Variable Differential Transformers (LVDTs) are used to measure the displacement of the pile very accurately. However, vibrations can introduce spikes in the measured data which need to be filtered out to produce correct results. For example, nearby roadworks may induce enough vibrations in the ground so that the data recorded through the LVDTs is distorted.

Besides measuring displacement, strain can be measured in piles through the use of different systems, such as fibre optics. Several types of measurement systems were discussed in the previous section.

An example of the different results two strain gauge measurements systems can give is shown in Figure 2.17b. The high sensitivity of these fibre optics mean that the data is susceptible to noise. Additionally, concrete curing and debonding between the instrument and the surrounding concrete can affect these readings.

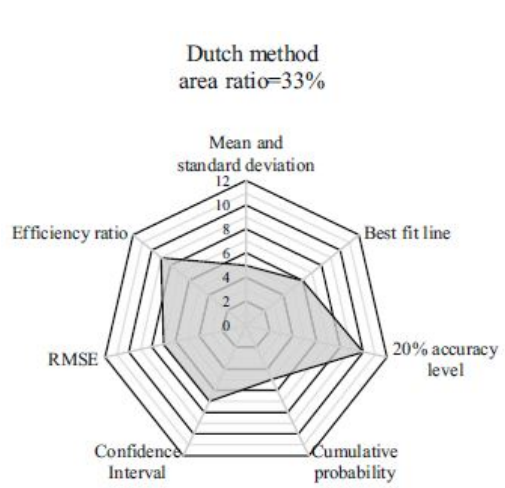

(a) Assessment of Dutch method based on investigated criteria from Heidarie Golofzani et al. (2020)

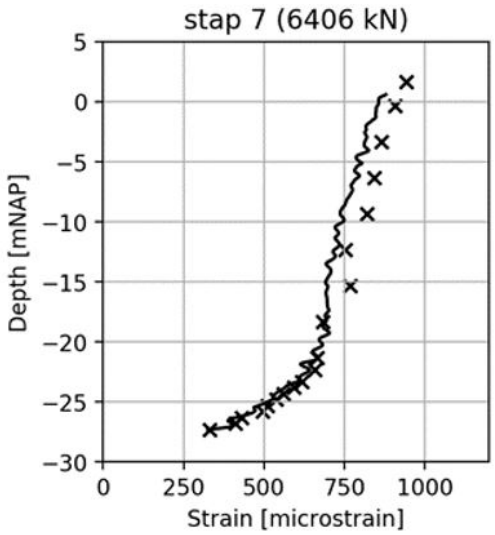

(b) Comparison between BOFDA (continuous) and FBG measurements (Duffy et al. 2021)

Figure 2.17: Illustrations regarding prediction and measurement uncertainties

In summary, predictions and analyses on pile capacities are influenced by many sources of uncertainties, such as spatial variability, measurement and transformation errors, and human error and bias in the interpretation of load test data.

2.5 Dutch Pile Design Method

Dutch practice is described in the standard NEN9997-1 (NEN 2017). This section will present the main steps required to calculate the pile capacity according to the standard.

2.5.1 Total bearing capacity

The total bearing capacity of the pile is calculated by adding the base resistance and the shaft friction:

$$R_c = R_b + R_s \tag{2.1}$$

Where:

$$R_b = A_b \times q_b \tag{2.2}$$

And:

$$R_s = O_{s;\delta L} \times \int_{\delta L} q_{s;z} \times dz \tag{2.3}$$

With:

R_c = the bearing capacity of the pile; kN

R_b = the bearing capacity of the pile tip; kN

R_s = the pile shaft friction; kN

A_b = the area of the pile tip; m^2

q_b = the pile tip resistance; kN/m^2

$O_{s;\delta L}$ = the average circumference of the pile shaft in the layer of the pile tip; m

δL = the length of the part of the pile which may be considered in shaft friction calculations (see NEN (2017, p. 161) for more details); m

$q_{s;z}$ = the pile shaft friction at depth z; kN/m^2

z = the vertical direction

2.5.2 Base resistance

The ultimate pile tip resistance is calculated as following (NEN 2017, p. 162):

$$q_{b;max} = \frac{1}{2} \times \alpha_p \times \beta \times s \times q_{c,avg} \tag{2.4}$$

With:

$q_{b;max}$ = maximum pile tip capacity $\leq$ 15 MPa

α_p = the pile base reduction factor, examples of these are 0.63 for driven piles and 0.35 for anchor piles (see NEN (2017, p. 163-165) for details)

β = Factor taking into account pile tip shape (= 1 in thesis, see methodology)

s = factor taking into account shape of cross section of pile tip (= 1 in thesis, see methodology)

$q_{c,avg}$ = complex average of cone resistance around pile base, explained in following section

Koppejan averaging method (4D/8D method)

The method used to determine the values of $q_{c,avg}$ as written in NEN 9997-1 (NEN 2017) is called the 4D/8D or Koppejan method, proposed by van Mierlo and Koppejan (1952). The value is a complex average of the q_c around the pile tip. This factor is then multiplied by a factor α_p which varies per pile type and installation method used. The 4D/8D method returns a value of q_c influenced by the soil 0.7D to 4D under the pile tip, and 8D above the pile tip.

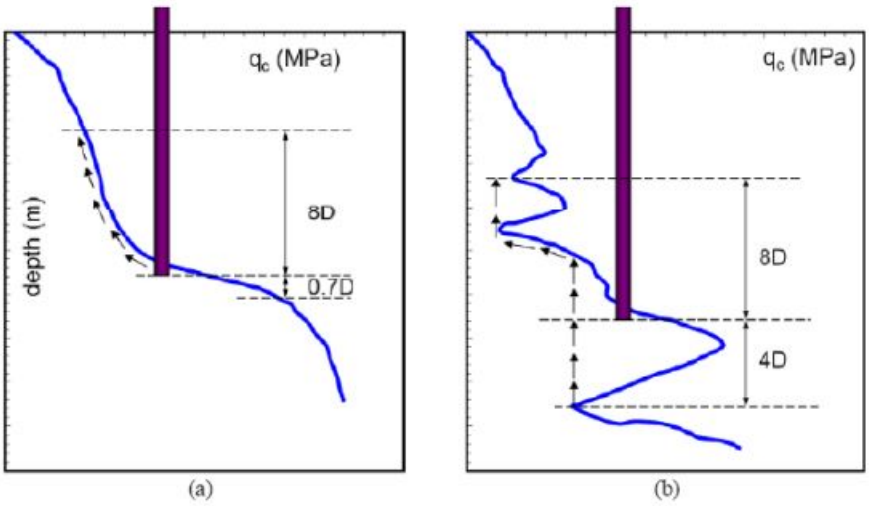

Figure 2.18: Calculation of $q_{c,avg}$ according to Koppejan (Xu 2007)

Koppejan's method utilises the minimum path rule while determining the values of q_c. To calculate $q_{c,I,avg}$, one takes the average q_c values ranging from 0.7 to 4D beneath the pile tip. The selected value is the minimum of those averages. Figure 2.18 shows how $q_{c,II,avg}$ and $q_{c,III,avg}$ is found using the minimum path rule. Starting from the pile base, the line is followed upwards. For every measurement interval, the recorded q_c value is considered. If this value exceeds the minimum q_c value encountered along this path, the value is limited to this minimum value. Otherwise, the actual value is recorded and is deemed the limiting resistance for measurements further along the path. Thereafter, the average q_c is taken over the depth range for all the recorded q_c values. In short, the process can be formulated as:

$q_{c,I,avg}$ = the minimum of the average 0.7-4D below the pile tip

$q_{c,II,avg}$ = the average of the minimums 0.7-4D below the pile tip

$q_{c,III,avg}$ = the average of the minimums 0-8D above the pile tip

2.5.3 Shaft friction

The shaft friction is found via (NEN 2017, p. 165-166):

$$q_{s;z} = \alpha_s \times q_{c;z} \tag{2.5}$$

With:

$q_{s;z}$ = the pile shaft friction at depth z; with z in m

α_s = the reduction factor (see NEN (2017, p. 163-165) for details)

$q_{c;z}$ = the cone resistance, limited to 12 MPa for layers $<$ 1 m and 15 MPa for layers $\geq$ 1 m (see NEN (2017, p. 166) for details)

The process used to determine the value for $q_{c;z}$ is not straightforward, and is described in full detail in NEN9997-1, page 166.

Clarification on 'limiting' In the thesis, the effects of limiting prescribed by the NEN are investigated. Limiting rules are applied at two separate points in the calculation. First, the maximum base resistance q_b is set at 15 MPa (described in Section 2.5.2). In this thesis, the combination of $q_{c,avg}$ and the determined α_p factors never produce a value of q_b above 15 MPa.

The other limiting rule applied by the NEN is when calculating the shaft friction (Section 2.5.3). This limits q_c values along the shaft to a maximum of 15 MPa if the layer has a thickness $\geq$ 1 m, and 12 MPa if the layer has a thickness $<$ 1 m. Therefore, when evaluating limiting in this thesis, only the q_c limiting along the shaft is shown, due to the q_b values at the base never exceeding 15 MPa.

2.6 Literature review: conclusions

The literature generally agrees on the identification and importance of installation effects, although there is no clear consensus on the influence of a particular factor and on interaction between installation variables. Research on installation effects indicates possible consequences and provides some recommendations, though tests performed are usually small scale and site-specific. There is a clear agreement in the literature that more investigation is required, with several papers proposing to review tests at a grander scale.

The reviewed literature describes several pile design methods. While it is agreed that some methods are better than others, there is no general recommendation for a specific design method under certain conditions. Papers cite differing soil conditions and human input as the most substantial reasons for inaccurate prediction results. Due to the varied use of pile design methods, it is difficult to directly compare predictions of piles between different methods and to evaluate the performance of a certain method itself.

Uncertainties in general pose a problem regarding the pile design. It is clearly stated in the literature that uncertainties are encountered throughout the whole process, from the design phase through the curing of concrete. However, the huge variability of sources makes it difficult to provide methods to curtail their effects. For this reason, the literature suggests studying the uncertainties so that researchers are not misled by them.

In summary, there is a lack of understanding on the effects of installation variables and how these interact with each other. A database driven approach with a broader view may provide more information on the topic. Additionally, a consensus on which pile design method to utilise under specific circumstances is lacking. The use of numerous pile design methods makes evaluation of a distinct method difficult and poses a challenge when comparing pile capacity predictions. Uncertainties in the process are significant and ever present, but are understood and can be accounted for during human interpretation of results.

Identified gaps and problems in the previous research are:

- Lack of understanding of specific installation effects.
- Insufficient knowledge on interaction between installation variables.
- No database studies performed, causing difficulty with translating findings to a broader picture.

- Varying design methods, problematic for direct comparisons and evaluation of method.

This thesis will try to address the above-mentioned gaps and problems in the literature with a database driven, broad scale approach. By comparing and analysing pile test results using the Dutch design method, the goal is to gain an improved understanding of the installation effects, the Dutch design method, and the alpha factors.

Chapter 3

Methodology

The methodology consists of the following steps:

- Finding suitable pile test data
- Importing tests data
- Determination of soil profile
- Determination of pile factors
- Calculate pile capacity
- Predicting load-settlement curves
- Evaluation and refinement of results

All relevant data presented in the pile test database is stored digitally, as either a pdf document, Excel sheet or picture. The script that calculates the pile capacity according to the NEN9997-1 method is kindly provided by Kevin Duffy. This script is only slightly modified in some areas, mainly to account for the more limited availability of soil data in the database. Code to import and interpolate CPT data and load-settlement curves is written by the author, as is the script to produce load-settlement predictions. Scripts can be provided upon request. Each step is described in more detail below.

3.1 Step 1: Finding suitable pile test data

The first step in the process of starting a database study is finding reports, and selecting which ones are suitable for the database. Several sources have been consulted, such as research programmes from TU Delft, test reports from Dutch piling companies and the archive at Deltares. In order to be selected, reports need to contain at least detailed information on the pile design, CPT profiles and load-settlement data. In addition, a preference is given to static load tests and reports which allow the separation of load into shaft friction and base resistance. This can be achieved, for example, by including strain measurements along the pile. Those findings can be used to reliably determine α factors. Other interesting findings in reports, such as excavation of the piles after testing, can provide valuable insights in the accuracy of assumptions made during the design phase. Dynamic load tests are not selected due to these lacking in accuracy, but rapid load tests can work to evaluate findings made with static load test reports. An overview of the database discussed in this report is given in Table 3.1

Test name	Screw or screw-injection	Pile type	No. of piles	Load test type	Separation of shaft/base resistance	Extra investigation on:
Maasvlakte 2	Screw-injection	Type 3	4	Static	Yes, strain data	Grout sand content
Beemster	Screw	Type 1	4	Static	Yes, strain data	Pile tip shape
Rosmalen	Screw-injection	Type 3	5	Static	Yes, separate load cell	Pile tip shape; excavated piles
Limelette	Screw	Type 1 and 2	10	Static	No	Excavated piles
SON	Screw-injection	Type 3	3	Rapid	No	

Table 3.1: Overview of test database reviewed in report.

3.2 Step 2: Importing test data

With the test reports selected, the next step is to import the relevant data required to calculate capacity and predict load-settlement behaviour. Due to most of the data being available only on paper or as an image, a method is required to read the visual data and convert it into a datasheet, such as a .csv or.xlsx. The program used to do this is WebPlotDigitizer by Rohatgi (2021). After setting the range and inclination of the axes, the program is able to filter out the relevant data. This can be manually adjusted to account for small mistakes. In the case where data cannot be accurately filtered from the background, the data is outlined in a bright colour by the user, so that WebPlotDigitizer is able to extract the data. An example of how one profile is extracted is given in Figure 3.1.

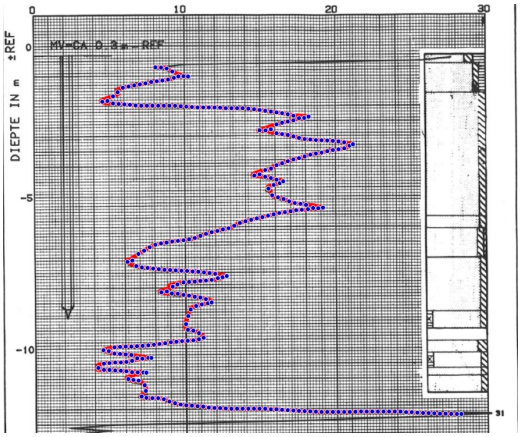

(a) Blue dots represent data extraction performed by WebPlotDigitizer.

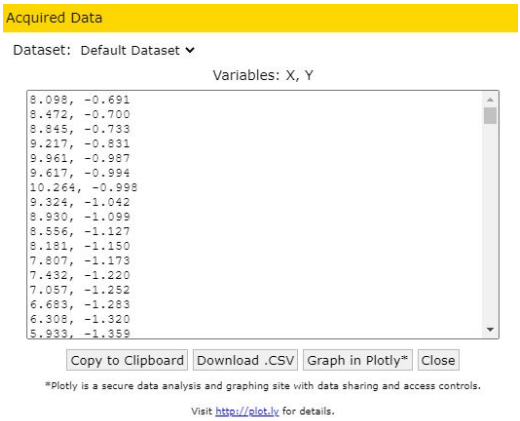

(b) Example of recorded data from WebPlotDigitizer, which can be stored as a .csv file.

Figure 3.1

The same process is then followed to store load-settlement data of the load tests, if the data was not available otherwise. However, rather than a continuous line like a CPT profile, the load-settlement data is often recorded once per load step, simplifying the procedure.

For each pile test, the pile parameters and dimensions are then recorded from the reports and stored to be used in the code. These numbers represent data such as the pile length, base and shaft diameter and pile tip level.

Finally, the load-settlement curves from NEN9997-1 must be imported (shown under step 5 in Figure 3.3), so that they can be used as a look-up table in the code. This allows the prediction of a pile response, based on the calculated capacity and input variables. The x and y values of each line are provided in an Excel sheet, and therefore do not need to be extracted using WebPlotDigitizer.

3.3 Step 3: Determination of soil profile

For the program to accurately calculate the bearing capacity of a pile, the soil profile must be input correctly. As not all test reports came with data on sleeve friction and friction ratio, each soil layer must be classified separately. Where available, soil investigations in the reports are closely studied and compared with the soil classification method by Robertson (2016). When all soil layers have been identified, each layer will be classified as one of the soil types described in NEN9997-1: sand, clay, very sandy silt, slightly sandy silt or peat. Based on the classification, an appropriate α_s factor is then set for that layer. An example of how this would be done in the code is shown in Figure 3.2b.

The previously extracted CPT profile is then imported into the code. As the x and y values are not evenly spaced, 1D interpolation is performed, which provides an evenly spaced number of coordinates which accurately represents the recorded q_c values in the original profile. The result of this is presented in Figure 3.2a. With both the q_c values and soil classification correctly correlated, the next step in the code is to calculate the pile capacity following the Dutch design method.

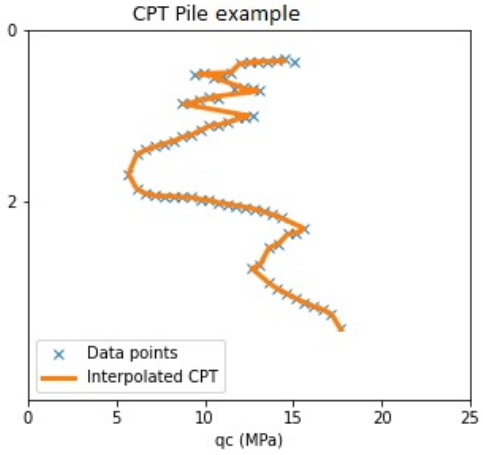

(a) Example of interpolated CPT (orange) compared to data points (blue).

Condition	*Soil class*	*α*
Depth > -2m:	Peat	0
-2m > Depth > -5 m:	Clay	0.03
Depth < -5m:	Sand	0.01

(b) Example of how soil would be classified in code.

Figure 3.2

3.4 Step 4: Determination of pile factors

Two of the tests in the database are instrumented with strain gauges, and one has the pile tip connected to an independent load cell. Therefore, based on these reports, it is possible to find representative α_p and α_s factors established on these measurements.

The shaft factor α_s is calculated by:

$$\alpha_s = \frac{\delta F}{\delta L * O} \Big/ q_c \tag{3.1}$$

With δF the difference in force along the pile [kN]; δL the distance along the pile on which the force acts [m]; O the circumference of the pile [m]; and q_c the average cone resistance along the pile [MPa].

The base factor α_p is found using:

$$\alpha_p = \frac{F_b}{A_{tip}} \Big/ q_{c,avg} \tag{3.2}$$

With F_b the force at the base of the pile [kN]; A the area of the pile tip [m^2]; and $q_{c,avg}$ the calculated average cone resistance at the base of the pile [MPa], as documented in NEN9997-1.

For a pile test with a separate load cell for the pile tip, the total load on the pile can be easily split between the pile base (measured separately) and the pile shaft (total load minus the pile base load). These values can then be used to find the corresponding α factors.

For the pile tests instrumented with strain gauges, the recorded strain must first be converted to force. In the case of Maasvlakte 2, the tangent stiffness method is used, as described in the report by Duffy et al. (2021). The calculations performed in this thesis, for the Beemster test, are done with the following equation:

$$F = \epsilon \times E \times A \tag{3.3}$$

Where F is the force in kN; ϵ the strain [-]; E the Young's modulus [kPa]; and A the surface area [m^2]. The stiffness of the pile $E * A$ can be calculated by multiplying the cross-sectional area of the pile (A) with a Young's modulus (E) suitable for the type of material used.

3.5 Step 5: Calculate pile capacity

The program employs the NEN9997-1 calculation method, described in detail in Section 2.5. With the parameters of the pile and the soil profile classification defined, only a few remaining factors must be set before the capacity of the pile can be calculated. These are β, s, α_p and α_s.

Factor β takes into account the pile tip shape. This depends on two values. First, the distance from the start of the pile tip to the widest part of the tip, H, which is 0 for all considered piles. Secondly, the fraction of the squared equivalent tip diameter over the squared equivalent shaft diameter, $\frac{D_{eq}^2}{d_{eq}^2}$. For all screw-injection piles, the shaft and base diameter are equal and thus the fraction results in 1. With $H = 0$ and $\frac{D_{eq}^2}{D_{eq}^2} = 1$, the correct selection of β according to the NEN is a value of 1. Therefore, β for all screw-injection piles is equal to 1. In order to directly compare load-settlement data between screw and screw-injection piles, it is chosen to apply the same β factor of 1 to all other piles as well. The factor s takes into account the shape of the cross section of the pile base. For round piles, the equation for s returns a value of 1. As all piles in the database are round, factor $s = 1$ is applied to every pile.

The α_p and α_s factors, while prescribed in NEN9997-1, will be subject to variation according to calculations in the analysis, as described in the previous step.

Based on the given inputs, the program will then calculate the total shaft friction $R_{s;k;max}$ and base resistance $R_{b,k;max}$ of the pile. These can then be used to draw a predicted load-settlement response.

3.6 Step 6: Predicting load-settlement curves

With the maximum base capacity $R_{b,k;max}$ and shaft friction $R_{s;k;max}$ now determined, the program is able to produce a load-settlement response based on those numbers. This behaviour prediction is based on the prescribed load-settlement curves in NEN9997-1, as shown in Figure 3.3. The base mobilisation is drawn to the left, while the shaft mobilisation is presented to the right. The figures allow the selection of three options. Curve 1 represents behaviour found in soil displacing piles, prescribed for driven and screwed piles. Curve 2 is prescribed for soil replacing and micropiles, such

as Continuous Flight Auger and anchor piles. Curve 3 considers piles outside of the scope of this report.

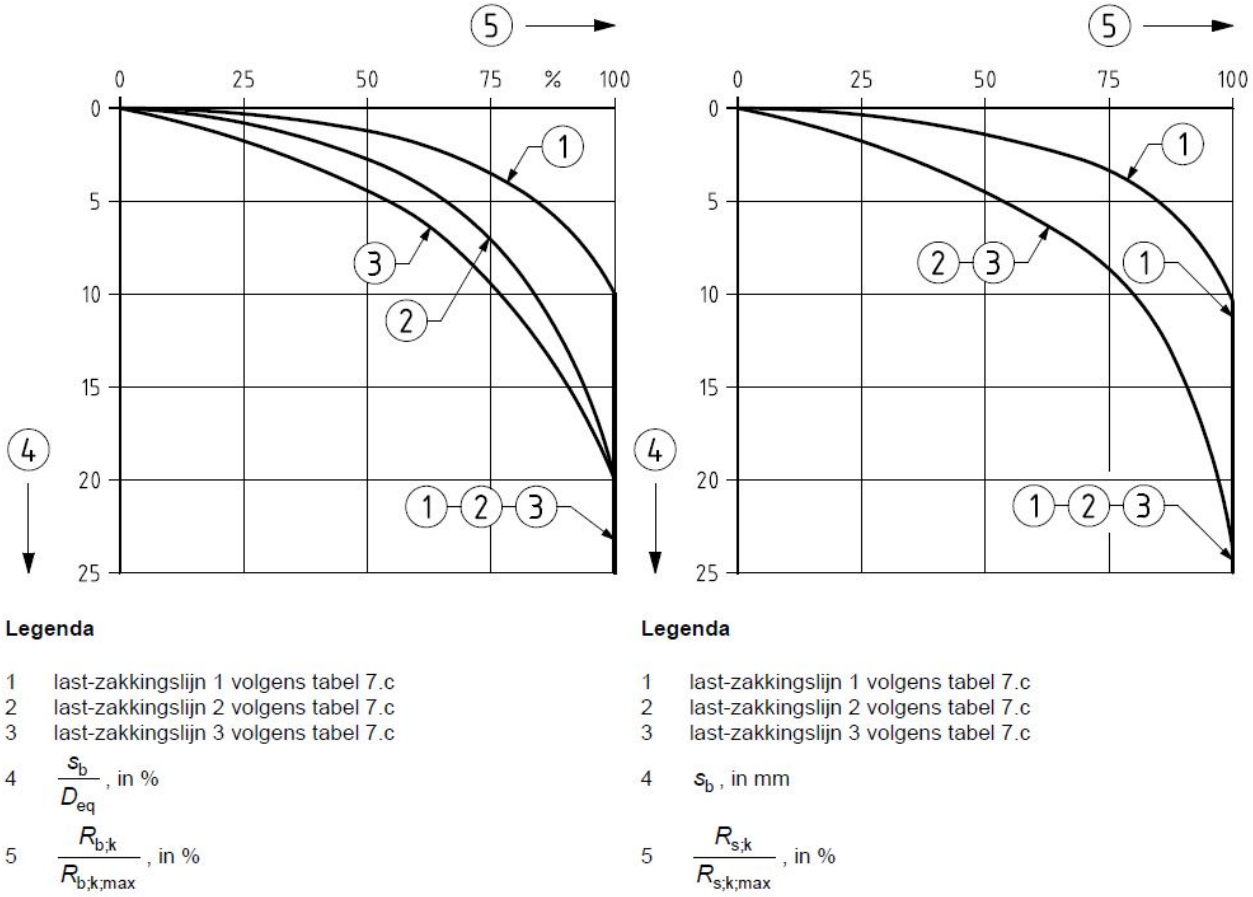

Figure 3.3: Load-settlement curves from section 7.6.4.2. Base mobilisation on left, shaft mobilisation on right (NEN 2017).

The graph on the left in Figure 3.3 shows the mobilisation of the base resistance. The vertical axis is the normalised base settlement, defined as $\frac{s_b}{D_{eq}}$, in %. Here, s_b is the base settlement, in mm; and D_{eq} is the equivalent diameter of the pile base, in mm. The horizontal axis is the percentage of the base mobilisation, defined as $\frac{R_{b;k}}{R_{b;k;max}}$, in %. The value $R_{b;k;max}$ is - the in the previous step - calculated maximum base resistance, in kN; and $R_{b;k}$ is the load on the base at a given s_b, in kN.
The graph to the right in Figure 3.3 shows the mobilisation of the shaft resistance. The vertical axis is the base settlement s_b, in mm. The horizontal axis is the percentage of shaft mobilisation, defined as $\frac{R_{s;k}}{R_{s;k;max}}$. The value $R_{s;k;max}$ is - the in the previous step - calculated maximum shaft resistance, in kN; and $R_{b;k}$ is the load on the shaft at a given s_b, in kN.

Like the CPT profile, the imported data first needs to be interpolated so that all values are equally spaced. The interpolation step size is 0.1 along both y-axes of the graphs shown in Figure 3.3. This means that each curve is represented with a total of 250 coordinates, which provides fast performance of the code and good data resolution.
Though, this presents a problem. The vertical axes of the two graphs in Figure 3.3 do not have the same unit. The y-axis for the base mobilisation is represented as $\frac{s_b}{D_{eq}}$, in %. This is a normalised value of base settlement, divided by the equivalent diameter of the pile base; in percentage. The y-axis of the shaft mobilisation is simply represented as s_b, in mm. Therefore, the calculated load for each y value cannot simply be added to each other.

However, because the factor D_{eq} is known, a solution can be found. The step size for the shaft mobilisation is set at 0.1 mm. This provides a high data resolution but does not slow down the code noticeably. For the base mobilisation, the step size is set as $\frac{0.1mm}{D_{eq}} * 100\%$. This means that for every data point generated, the actual value of s_b is precisely the same: and thus the load at the base and along the shaft at a given settlement can be easily summed to find the total load on the pile.

Simply put, the process works as follows: for a given value of s_b, the program looks up the percentage of mobilisation on the load-settlement curves. Based on the percentage of mobilisation and the known maximum load, the load at the given value of s_b is calculated. This process is then repeated for all defined values of s_b.
The load-settlement prediction can then be plotted, together with the previously imported measured load-settlement data from the actual pile test. An example result is shown in Figure 3.4.

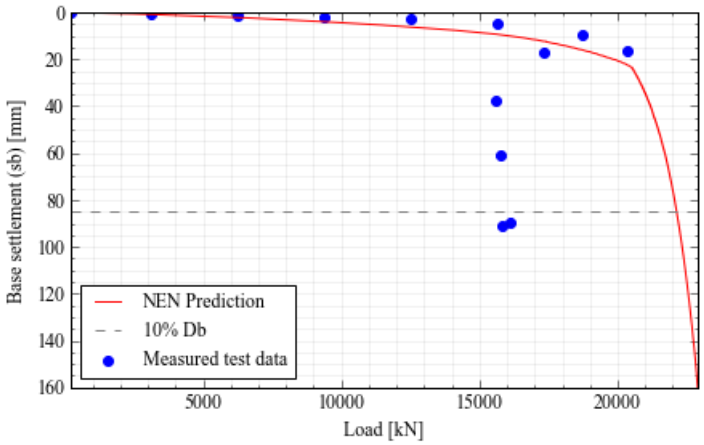

Figure 3.4: Example of finalised load-settlement prediction (red line), plotted with measured test data (blue dots).

An important note is that this thesis presents the load-settlement graphs in terms of base settlement s_b, rather than pile head settlement s_0. The NEN prediction method produces results in terms of s_b, and then backcalculates the head settlement s_0 through a simplified calculation using the stiffness of the pile. That introduces a significant uncertainty to the calculated s_0 values. The considered pile test data provides s_b measurements which can be considered more reliable than the NEN method of backcalculating s_0. The tests at Maasvlakte 2 and Beemster have provided load response graphs in terms of s_b, through strain data recordings and stiffness measurements. Although the raw strain data has not been published, the tests at Limelette and Sonate have also presented the load-settlement results in terms of s_b, through the strain gauges installed in the piles. The pile load test at Rosmalen has been able to calculate base settlement for pile 3, due to a separate load measurement and stiffness measurement of the tube directly connected to the pile tip.
For continuity in the thesis, the load-settlements graphs for the other piles at Rosmalen is also presented in s_b. It is argued that the choice to present all load-settlement graphs in this thesis in terms of s_b rather than s_0 introduces the least amount of uncertainty to the results.

3.7 Step 7: Evaluation and refinement of results

With the load-settlement response now drawn, it can be compared to the measured test data. In order to get the representation as close as possible, the factors α_p and α_s might be slightly changed to see how this affects the final result.
Additionally, in to investigate the influence of multiple variables, such as the difference between load-settlement curve 1 and 2, or the effect of q_c limiting, runs are made with these settings and then

compared to one another.

This will allow for a thorough investigation of the influence of these parameters, with the aim of recommending α_p and α_s factors, and finding how the load-settlement behaviour of screw and screw-injection piles is best represented.

Chapter 4

Results pile test database analysis

This chapter presents the results and analysis of the pile load tests selected in the database. Each pile test is discussed in a separate section. A section is subdivided in the following parts: a short introduction, an overview of the test, notes on the test, pile factor determination, results and analysis, and a conclusion. In the case of Maasvlakte 2, the laboratory test report is also included as a subsection.

4.1 Maasvlakte 2

The screw-injection pile tests at Maasvlakte 2 (Duffy et al. 2021) were performed at Amaliahaven in Rotterdam, in December 2019 and January 2020. These tests had two aims: to find project specific pile class factors, and to update the national pile class factors. Four screw-injection piles were installed employing grout injection during installation. Additionally, in- and outcoming samples of grout were taken in order to investigate transport of soil during installation. Out of the tests in the database, Maasvlakte 2 has the largest amount of data, with the highest level of detail and accuracy. Therefore, this data is considered to be the best available in the thesis.

4.1.1 Maasvlakte 2 - Overview

Ground investigation

The subsurface of the site can be described as follows; with depth in m relative to NAP (Duffy et al. 2021):

- +4 m to -15 m: moderately dense to dense sand, with pockets of clay and very silty sand.
- -15 m to -23 m: interlaminated and/or mixture of sand and clayey silty sand.
- -23 m to -24 m: 1 m bed of stiff clay
- -24 m to -38 m: dense to extremely dense sand.
- < -38 m: loose to moderately dense clayey sand.

The CPT data at the site, together with a schematic overview of the soil layers, is illustrated in Figure 4.1.

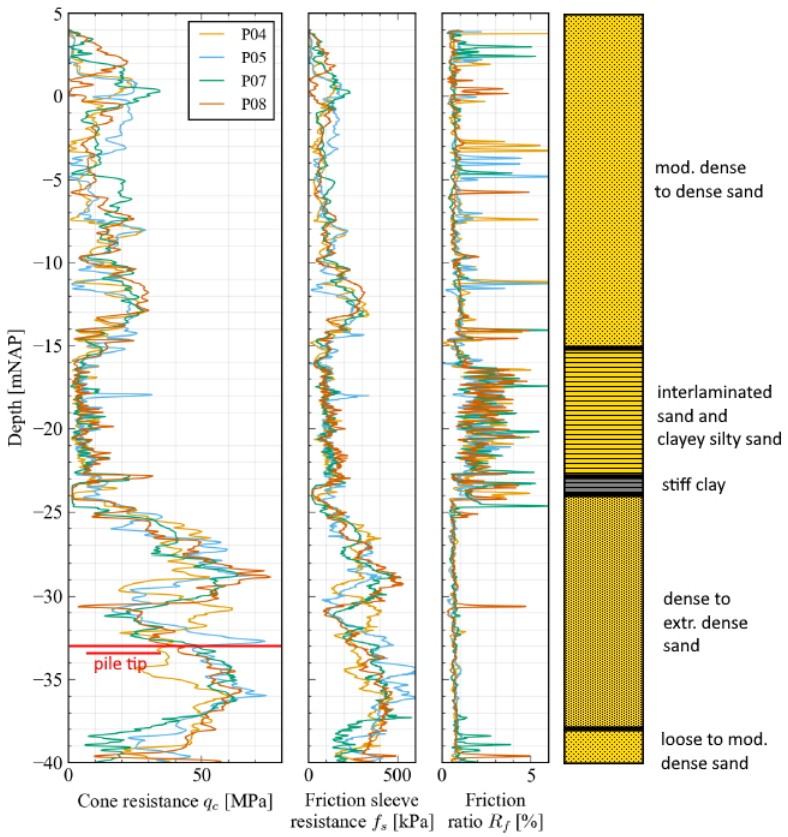

Figure 4.1: CPT data and soil classification for Maasvlakte 2, edited from Duffy et al. (2021).

Pile specifications

Four piles were installed, named P04, P05, P07 and P08. Geometry and relevant information is provided in Table 4.1. An image and schematic drawing are shown in Figure 4.2.

All four piles are screw-injection piles. These were provided by Terracon Funderingstechniek B.V. and named in-house as the 'Terr-Econ' pile system, classified in this thesis as Type 3 (screw pile with permanent steel casing). The piles are composed of S355 steel, with a wall thickness of 24 mm, outer shaft diameter of 0.61 m and base diameter of 0.85 m. The flow of grout is enabled through a steel conduit with diameter 48.3 mm along the piles' central axes, ejected horizontally outwards through three outlets at the pile tip. Two steel reservation tubes were placed along the length of the pile to insert the fibre optics cables after pile installation.

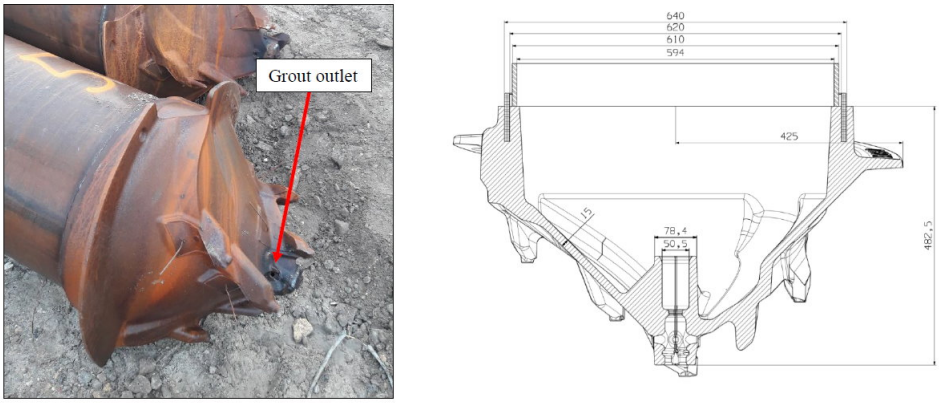

Figure 4.2: Picture and schematic drawing of pile tip and dimensions (Duffy et al. 2021).

	P04	P05	P07	P08
Pile length [m]	37.02	37.06	34.98	34.06
Pile head level [mNAP]	4.00	4.00	4.00	4.00
Pile toe level [mNAP]	-33.02	-33.06	-30.98	-30.06
Target pile toe level	-33.00	-33.00	-31.00	-30.00
Pleistocene sand depth [mNAP]	-24.15	-24.15	-24.70	-24.20
Inner diameter – steel tube[m]	0.594			
Outer diameter – steel tube [m]	0.610			
Maximum diameter – screw tip [m]	0.850			
$q_{c,avg,report}$ **[MPa]***	35.64	31.79	22.10	17.30
$q_{c,avg,Thesis}$ **[MPa]***	24.78	36.44	16.76	11.79
Installation date	28/10/19	24/10/19	29/10/19	28/10/19
Installation duration [mins]	81	110	97	71
Grout consumed [m^3]	13.94†	15.76	18.08	12.01
Concrete consumed [m^3]‡	10.26	10.27	9.69	9.44
Testing date [DD/MM/YY]	10/12/19	12/12/19§	16/01/20	17/12/20
Anchor test [DD/MM/YY]	-	11/12/19	15/01/20	16/12/20
No. days between installation and testing	43	49	78	50

Table 4.1: Overview of specifications, edited from Duffy et al. (2021).

The piles were installed with a Woltman HDPR 900 drilling rig, with an IHC PD45 rotary head providing torque to the pile. The software used to provide drilling-related measurements was provided by Tomer Systems B.V..

The steel auxiliary tubes were installed using a combination of pulldown forces and screwing, during which a grout mix was ejected though the three holes at the pile tip. The type of grout used is Beamix GM41 with strength class > 20 N/mm^2 and a water-cement ratio of 2.0. No upward lifting was performed during installation, with rotations both left and right depending on the difficulty of penetration. The grout injection rate was limited to 200 L/min. After the pile tip reached target depth and performed an additional half revolution, grout injection was halted.

After installation of pile P05, erroneous measurements were observed from approximately -25 m NAP. These were resolved before installing subsequent piles after a software bug was fixed. Time-independent parameters have not been affected by the bug.

After installation of the pile, the grout injection conduit was cut off to the desired height. To enable the installation of the fibre optics, two recesses of 5 cm were cut out of the pile. After the placing of the sensors, the pile was filled with concrete of class C35/45, XC2, F4, CEM III/B 42.5 with particle size 4-16 mm. The pile cap was placed directly on top of the steel tube, after which steel fibre reinforced mortar of type BASF MasterEmaco T 1400 FR was poured through two inlets in the pile cap to ensure a full development of the pile cap and head interface.

Pile testing

The **test frame** used is a reaction frame, known as a 'spider's head', tied in by twelve grout anchors, six hydraulic jacks, six load cells, a transition piece and a pile cap.

Each hydraulic jack had a capacity of around 5000 kN, controlled automatically by a programmable logic controller at the hydraulic unit (capacity 700 bar). The oil pressure was measured throughout the test to verify the load cell readings although no records were kept. On top of each load cell was a calibrated load cell (dynanometer) with an accuracy of ± 1 kN.

The displacement of the pile head was measured using four linear variable differential transformers (LVDTs) with an accuracy of ± 0.01 mm. These were placed at four diametrically opposing ends of the pile. The displacement was measured relative to a reference frame. Cross-checking pile head settlements and inclination/elevation of the reference frame and grout anchors was performed using a total station and surveying prisms.

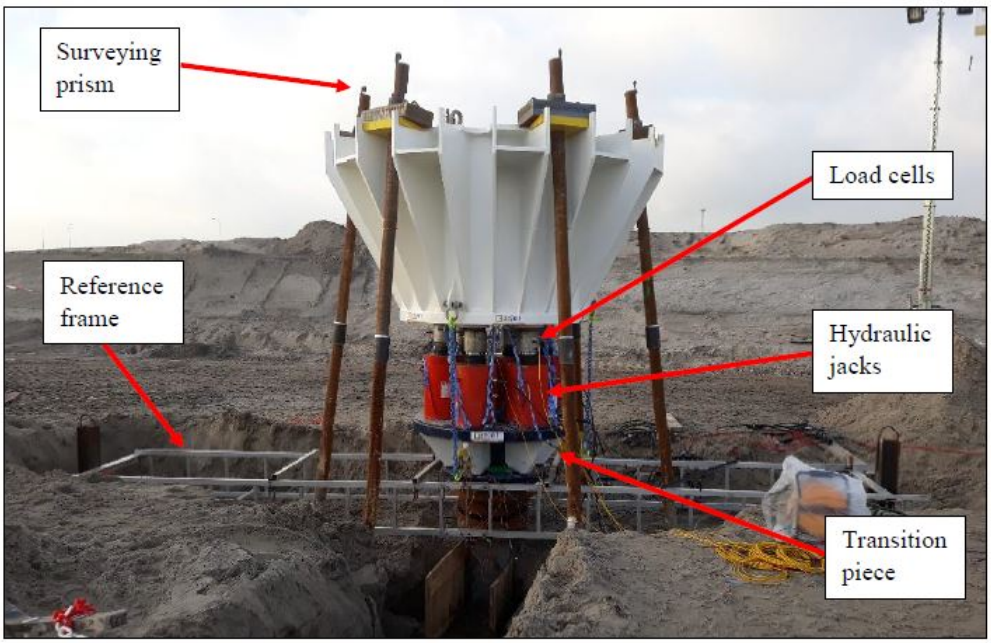

Figure 4.3: Reaction frame and reference frame (Duffy et al. 2021)

The **reaction force** for the pile tests was provided by a ring of twelve symmetrically place grout anchors attached to the reaction frame. Each anchor was at an angle of 8° from vertical, with a grout body design length of 9.5 m and a total anchor length of 40 m. The design of the anchors was realised

by MariTeam. The anchors were positioned in such a way that the grout body of each anchor was at least 5 m from the pile shaft. The installation of the anchors was carried out by High 5 Solutions using self-boring displacement screw-injection anchors in accordance with CUR166.

The **pile loading scheme** was carried out as described in NPR7201 (NPR 2017), but with the omission of the unload/reload cycles following each load step. However, due to difficulties with achieving the required capacity in the test frame, several unload/reload cycles were performed throughout the latter part of the pile tests. The load scheme and the unload/reload cycles for pile P04 are depicted in Figure 4.4.

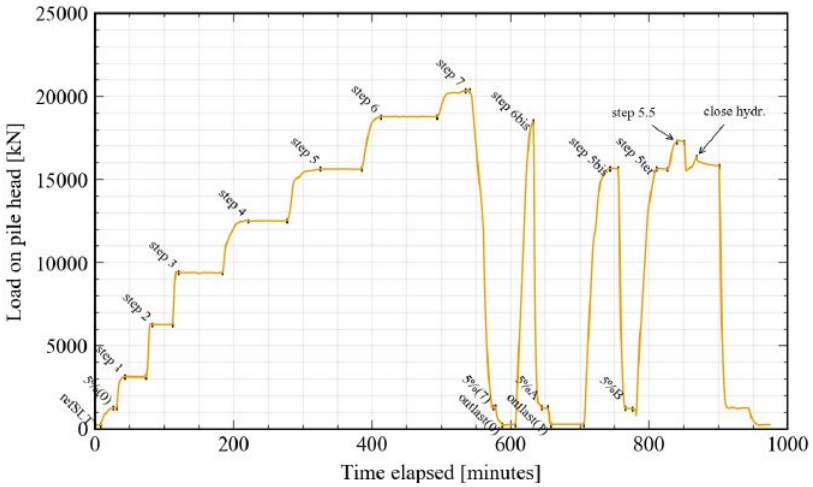

Figure 4.4: Load against time graph for P04 (Duffy et al. 2021).

Pile instrumentation

All piles were instrumented across their length using two fibre optic measurement systems. The two methods used are Fibre Bragg Grating (FBG) and Brillouin Optical Frequency Domain Analysis (BOFDA). These techniques are described in more detail in Section 2.4.5. The strain data measurements enable the calculation of force distributions throughout the piles, which allow for the determination of α_s and α_p factors.

The FBG logger was the Micron Optics SM125 and the fibre type used was FBGS SMW-01, which is a glass fibre reinforced polymer (GFRP) fibre. The system provided strain readings every 10 s, from gratings placed along the length of the pile. Each pile had two fibres at diametrically opposing sides of the tube.

The BOFDA logger was the fibrisTerre 2505 with the sensing cable Solifos BRUsens DSS v9. This had a measuring frequency of 4 minutes. The fibre is encased in a metal tube in order to increase the robustness of the cable. Each pile had two BOFDA lines, arranged in a loop with one in each reservation tube alongside the FBG cables, shown in Figure 4.5.

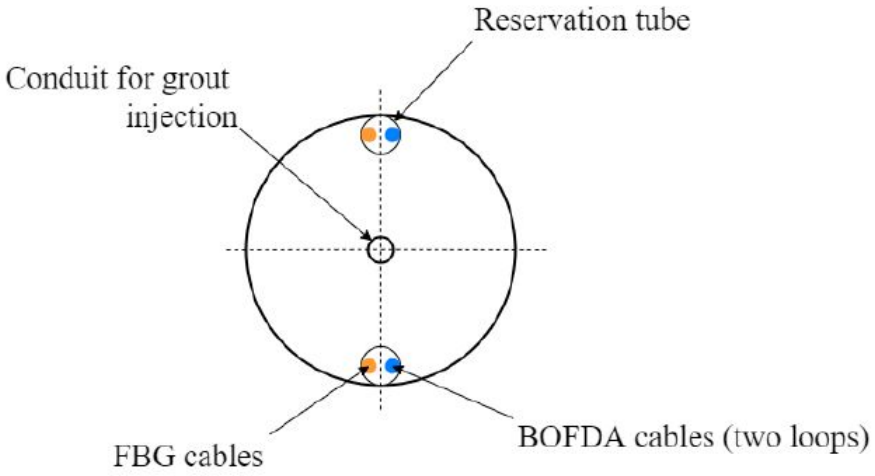

Figure 4.5: Configuration of fibre optic sensors in the pile (Duffy et al. 2021).

After the installation of the fibres in the reservation tube, grout was poured in the tube, while the ends of the cables were placed in a protective box attached to the pile. No prestressing of the fibres was carried out. All cables within the same measurement type were spliced together before their connection to a data logger. No temperature correction was applied to the readings as it was assumed that the temperature remained relatively constant over the course of the pile test.

In addition to the load test, samples were taken of both the incoming and outcoming grout. The aim of this extra analysis was to investigate the transport of soil out of the borehole during installation of SI piles. The volume and mass for each incoming and outcoming grout sample was recorded. Thereafter, the approximate sand content could be calculated in the outcoming grout. Sand content between 30 and 40% was found in the outcoming samples.

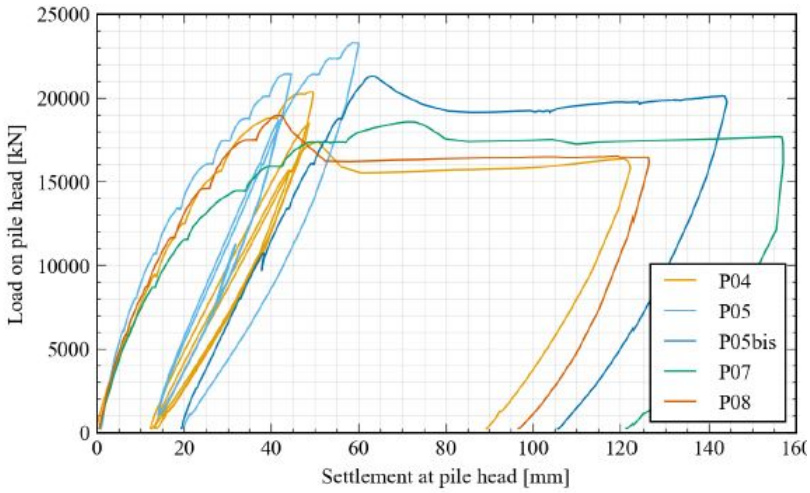

Figure 4.6: Load versus pile head settlement (Duffy et al. 2021).

4.1.2 Maasvlakte 2 - Test notes

- Pile P04 went out of horizontal during load step 7. This required unloading to 0, where it was found that two grout anchors had failed. Two more anchors were removed to maintain symmetry. Thereafter, two more unload/reload cycles were performed.
- Pile P05 underwent six cyclical loads up to 4000 kN to test the grout anchors. Failure in one

caused a second one to be removed. Two unload/reload cycles were performed to reduce shaft friction in the upper part of the pile. As the pile did not reach geotechnical failure, a second test on the pile was carried out.

- Pile P07 also underwent six cyclical loads to test the grout anchors, with none failing. The strain readings for this pile are stated to lack credibility, caused by scattered readings and a deviation in the sand layer when compared to the other piles.
- Pile P08 was also cyclically loaded to test the grout anchors, with none failing. Failure occurred during load step 7 without any unload/reload cycles being taken.
- A sudden loss in capacity (strain softening) was seen during loading for all piles. This is apparent in Figure 4.6.
- Outcoming grout samples during installation revealed a sand content of 30-40%, compared to 0% for the incoming samples.

4.1.3 Maasvlakte 2 - Pile factor determination

The variables used for predicting pile capacities have been extensively described in the report by Duffy et al. (2021). These values are supported by detailed strain readings and form the base for the further analysis in this section. Note that the factors are determined without any q_c limiting, as this would severely underestimate the capacity in the lower sand layers, which regularly exceed q_c values of 50 MPa. This is discussed in more detail in the following subsection (see Figure 4.7).

α_s **clay** The value of α_s for the clay layer is simply taken from NEN 9997-1, which is 0.03. Due to its shallow thickness, this layer does not have a significant influence on the shaft friction. Therefore, no extra investigation in this factor has been performed.

α_s **sand** Strain data readings during the Maasvlakte 2 tests indicated an average peak α_s of 0.011. However, due to the aforementioned strain softening, this value is not regarded as safe in the report by Duffy et al. (2021), and a value of 0.010 is proposed instead. Though, as this thesis focuses on the geotechnical rather than the structural properties of the pile, the measured α_s of 0.011 is used.

α_p At large settlements of around $20\%D_b$, strain data analysis showed an average peak α_p of 0.35. This value of 0.35 is used for the analysis in the following subsection. It is noted by Duffy et al. (2021) that this value is too high when predicting capacity at lower settlements, recommending an α_p of 0.30 for settlements at $10\%D_b$.

4.1.4 Maasvlakte 2 - Analysis and results

In the analysis and recommendations by Duffy et al. (2021), different mobilisation curves (compared to NEN9997-1) are suggested. It must be noted that the analysis in this thesis does not use the curves proposed by the report, but rather investigates the mobilisation curves as prescribed in NEN9997-1.

The report by used several CPTs around the pile to produce an average q_c profile. This thesis only uses a CPT profile at the centre of each pile. Therefore, the calculated $q_{c,avg}$ differs between the report and this thesis. Table 4.1 lists these values.

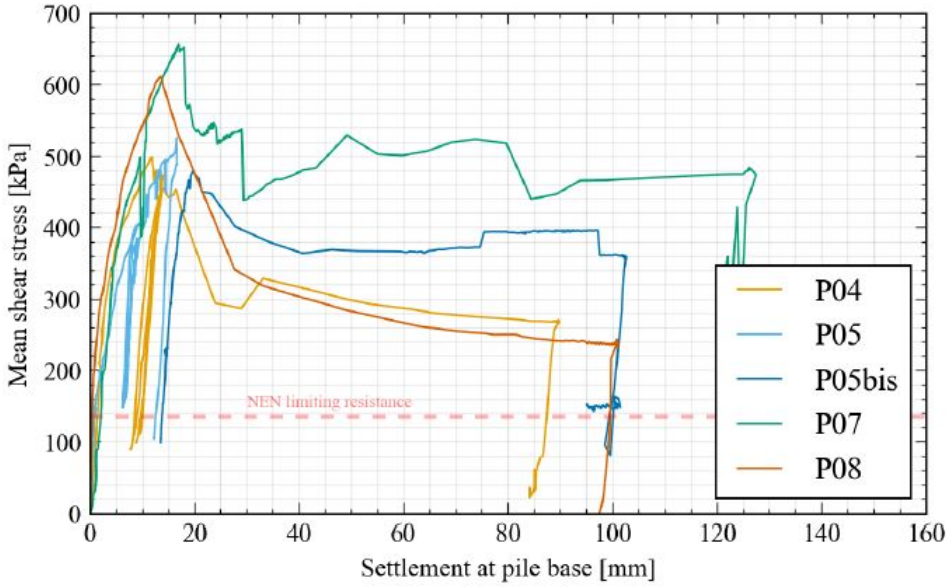

Figure 4.7: Mean shear stress against base settlement, with NEN limiting resistance $\alpha_s \times 15$ MPa shown (Duffy et al. 2021).

As described previously, in order to accurately depict the pile capacity, no q_c limiting for the shaft friction was performed at Maasvlakte 2. Figure 4.7 clearly illustrates that the piles exhibit a mean shear stress much higher than would be allowed by limiting q_c values to maximum of 15 MPa, as prescribed by NEN9997-1.

Regarding the limiting of maximum base resistance q_b, the limit of 15 MPa is only reached with an α_p factor above 0.41 for pile P05, which has the highest $q_{c,avg}$ value. As an α_p of 0.41 is higher than the peak value of 0.35 determined in the report by Duffy et al. (2021), the NEN9997-1 practice of limiting q_b to 15 MPa has no effect on these piles, with the stated values of α_p.

In order to investigate the effect of different load-settlement curves, q_c limiting and the currently prescribed α factors, a comparison is presented in Figure 4.8. Unless otherwise stated, the predictions have been made using an α_p of 0.35, α_s in sand of 0.011, α_s in clay of 0.03, and no q_c limiting. All graphs are based on data of pile P08. Because of the sudden loss in capacity due to strain softening, the comparison focuses on the data points before this occurs.

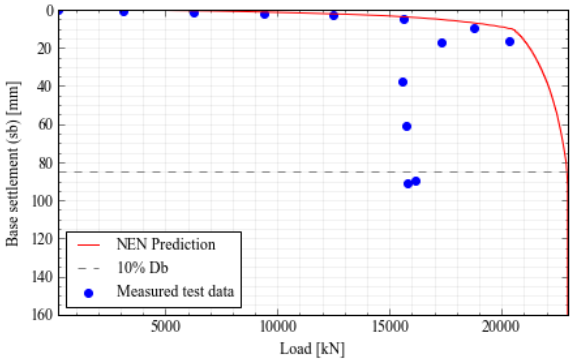

(a) Load-settlement curve 1.

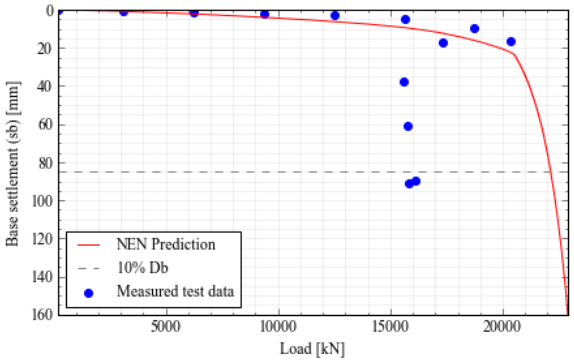

(b) Load-settlement curve 2.

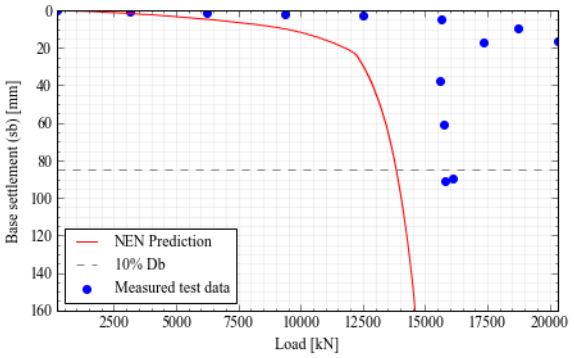

(c) Load-settlement curve 2, with q_c limiting.

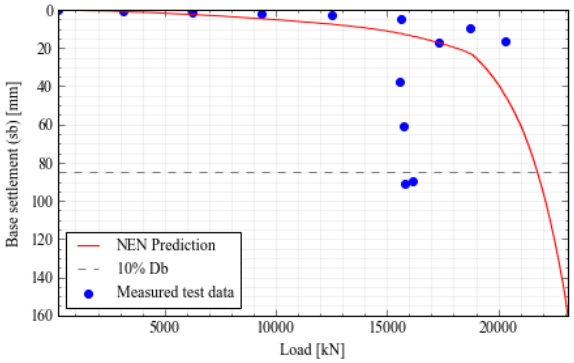

(d) Curve 2 with NEN $\alpha_p = 0.63$ and $\alpha_s = 0.009$.

Figure 4.8: Presentation of different load-settlement curves, effect of limiting q_c, and NEN9997-1 prescribed α_p and α_s. Based on data from pile P04.

The first figure (4.8a) shows the prediction with load-settlement curve 1. Compared to the measured data points, the mobilisation at lower settlements is noticeably stiffer.

Figure 4.8b presents load-settlement curve 2. Compared to curve 1, the predicted mobilisation follows the data points significantly better.

Figure 4.8c indicates the effect of limiting q_c along the shaft to a maximum of 15 MPa, as per NEN9997-1. However, it is clear to see that this severely underestimates the pile capacity. This is to be expected when the lower part of the pile is founded in sand with q_c values almost four times that of 15.

The currently prescribed α_p of 0.63 and α_s in sand of 0.009 are applied in Figure 4.8d. Due to the length of the piles, the reduction of shaft friction is more than the gain in base resistance. These values do not accurately predict the load-settlement behaviour of the pile.

Based on these findings, it is argued that load-settlement curve 2 with no q_c limiting along the shaft is the best representation of the true pile response. Figure 4.9a to d shows the load-settlement predictions for all four piles with these variables. With the α factors proposed by Duffy et al. (2021), the initial behaviour of the piles is predicted well, with the exception of pile P07. The following findings are noted:

- The sudden strain-softening behaviour seen in the piles (Figure 4.6) requires more investigation, and is the motivation for the laboratory test described in Section 4.1.5.
- The mobilisation of the piles is incorrectly predicted after strain softening occurs.

- Load-settlement curve 2, without limiting q_c values, provides the most realistic prediction.
- An α_p of 0.35 and α_s in sand of 0.011 are appropriate to predict the initial pile response.
- The comparison in sand content between in- and outgoing grout samples support the claim that these piles are not fully soil displacing piles, with sand content reaching 30-40% in the outcoming samples.
- It is argued that the use of load-settlement curve 2 and no q_c limiting is correct for these piles. These options highlight the less stiff shaft and base mobilisation of the screw-injection piles, which resembles behaviour found on (partly) soil replacing piles.

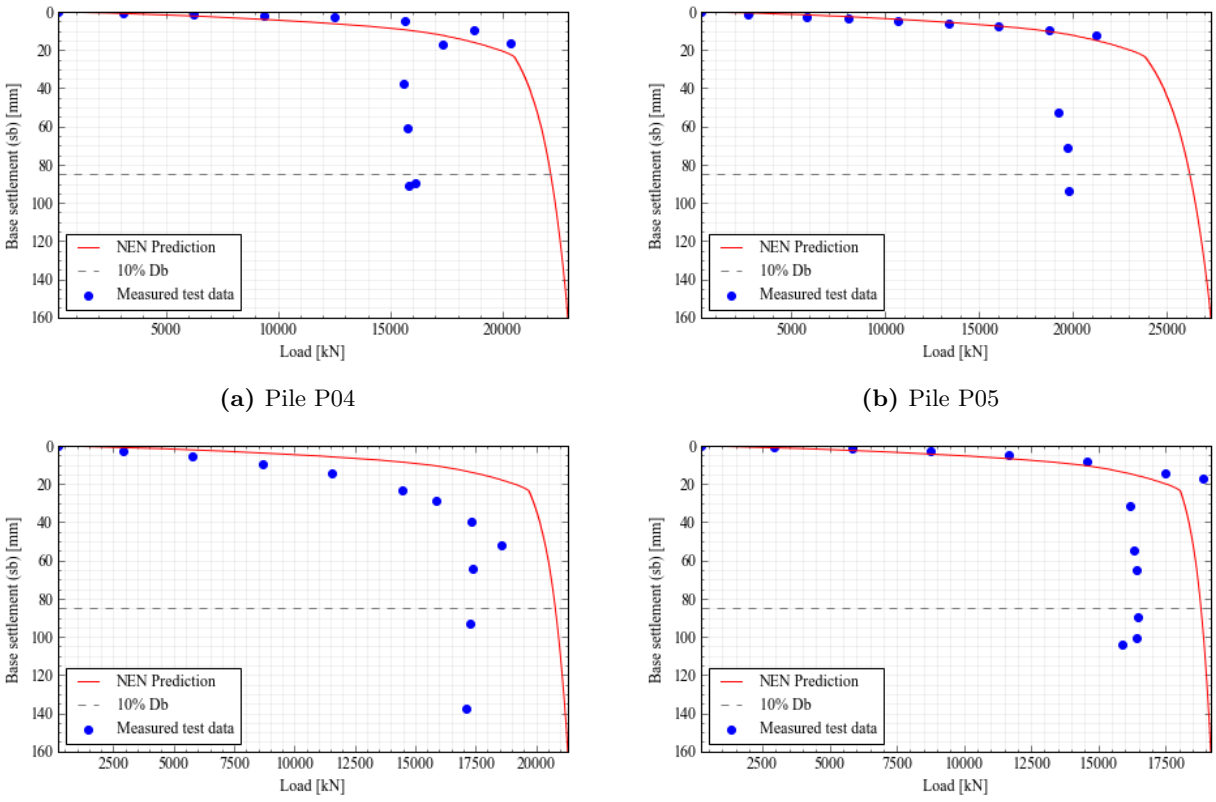

(a) Pile P04 **(b)** Pile P05

(c) Pile P07 **(d)** Pile P08

Figure 4.9: Load settlement predictions for Maasvlakte 2 piles using load-settlement curve 2, with α_p 0.35 , α_s in sand 0.013, α_s in clay 0.03.

4.1.5 Maasvlakte 2 - Grout debonding laboratory experiment

Strain-softening at Maasvlakte 2

During the load testing of the piles at Maasvlakte 2, it was observed that in all piles there was significant softening after reaching a peak shear stress of around 650 kPa. This behaviour can be seen in Figures 4.10a and 4.10b.

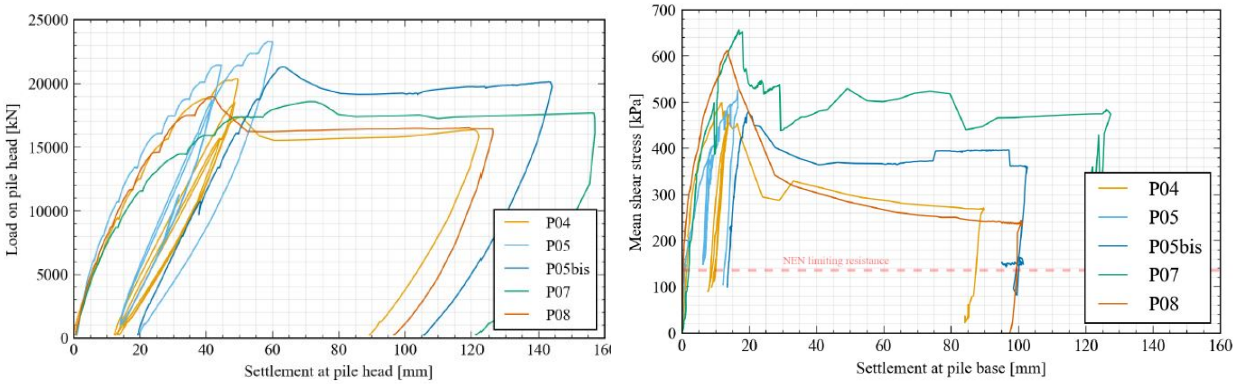

(a) Load versus pile head settlement (Duffy et al. 2021)

(b) Mean shear stress against base settlement, with NEN limiting resistance $\alpha_s \times 15$ MPa shown (Duffy et al. 2021).

Figure 4.10

This sudden loss of strength of the pile was not attributed to softening of the soil, but rather it was suggested that structural failure occurred along the steel-grout interface, due to the influence of the high normal forces ($\pm$ 1400 kPa) acting on the grout. An example of how the shear strength may behave between the grout and steel is shown in Figure 4.11, together with a visual clarification of the circumstances in situ. The shear strength is a combination of adhesive forces and frictional forces between the steel and grout. Just before failure, the peak shear strength is reached. After failure, this quickly reduces asymptotically towards a residual stress level.

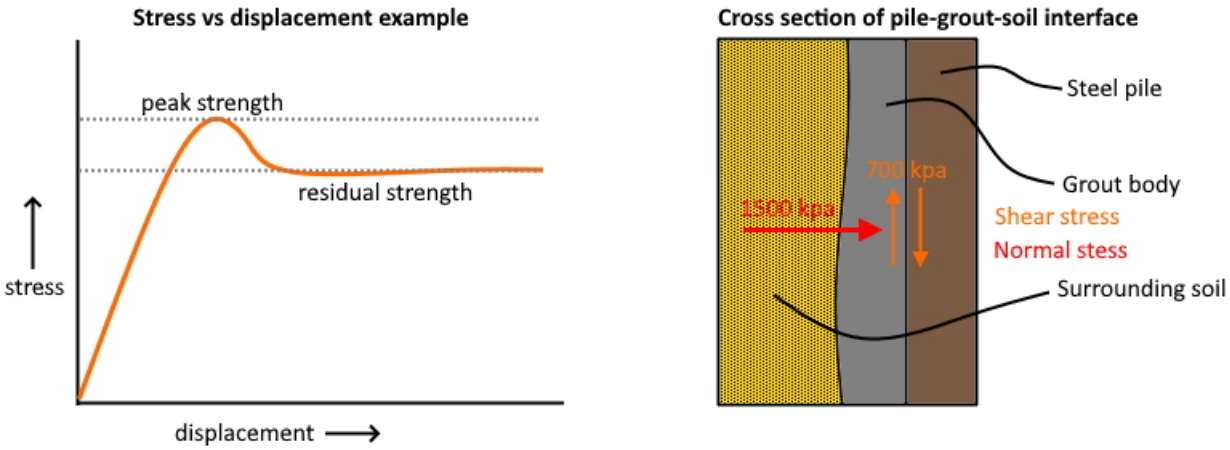

Figure 4.11: Left: schematic example of stress versus displacement along steel-grout interface; Right: schematic cross subsubsection of situation underground

In order to investigate the behaviour of the interface between steel and grout, a test using the shear box is proposed. The test aims to reproduce the circumstances similar to those found during the Maasvlakte 2 load tests.

Principle of shear box test

The shear box machine used during lab testing is shown in Figure 4.12. A cross section of the sample holder is shown in Figure 4.13. The main focus of the shear box test is to exert a force along the horizontal plane, in this case the boundary between the steel and grout. This is made possible by splitting the sample holder in two parts: the upper half which cannot move, and the bottom half, which is displaced by the shear machine. This creates a horizontal shear force along the centre of the sample holder, indicated by the two orange arrows in Figure 4.13. This shear force is provided by the machine using a hydraulic system.

A vertical normal stress is applied to the sample using weights on a lever arm. This is to simulate the forces experienced by the sample in situ. The normal stress is provided by weights on a lever arm, whereby the arm provides x10 leverage. The forces from the lever arm are distributed evenly on top of the sample using a steel cap.

A force meter records the increasing shear forces on the sample. When the sample starts to deform, LVDTs measure the horizontal and vertical displacements. The vertical displacements are measured because these provide insight on whether compaction or dilation has occurred. In summary, the shear box test captures the following data:

- Shear stress (horizontal) along steel-grout interface.
- Normal stress (vertical) exerted by lever arm over area of sample.
- Force and displacement readings from force gauge and LVDTs.

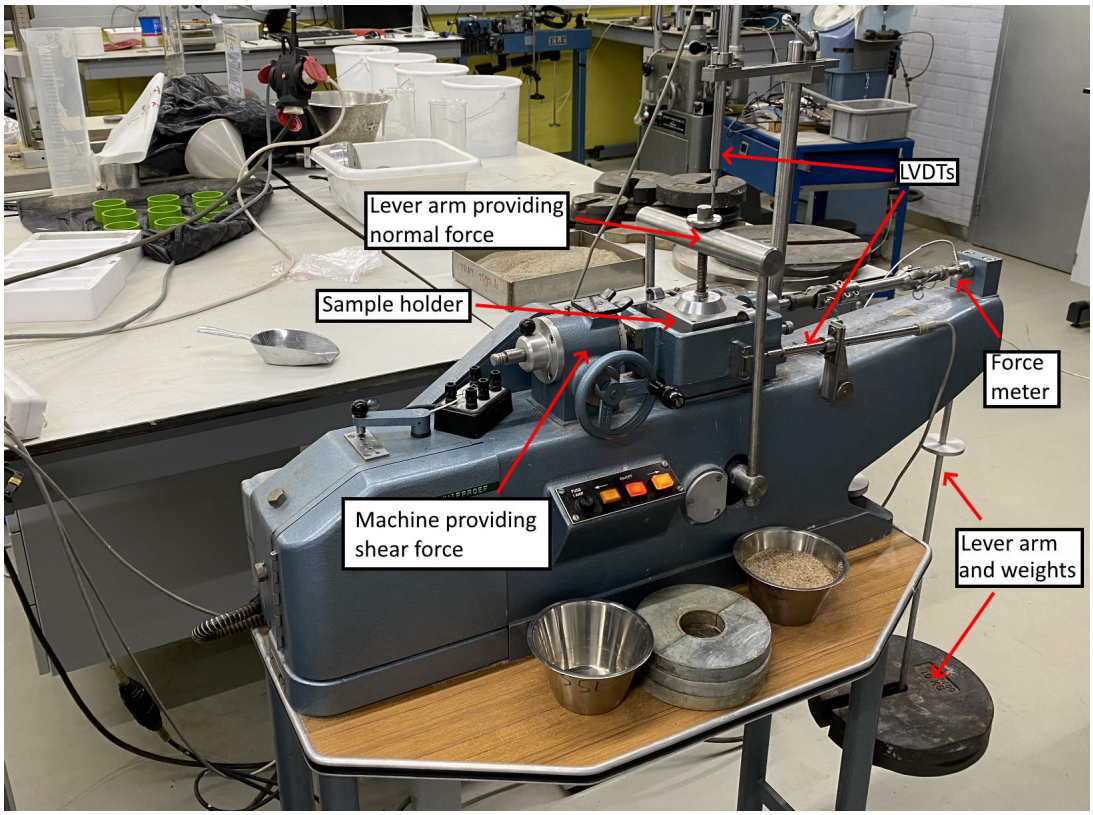

Figure 4.12: Shear box machine as used in tests.

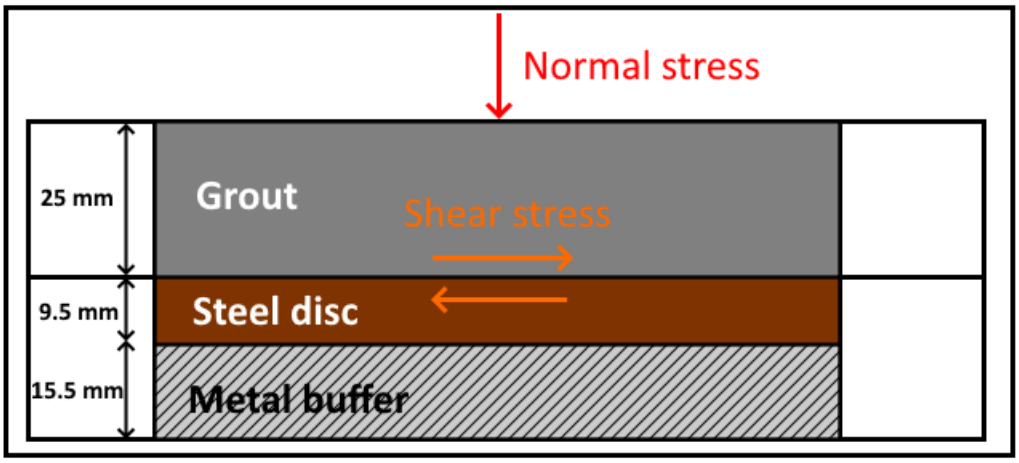

Figure 4.13: Sample in holder for shear box test.

Test Samples

The focus on the lab test is on the adhesive force of the steel/grout interface. Several properties of the steel and grout are varied to investigate the influence on the adhesive force. The water-cement factor (WCF) of the grout is thought to have a significant effect, with lower WCF values (more cement) expected to provide a more adhesion. Additionally, the presence of sand may influence the resistance of the steel/grout interface. To investigate these theories, four grout mixes were made, with differing water-cement ratios (WCF) and one with a sand content of 30%. The cement used to create the grout mixes is 'Bruil Groutmortel GPM350', specifically designed for use with screw-injection and anchor piles. The grout has a noted tensile strength of ≤ 5 N/mm^2 and a compressive strength of ≤ 35 N/mm^2.

The roughness of the steel is also thought to have a significant influence. A rougher area will increase frictional resistance, but most importantly provides a larger surface area for the grout to bind to, thus increasing the adhesive strength. Two grades of steel coarseness, described Rough (> 32 µm) and Smooth (< 4 µm) are tested and evaluated.

The samples consist of steel discs with diameter 58.5 mm and thickness 9.5 mm, bonded to differing grout mixes with a similar diameter but varying thickness (± 22 mm). The smaller diameter of the steel discs was caused by manufacturing limitations, but is within tolerance and should only influence the calculations for converting force to stress. The difference in grout thickness is due to particle settlement in the grout mixes with high WCF values. However, this too does not pose a problem as the surface area on which the normal force acts is the same for all samples; and so is the steel/grout interface on which the shear forces are exerted.

Sample ID	Steel surface	WCF	Sand volume
1R-A	Rough	1	-
1R-B (broken)	Rough	1	-
1S	Smooth	1	-
2R	Rough	1.5	-
2S	Smooth	1.5	-
3R-A (broken)	Rough	2	-
3R-B	Rough	2	-
4R	Rough	1 (1.25)	30%
4S	Smooth	1 (1.25)	30%

Table 4.2: Overview of test samples (values in brackets denote WCF without inclusion of sand volume)

The first number in the Sample ID (1,2,3 or 4) indicates the grout mix. The second letter, R or S, indicates whether the steel disc is Rough (> 32 µm) or Smooth (< 4 µm). The final letter, A or B is to distinguish between to identical samples.

The four different grout mixes were carefully mixed in the laboratory, with the volume of each ingredient measured accurately using a beaker and weighed precisely with an electronic scale. Each sample was then poured in a correspondingly marked mould, as shown in Figure 4.14a. The samples were allowed to cure submerged in water after a day, for a total of 12 days (Figure 4.14b).

(a) Grout samples immediately after pouring.

(b) Grout samples, curing submerged in water for 12 days.

Figure 4.14

The samples were retrieved from their mould after 12 days. Samples 1R-B and 3R-B broke after extraction of their mould. Therefore, tests on these samples have been omitted from this section. The remaining samples were all removed from their mould without incident. Notably, all samples had a lightly coloured, thin (<0.5 mm) and soft layer on top. This could easily be scratched by a fingernail. This was likely caused due to the grout being in contact with water immediately before extracting the samples.

Test Procedure

The hypothesis is that failure along the steel-grout interface occurs around the observed 650 kPa shear stress only when under a normal stress of around 1400 kPa. With lower normal stresses, the steel-grout interface is not expected to fail at a shear stress of 650 kPa.

Therefore, a 4-step loading procedure is suggested which allows for a consistent increase of normal stress ranging from around 912 to 1459 kPa. Table 4.3 shows the procedure.

Load step	1	2	3	4
Weights on arm [kg]	25	30	35	40
Force on sample [N]	2452.5	2943	3433.5	3924
Stress on sample [kPa]	912	1094	1276	1459

Table 4.3: Load step procedure

Starting at load step 1, the shear stress will be allowed to increase to 700 kPa. If failure has not occurred, the shear stress will be reduced after which the normal force on the sample will be increased by the amount described in load step 2. Load step 2 can now be performed by again increasing the shear stress to 700 kPa. This process repeats until failure, or until load step 4 is reached, where the shear stress will be increased past 700 kPa if needed to reach failure.

Results and analysis

Sample 1R-A Sample 1R-A was loaded in four steps, starting with 25kg at the lever arm, translating to a normal force of 912 kPa. The shear stress was then increased to above 700 kPa, to simulate the conditions present at Maasvlakte 2. If failure did not occur, the sample was unloaded slightly and more weight was added to the lever arm. This is shown in Figure 4.15b. The weight was increased to 30 kg around 500 s, to 35 kg at 600 s and finally to 40 kg at 700 s. In none of the load steps, failure occurred under 800 kPa. Figure 4.15a shows the almost non-existent influence of the load steps on the response, around a horizontal displacement of 3 mm. During the final step with 40 kg on the arm (normal force 1459 kPa) the sample was sheared to failure.

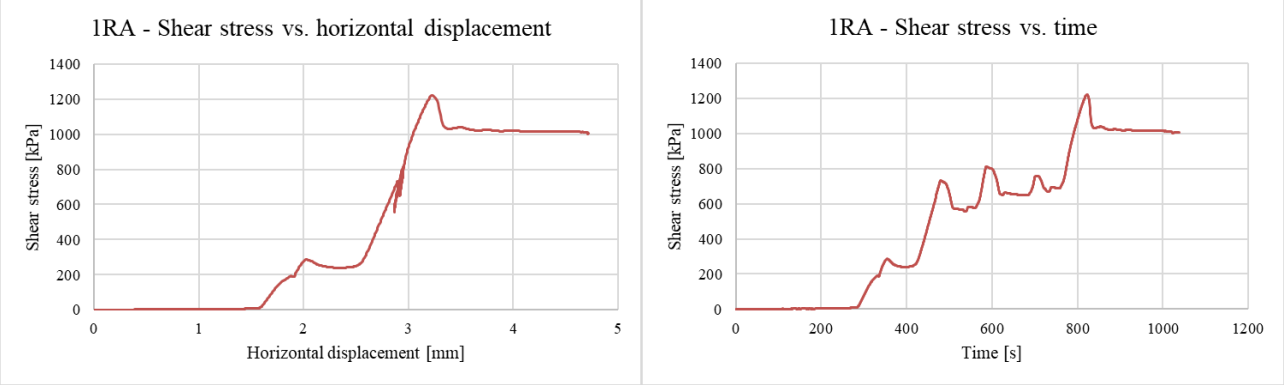

(a) Sample 1R-A. Shear stress against horizontal displacement.

(b) Sample 1R-A. Shear stress against time. The different load steps are clearly visible.

Figure 4.15

The reason for the initial bump visible in Figure 4.15a at 2 mm is uncertain, as no chipping occurred on the sample, proven by Figure 4.16a. This bump may be caused by the slack in the sample holder, due to the sample's 58.5 mm diameter instead of the originally intended 59.5 mm.

(a) Sample 1R-A after shear test.

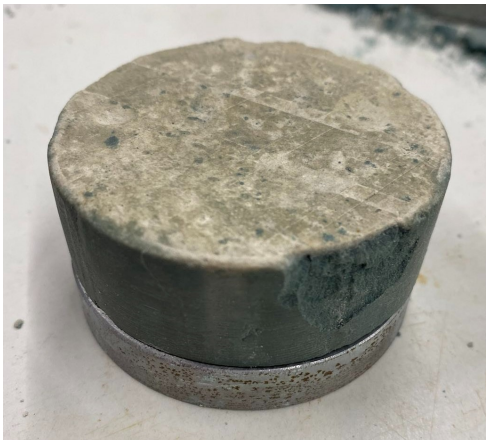

(b) Sample 1R-A after load test with 70 kg on lever arm.

Figure 4.16

Adhesive failure of sample 1R-A occurred at a shear stress of **1222 kPa** under a normal stress of **1459 kPa**.

After the shear test, due to the sample remaining intact, the influence of normal stress was investigated by placing the sample back in the box and increasing the mass on the lever arm to the maximum value of 70 kg. This translated into and exerted normal force on the sample of 2550 kPa. No shearing was performed. After unloading, the state of the sample is shown in Figure 4.16b. The only significant chipping is shown in the forefront, although a weakness in this area may have been caused by the shear test performed previously.

Sample 1S Sample 1S was the first sample to be tested with a smooth steel disc. In accordance with the proposed load scheme, the sample was loaded to around 700 kPa with 25 kg on the lever arm. However, failure occurred during the first load step at only 379 kPa. After this, it was decided to perform the load steps anyway, to gain some insight on the effect of normal force on the frictional resistance of the steel/grout interface. The recorded data is drawn in Figure 4.17a.

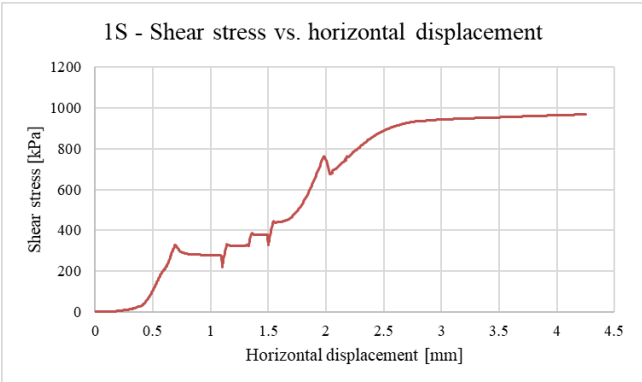

(a) Sample 1S. Shear stress against horizontal displacement.

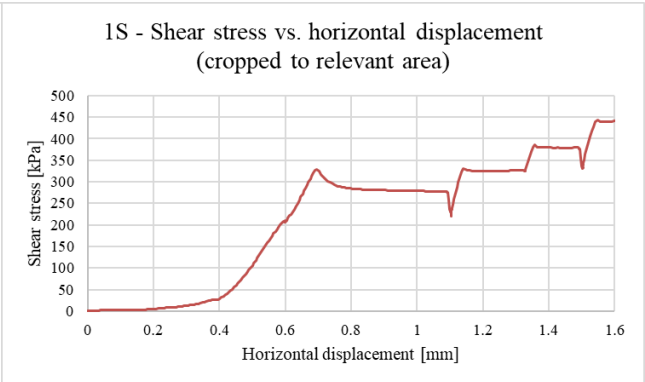

(b) Sample 1S. Shear stress against horizontal displacement, limited to the relevant part only.

Figure 4.17

After each increase of normal force, the sample presented an expected response: a swift increase to a higher shear stress and immediately settling at this new level. However, during the 40 kg load step, the sample suddenly gained an immense amount of shear resistance. When this reached a maximum of

close to 1000 kPa, the test was stopped in order to investigate what caused this unsuspected behaviour.

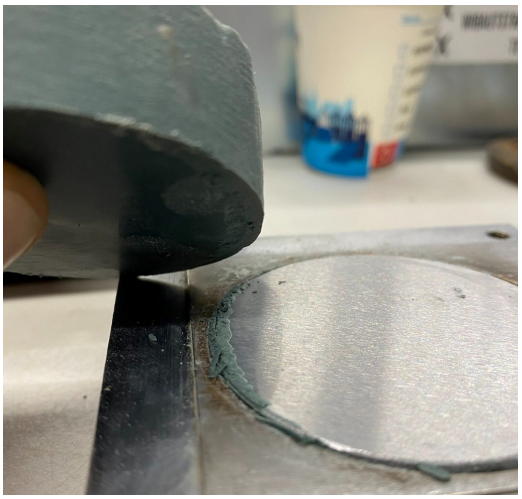

(a) Sample 1S after test. Note remaining grout of the edge of the steel plate, caused by the inclination.

(b) Sample 1S during test. The inclination of the sample is demonstrated by the uneven space along the top and bottom of the sample holder.

Figure 4.18

Figures 4.18a and 4.18b indicate the root cause of the problem: during the last load step, the sample started to incline. Therefore, instead of shearing the interface between the steel and grout, part of the grout itself was sheared. Shavings off the side of the sample and remaining grout on the steel disc, both shown in Figure 4.18a, support this claim. One will find that this problem affected several of the samples, though on none was it as clear-cut as on the last load step at sample 1S. Besides the sheared-off edge, no chipping occurred on this sample.

Adhesive failure of sample 1S occurred at a shear stress of **379 kPa** under a normal stress of **912 kPa**.

Sample 2R After the results of 1R-A and 1S, it was decided to only shear the samples with 40 kg on the lever arm. This would prevent (some) samples failing under a low normal force. It was thought that this ensured all samples could be directly compared to each other.

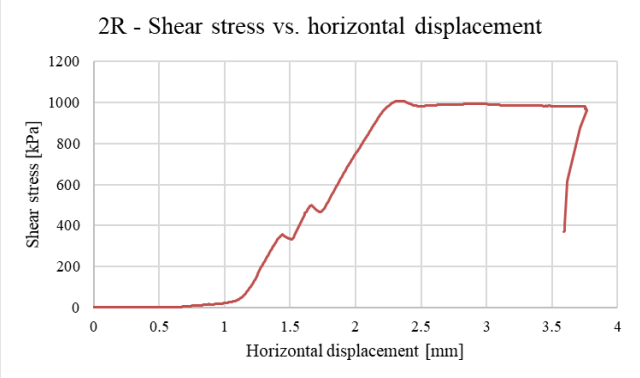

(a) Sample 2R. Shear stress against horizontal displacement.

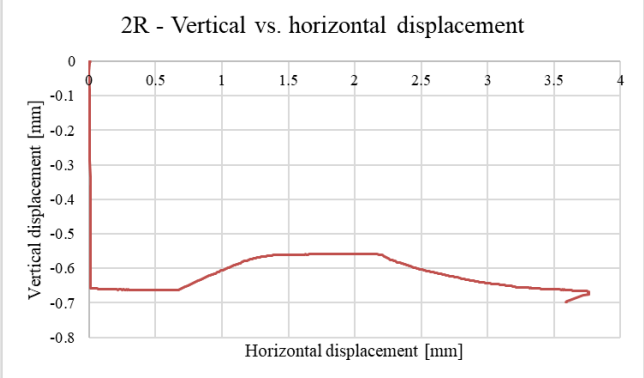

(b) Sample 2R. Vertical displacement against horizontal displacement.

Figure 4.19

Figure 4.19a shows two noticeable bumps in the response. Inspection of the sample after the test (Figure 4.20a) suggests this to be caused by chipping of the grout.

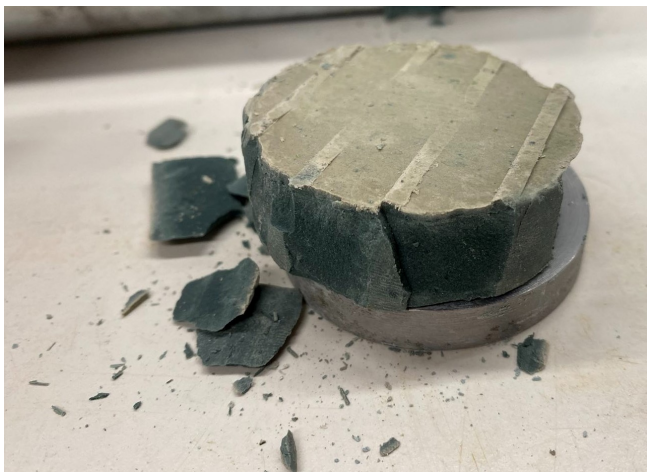

(a) Sample 2R after the test.

(b) Sample 2R after testing. Note the increased grout residue on one half of the steel disc, possible due to inclination of the sample.

Figure 4.20

Adhesive failure of sample 2R occurred at a shear stress of **1007 kPa** under a normal stress of **1459 kPa.**

Sample 2S Due to surprising behaviour of the measurement data, it was believed the sample had failed. However, after the sample was inspected it showed that the bond between the steel and grout was not yet broken. Though, significant amounts of grout had chipped off the sample, likely causing the unusual data shown in Figure 4.21a. The sample was then tested again. In order not to overwrite the original data, the retest was named 2Sbis. However, the sample itself remains 2S.

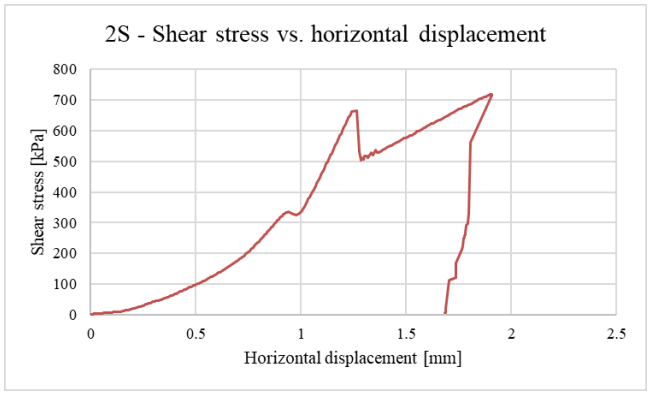

(a) Sample 2S. Shear stress against horizontal displacement.

(b) Sample 2S. Still bonded to the steel disc after the end of the initial test.

Figure 4.21

Figure 4.22a presents the measured data from the retest. As seen on sample 1S, there is an unexpected increase in shear strength after failure (at 500 kPa). This was caused by inclination of the sample, rendering the data after 1.5 mm of horizontal displacement useless. The result of the test, limited to the relevant part of the line only, is shown in Figure 4.22b. Chipping of the grout caused the bump in the line around 1.1 mm, as shown in Figure 4.23b. The reduced structural integrity of the grout due to a higher WCF is illustrated by the numerous fractures and chippings in the grout sample.

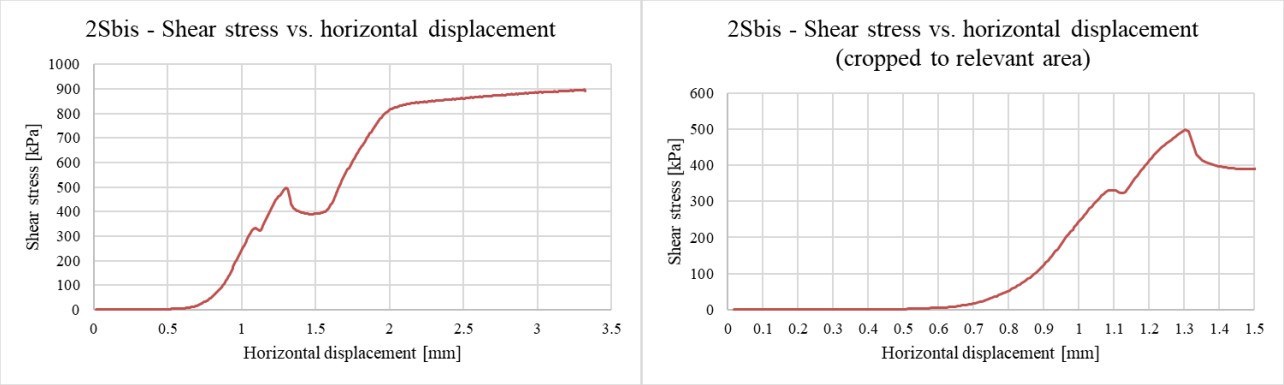

(a) Sample 2S. Shear stress against horizontal displacement.

(b) Sample 2S. Shear stress against horizontal displacement, limited to the relevant part only.

Figure 4.22

Adhesive failure of sample 2S occurred at a shear stress of **500 kPa** under a normal stress of **1459 kPa**.

(a) Sample 2S before test.

(b) Sample 2S after test.

Figure 4.23

Sample 3R-B The other identical sample, 3R-A, had broken during extraction from the mould. The second sample, 3R-B was successfully retrieved from the mould, although not completely unscathed (see Figure 4.25a). For an unknown reason, no vertical displacement was recorded during the test of 3R-B.

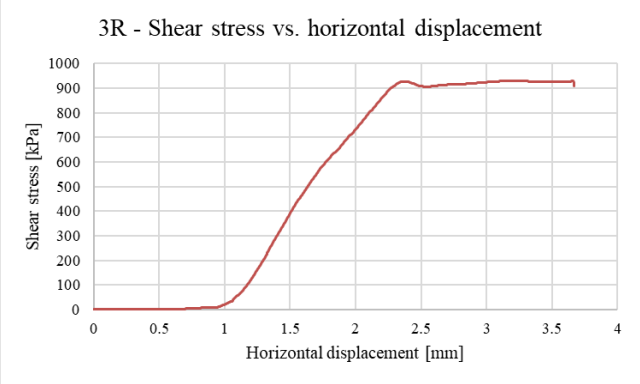

(a) Sample 3R-B. Shear stress against horizontal displacement.

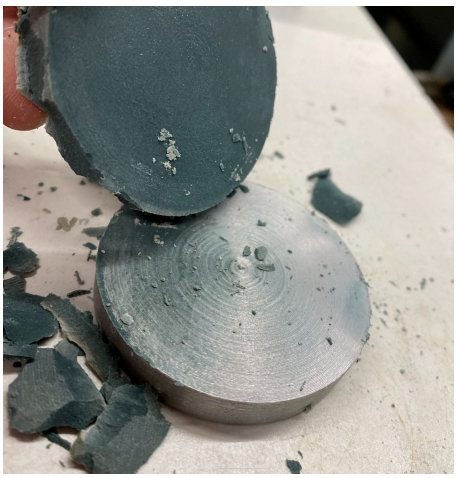

(b) Sample 3R-B. Shear stress against horizontal displacement, limited to the relevant part only.

Figure 4.24

Adhesive failure of sample 3R-B occurred at a shear stress of **927 kPa** under a normal stress of **1459 kPa**.

(a) Sample 3R before test.

(b) Sample 3R after test.

Figure 4.25

Sample 4R Sample 4R is the first of the two samples with a sand content of 30%. The two small bumps after 1 mm, shown in Figure 4.26a, seem to be caused by chipping of the grout. Although, Figure 4.26b shows that fracturing and chipping of the grout remains very limited.

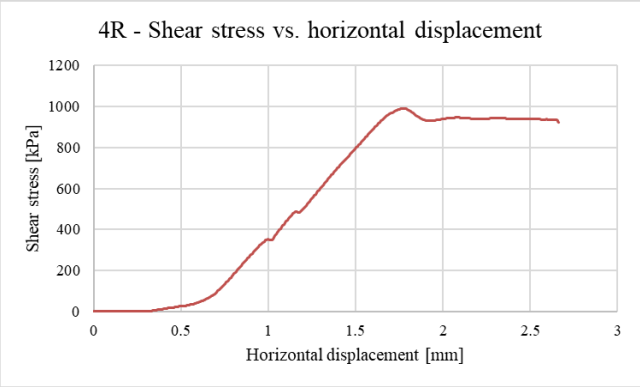

(a) Sample 4R. Shear stress against horizontal displacement.

(b) Sample 4R after test. Only a very small amount of fracturing and chipping is visible.

Figure 4.26

Adhesive failure of sample 4R occurred at a shear stress of **988 kPa** under a normal stress **1459 kPa**.

Sample 4S The final test was performed on sample 4S. The measurements shown in Figure 4.27a closely resemble those of samples 2S and 1S: after failure, the inclination of the sample caused the grout itself to be sheared, in addition to the steel/grout interface, sharply increasing the measured shear stress. The stress increases again in value after a horizontal displacement of 1.1 mm, after which the results are considered unreliable. Therefore, only the relevant part of the data is represented in Figure 4.27b.

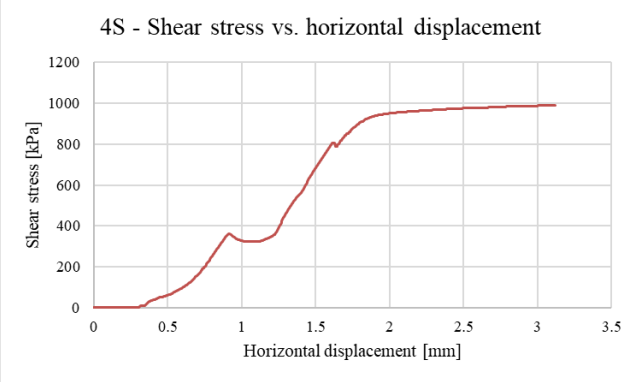

(a) Sample 4S. Shear stress against horizontal displacement.

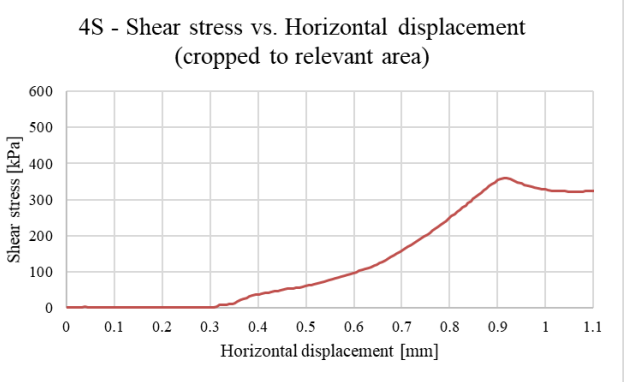

(b) Sample 4S. Shear stress against horizontal displacement, limited to the relevant part only.

Figure 4.27

The reduction of shear stress after reaching 360 kPa signifies adhesive failure. It could not possibly be explained by chipping of the grout, as the sample remained intact after the test, as shown by Figure 4.28a. Though, the left side of the grout is clearly shaven off, as was found in samples 2S and 1S. Figure 4.28b pictures the 'inclination problem': the sample holder has evidently deviated from the horizontal. However, as the focus on the tests lies on the adhesive failure, what happens afterwards is not of significant importance. Therefore, the results of the laboratory experiment are not affected by the inclination of samples.

(a) Sample 4S after test. Note the shaving and grout residue on the left side of the sample.

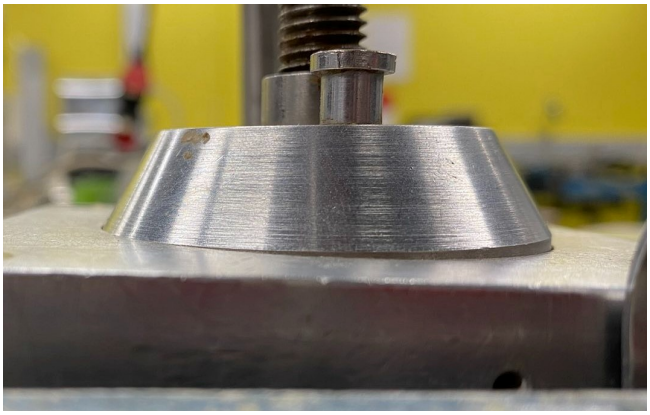

(b) Sample 4S during test. Inclination of the sample is clearly shown.

Figure 4.28

Adhesive failure of sample 4S occurred at a shear stress of **360 kPa** under a normal stress of **1459 kPa**.

Grout debonding: results

The overall results from the shear box tests are presented in Table 4.4, and shown graphically in Figure 4.29.

Sample	Disc roughness	WCF	Shear stress [kPa]	Normal stress [kPa]
1R-A	Rough, >32 µm	1	1222	1459
1S	Smooth, <4 µm	1	379	912
2R	Rough, >32 µm	1.5	1007	1459
2S	Smooth, <4 µm	1.5	500	1459
3R-B	Rough, >32 µm	2	927	1459
4R	Rough, >32 µm	1	988	1459
4S	Smooth, <4 µm	1	360	1459

Table 4.4: Overview of experiment results at adhesive failure.

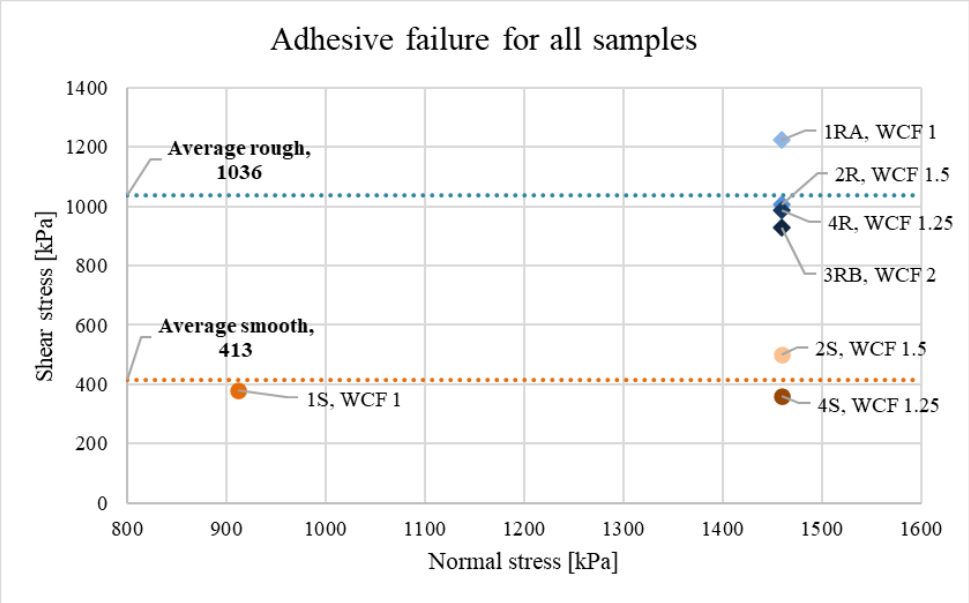

Figure 4.29: Graphical representation of adhesive failure. Rough samples are diamond shaped in shades of blue. Smooth samples are circular and in shades of orange. The dotted lines indicate the average shear stress at failure.

Because several load steps were performed after adhesive failure for sample 1S, it is possible draw these on a graph and determine the friction angle of the steel/grout interface. For sample 1S, the friction angle is approximated by $\phi = 17°$. For comparison, data from sample 1R-A is also added. In the case of sample 1R-A, all load steps were performed before failure. Therefore, only one value (the residual shear stress) is provided, being 1000 kPa. This is in line with all the other rough samples. The friction angle for 1R-A is approximated by $\phi = 35°$, although there is a significant uncertainty due to the limitation of one data point. The results have been plotted in Figure 4.30.

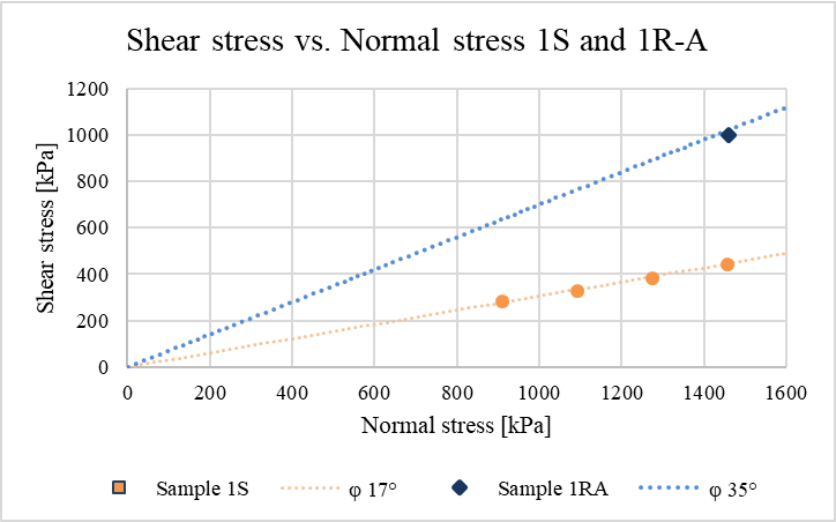

Figure 4.30: Shear stress plotted against normal stress, with friction angles indicated.

Overall, the results of the laboratory experiment on the debonding of the steel/grout interface indicate the following:

- There is a significant difference in shear stress at adhesive failure between the rough and smooth disc samples. The rough samples have an average shear stress at failure of 1036 kPa, while the smooth samples show an average shear stress of 413 kPa.
- Within the separate groups of rough and smooth samples, there is little variation between the measured shear stresses. All values are near the group average.
- The result of sample 1S indicates that above a certain value, the normal stress has no influence on the adhesive failure.
- Varying the water-cement factor (WCF) between 1 and 2 does not have a significant influence on the magnitude of adhesive failure. Only the structural integrity of the grout is affected.
- The results of the laboratory experiment demonstrate that in dense soils with high q_c values, debonding between the grout body and steel tube of the pile under high load can occur. This presents as a plausible explanation for the strain softening measured at Maasvlakte 2.

4.1.6 Maasvlakte 2 - Conclusions

Based on the analysis of the test at Maasvlakte 2 and the results of the laboratory experiment, the following can be concluded:

- The shear box experiments demonstrate that debonding between the grout body and the steel tube of the piles is a plausible explanation for the sudden strain softening measured during the load tests.
- The strain data analysis indicates a peak α_p of 0.35 and a peak α_s in sand of 0.011.
- A load-settlement prediction using curve 2 and aforementioned α factors fits the initial load-settlement data well.
- Limiting q_c values to a maximum of 15 MPa as prescribed by NEN9997-1 severely underestimates the shaft friction.
- Sand content in outcoming grout samples reached between 30 and 40%. This indicates that the piles are not fully soil displacing.
- The overall behaviour of the screw-injection piles at the Maasvlakte 2 test site more closely resembles load-settlement curve 2, indicating that these piles behave like (partly) soil replacing piles.

4.2 Beemster Scale test

After the change in α_p factors in NEN9997-1 in 2017, the Nederlandse Vereniging Aannemers Funderingswerken (NVAF) performed an instrumented test on several piles. The report (NVAF 2019) describes the process, analysis and interpretation of the test results. Four screw piles were tested, all instrumented with strain gauges.

4.2.1 Beemster - Overview

Ground investigation

For the test, an artificial sand layer was created with a thickness of around 4.5 m, surrounded by sheet pile walls (NVAF 2019). The sand has a particle size distribution of D_{50} = 0.2 - 0.35 mm. The top of this artificial layer is situated between NAP -3.4 to -3.5 m. The water level was kept well below the pile base level using drainage, well outside of the area of influence of the piles.
All of the encountered soil is sand, where one distinction can be made based on the q_c value of the lower part of the soil. An overview of this is given in Figure 4.31a. The soil layers are classified as listed below (in m NAP):

- -3.5 to -5.8 m: loose sand
- < -5.8 m: medium dense sand

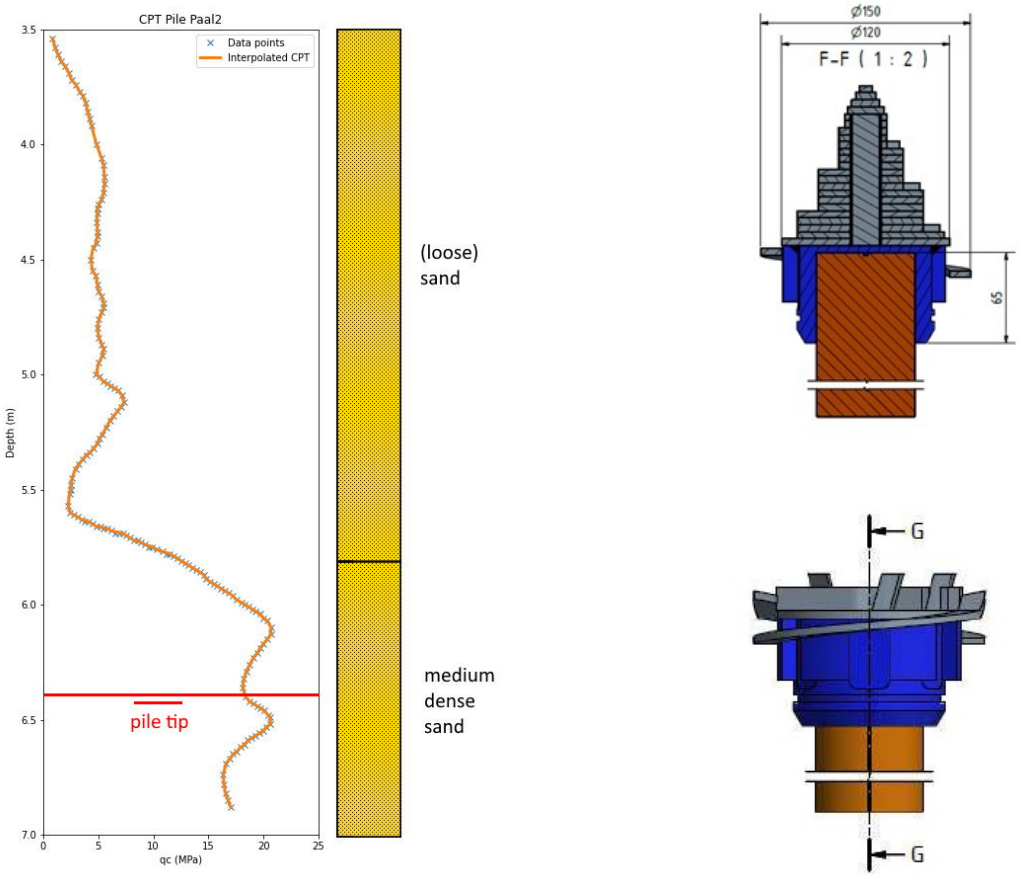

(a) CPT data and soil classification for Beemster scale test. **(b)** Comparison between pile tips (NVAF 2019)).

Figure 4.31

Pile specifications

In order to investigate the influence of differently shaped pile tips, two shapes were applied during the tests. These are a stepped conical screw tip with diameter 150 mm (Figure 4.31b, above), and a flat screw tip with teeth and a diameter 150 mm (Figure 4.31b, below).

The screw piles consist of a cylinder in the centre of the pile, with diameter 70 mm. On diametrically opposed sides of the cylinder, slots were made wherein the fibre optics were glued. This allowed for strain measurements along the pile with a resolution of 500 mm. The central steel cylinder was chosen so that the load could be transferred well to the pile tip.

The piles were installed with a drilling tube of inner diameter 120 mm. No grout injection was applied during or after installation of the piles.

The screwing of the piles was performed with a drilling rig build by Klemm, with a maximum drilling moment of 3 tonne×m and a pull down force of 4.5 tonne. After the target depth was reached, enough concrete was poured in the tube to completely fill the drilling tube.

After the installation, the position of the pile head was compared against the reference point to double check the level of the pile tip. It was seen that during the installation of the conical piles (2 and 6), the penetration close to the target depth was difficult. This was at 0.1 m and 0.3 m above the pile tip for pile 2 and 6, respectively.

Pile no	Ds [m]	Db [m]	Pile base [m]	Tip shape	Installation	Test	Test moment
Pile 2	0.12	0.15	-6.3	Cone	14/07/2017	15/08/2017	32 days after
Pile 3	0.12	0.15	-6.3	Flat	15/07/2017	14/08/2017	31 days after
Pile 6	0.12	0.15	-6.3	Cone	16/07/2017	17/08/2017	34 days after
Pile 7	0.12	0.15	-6.3	Flat	17/07/2017	16/08/2017	33 days after

Table 4.5: Overview of test piles Beemster.

Figure 4.32: Left to right: pile tips and centre steel cylinder; strain gauges installed along steel cylinder; piles after extraction (NVAF 2019).

Pile testing

The ballast of the **load frame** was provided by steel dragline mats, each with a mass of 5 to 6 tonnes. The ballast was positioned centrally above the pile, in a way so that there was no increase of ground pressure immediately surrounding the piles.

The **measuring frame** which registered the load at the pile head was placed at ground level. When deemed necessary, the frame was measured in between the load steps in comparison to a fixed reference point.

Figure 4.33: Load test setup used at Beemster Tests (NVAF 2019).

The pile head settlement was measured with digital potentiometers with a measuring range of 100,000 mm and a precision of 0.001 mm. The potentiometers were fixed to the measuring frame and in contact with the top of the pile.

To load the piles, a hydraulic jack was used from the brand Enerpac, type RRH 6010. This jack has a range of 250 mm and a maximum force of 576 kN at a pressure of 700 bar. At a later (unspecified) point in the test, a different jack was used. This was an Enerpac type CLS 150 with a maximum force of 1500 kN at 700 bar. This was chosen so that higher forces could be exerted at a lower hydraulic pressure.

The **load scheme** was carried out in accordance with NPR7201. Unload/reload cycles were carried out between each load step. This is illustrated in Figure 4.34.

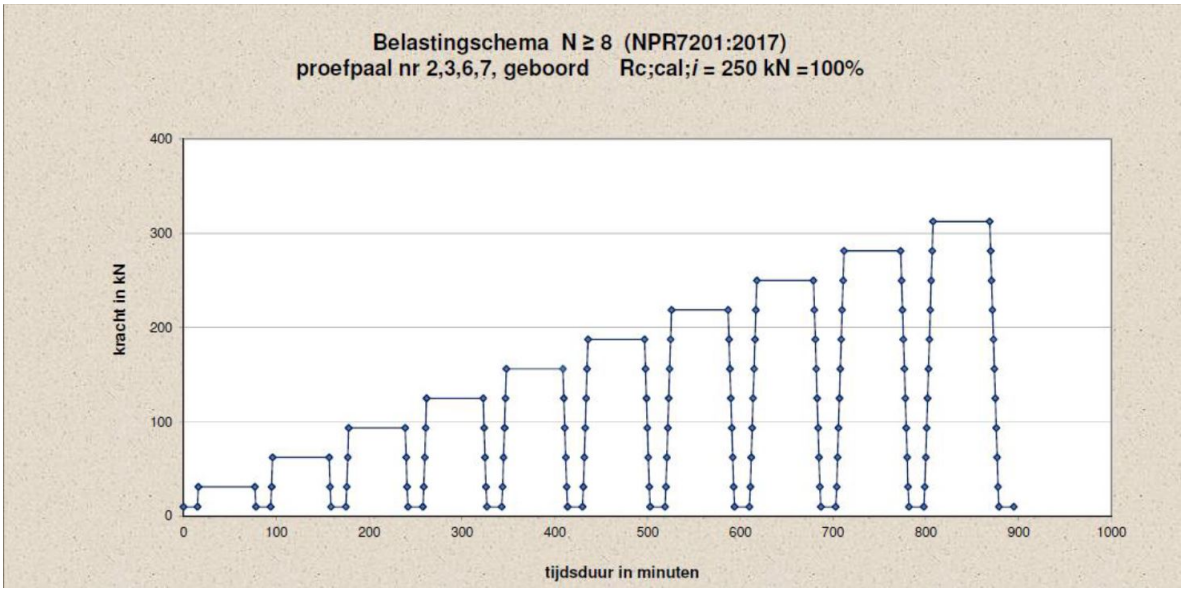

Figure 4.34: Load scheme performed in Beemster scale tests (NVAF 2019).

Pile instrumentation

The strain along the pile shaft was measured using fibre optic sensors, and were measured in microstrain (μm/m). The positions of the sensors are shown in Figure 4.32. All gauges used the working principle of the Fibre Bragg Grating (FBG) method. Each gauge was named based their side (left: A; right: B) and location in millimetres above the base of the pile (0 at the base, 200 at the highest gauge). This is shown in the right drawing in Figure 4.35. Strain gauge B100 would therefore indicate that it is situated 100 mm above the pile tip, on the right side.

4.2.2 Beemster - Test notes

- The cone shaped tip of Pile 6 sheared off during installation. It was found alongside the shaft of the pile around 30 cm above the pile tip. This problem is not described in detail by NVAF (2019), and introduces a significant uncertainty in the results of Pile 6.
- The strain readings regularly showed unexpected behaviour, reducing the reliability of this data. An example of this is the reversal of the yellow and grey line in the second to last load step in Figure 4.36a.

4.2.3 Beemster - Pile factor determination

For the Beemster scale test, a complete analysis was performed to derive the variables, independent from the interpretation of NVAF (2019). This was possible due to the availability of data on load, settlement, pile stiffness, and strain data. Therefore, the justification for these variables is more comprehensive compared to the other described pile tests.

In order to find the force distribution along the pile, which allows the calculation of α_s and α_p, the following equation must be used:

$$F = \epsilon \times E \times A \tag{4.1}$$

Where F is the force in kN; ϵ the strain [-]; E the Young's modulus GPa; and A the surface area m^2.

With the load at the top of the pile known and the strain readings given, only EA -the pile stiffness- is required to calculate the force at the location of the strain gauges.

Pile stiffness The stiffness of the pile (EA) can be calculated using the cross-sectional area of the steel cylinder and the surrounding concrete, being 70 mm and 120 mm, respectively. Multiplying the area with the Young's modulus (E) results in the pile stiffness. The E for steel is 210 GPa and 20 GPa for the used concrete. The centre table in Figure 4.35 shows the calculation steps. The resulting EA for these piles is 957.4 MN.

This result is very similar to what was calculated in the report (NVAF 2019). It was confirmed to be a good assumption: all piles were extracted and indicated shaft diameters around 120 mm, while tests to measure the stiffness demonstrated values near the calculated EA (NVAF 2019).

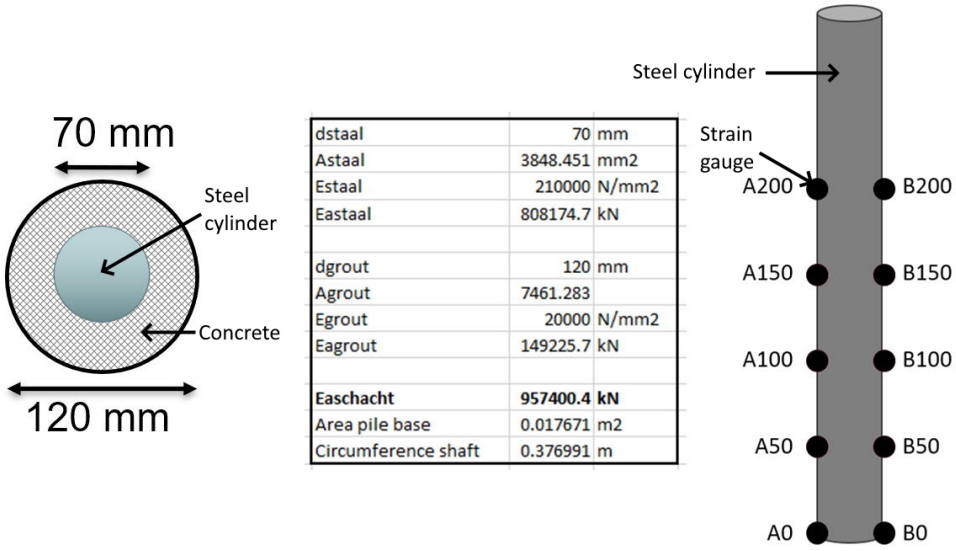

Figure 4.35: Left to right: schematic cross section of piles; stiffness calculation of piles; schematic overview of strain gauges and their location.

Strain to force conversion The FBG strain gauges (Figure 4.35, right) measure the change in length over a constant length, resulting in a value with no units. In combination with a calculated $E * A$ it can be used to find the force at the gauge location using Formula 4.1. An example of the strain data is given in Figure 4.36a.

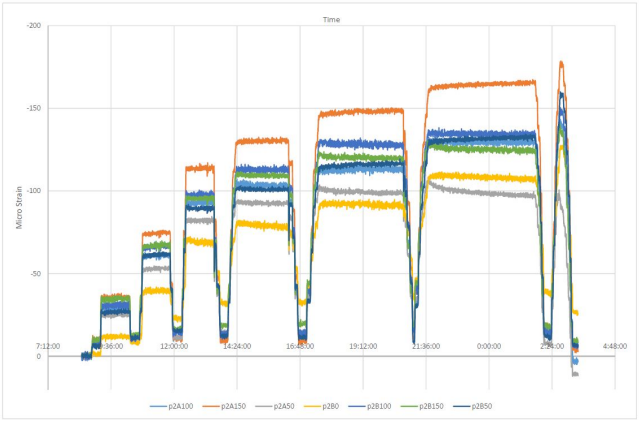

(a) Strain gauge readings from Pile 2. Note the reversal of the yellow and grey lines in the second to last load step (NVAF 2019).

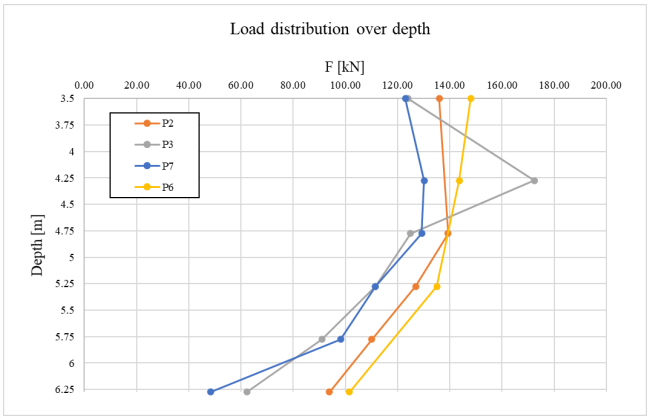

(b) Force, calculated from strain data, plotted against depth for all Beemster piles. Note the unreliability of the gauges 150 and 200 mm above the pile base.

Figure 4.36

Now, a force distribution along the pile can be calculated. This is shown in Figure 4.36b. Knowing the load at the top of the pile, it is now possible to determine how much of this force has dissipated into the soil. The difference between the measured force at the top and the calculated force at the strain gauges is attributed to the shaft friction F_s [kN]. In the same way, the difference in force between two levels of strain gauges can be calculated (e.g. between A150 and A100). This method enables the calculation of an α_s in each 'section' of the pile.

At the bottom gauges (A0/B0), after subtracting the shaft friction from the force at the top of the pile, a significant amount of force remains. This remaining force at the base, F_b [kN], is attributed to the pile tip. The value of F_b is required to find a corresponding α_p.

In order to find the α factors, **strain data from the final load step is used**. This is done because in earlier load steps, the shaft and base resistance may not yet be fully mobilised.

α_s sand Because of the unreliability of the strain gauges at level 200 and 150, sections *top-200* and *200-150* have not been included in the determination of α_s. This is because in these sections, a load higher than the applied load measured at the pile head could be found. In all other sections, an α_s value is calculated, which is then averaged for the whole pile. The results are presented in Table 4.6. The average α_s found for the Beemster scale piles is 0.012.

α_p The area of the pile tip is ordinarily taken as the circular cross section of the pile base. In this case, that would be a circle with a radius equal to 75 mm. However, cone-tipped piles 2 and 6 show significantly higher strain at the lowest strain gauge, as evidenced by Figure 4.37a. Whereas a sharp decline in strain is visible for piles 3 and 7 at the base, this does not occur for piles 2 and 6.

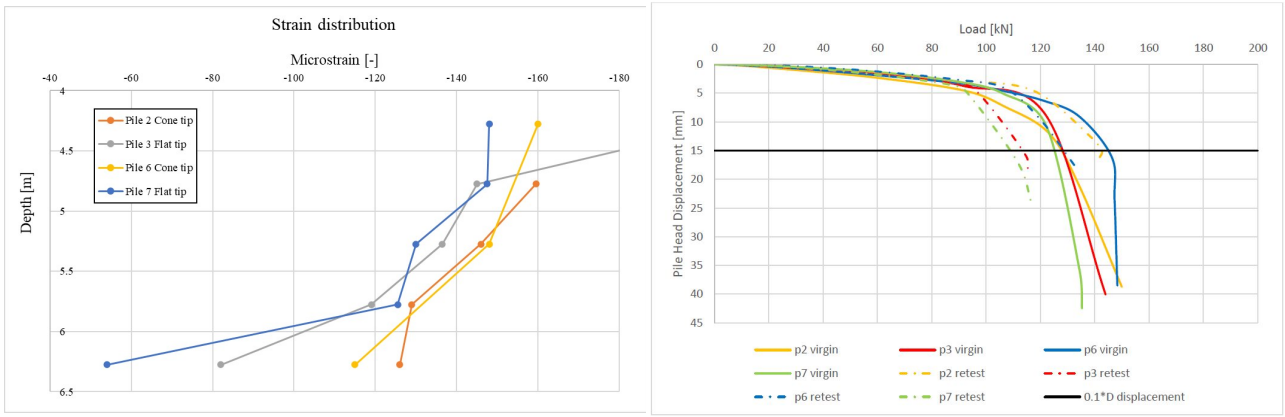

(a) Strain distribution along the length of the piles.

(b) Load-settlement data from report by NVAF (2019).

Figure 4.37

This means that a much higher force is attributed to the base of piles 2 and 6, which would lead to a much increased value of α_p. Yet, the pile tests show no difference in capacity between the different piles, and therefore these much higher α_p factors are unlikely to be representative. In the flat-tipped piles 3 and 7, the final strain gauge is practically at the base of the pile. However, on the piles with cone tips, there is still a significant distance to the actual pile base. Thus, the calculated load at A0/B0 is not truly the load at the tip of the pile. Therefore, the higher F_b for piles 2 and 6 needs to be distributed across the area of the cone, to provide reliable estimates of α_p. This area is calculated as a cone with radius 60 mm and height 115 mm, following the specifications shown in Figure 4.31b. The inner radius of 60 mm, without the screw flanges, is used to calculate the conical area. The previously mentioned dislocation of the cone tip towards the side of Pile 6 may also have influenced the strain reading at the bottom of the pile.

The α_p factors with and without the cone correction are displayed in Table 4.6. Clearly, the cone corrected α_p values are much more in line with piles 3 and 7, and other reviewed pile tests. Therefore, these cone corrected factors are considered the correct choice. The analysis indicates an average α_p of 0.27.

	α_s	α_p	α_p **(cone corrected)**
Pile 2	0.013	0.53	0.26
Pile 3	0.011	0.34	0.34
Pile 6	0.007	0.53	0.26
Pile 7	0.016	0.23	0.22
Average	0.12	0.4	0.27

Table 4.6: Results α factor analysis from strain readings. Note that the α_p factors corrected for conical area are considered leading.

4.2.4 Beemster - Analysis and results

Figure 4.38 shows how the α_p mobilises as base settlement increases. The graph clearly shows that the values are approaching their maximum value towards the last load step. In addition, large difference between the flat and cone tipped piles is indicated, if no correction is applied to the base area.

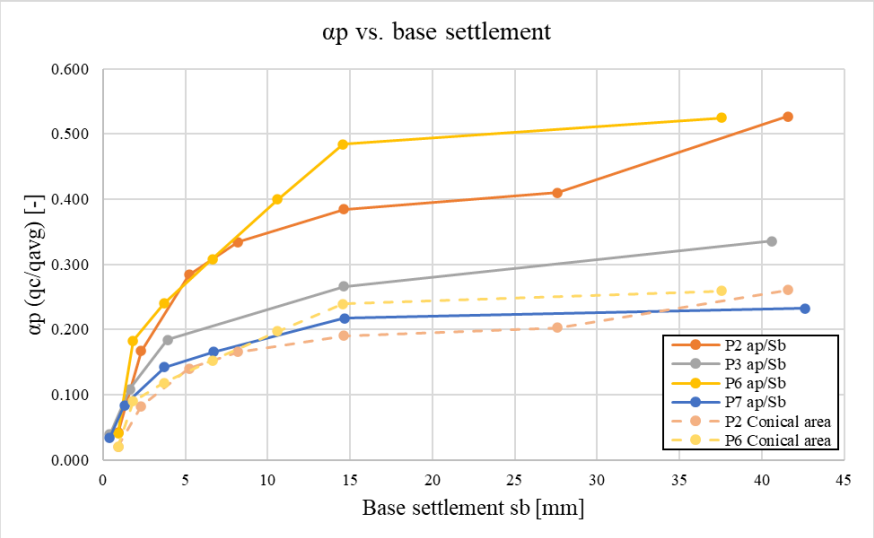

Figure 4.38: Mobilisation of α_p factor as base settlement s_b increases. Comparison between all piles, also including cone corrected values.

From Figure 4.38, it may be concluded that the α_p for all piles is near full mobilisation during the last load step. Second, it is obvious that applying a correction for the conical area (P2 and P6) provides results in line with the flat piles (P3 and P7). Therefore, it is clear that the strain readings at level A0/B0 are affected by the shape of the tip. The significant increase of distance from the strain gauge to the actual pile tip between the conical and flat tips is likely the most important factor.

Detailed load/displacement data can be seen in Figure 4.39, by plotting the values recorded by the load cell. Two load cells were used for each pile, but only load cell 1 (LC1) was determined to be working properly in all cases. Therefore, the data shown in Figure 4.39 is provided by load cell 1. These are indicated by blue dots and clearly show the unload/reload cycles performed during testing. Also plotted on Figures 4.39a-d are two combinations of load-settlement predictions. These are: grey, load-settlement curve 1; and orange, curve 2.

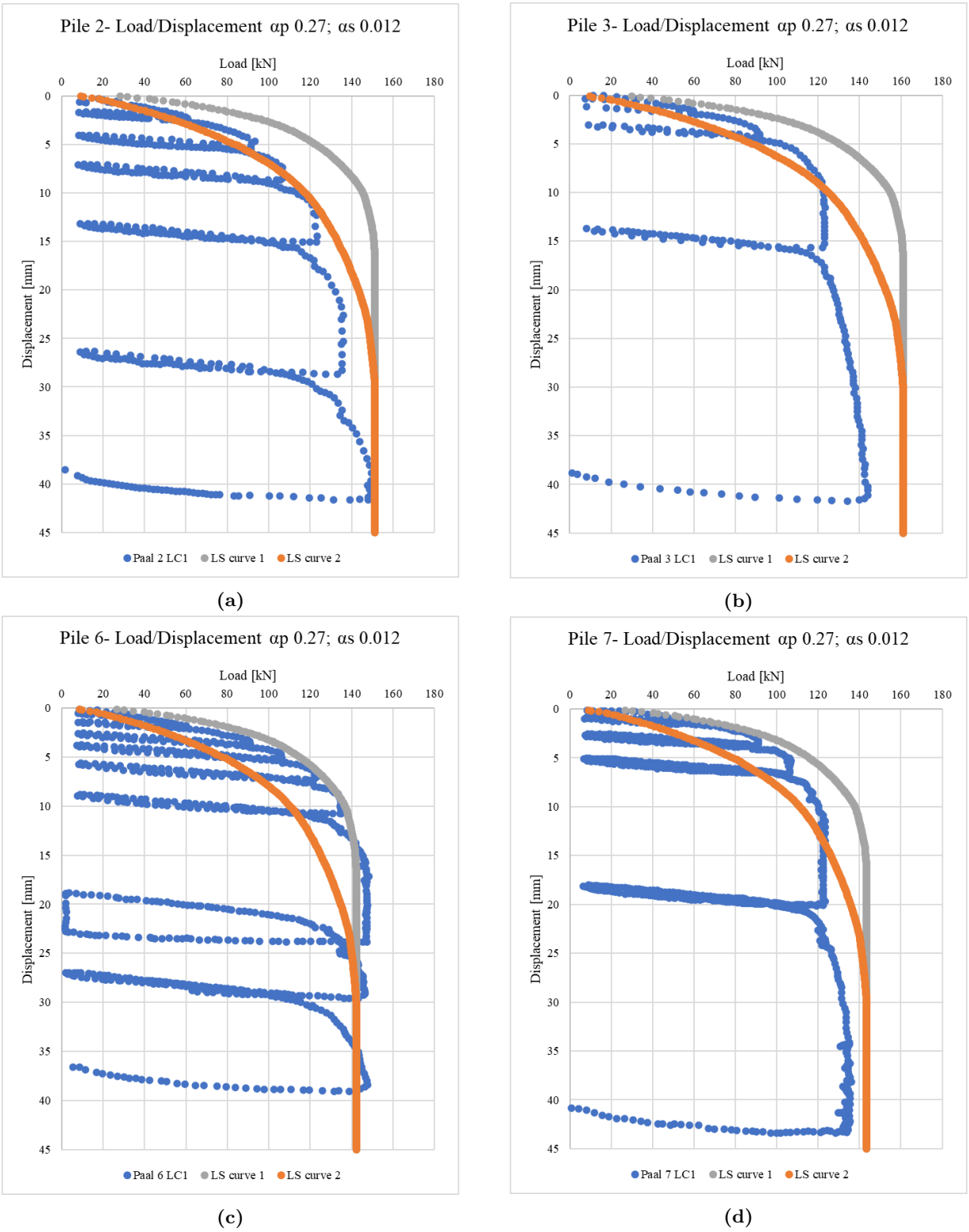

Figure 4.39: Comparison of different load-settlement curve options. Blue: load cell data; orange: curve 2; grey: curve 1.

From the different prediction options shown in Figures 4.39a-d, several observations can be made. Load-settlement curve 1 (grey line) behaves too stiff in comparison with the measured data. Additionally, no more resistance is mobilised after 15 mm of settlement. However, especially in Figures 4.39a, b and c, it can be seen that there is still more capacity generated. Therefore, load-settlement curve 1 is not the most representative choice.

The orange line depicts the prediction made with curve 2. The predicted resistance mobilises slower than the measured data. It appears that the shaft friction for these piles is generated quicker than curve 2 presents. However, the overall behaviour of these piles is better approximated by load-settlement curve 2.

The soft predicted response of the shaft friction may be a scale effect of the small dimensions of the pile. The NEN load-settlement prediction scales the base settlement with equivalent diameter, but *does not scale the shaft mobilisation*. This means that irrespective of the pile length and width, the shaft friction is fully mobilised at either 10 mm (curve 1) or 25 mm (curve 2). As these curves are based on real world tests, it is unlikely that such small piles have been included. Therefore, it may be concluded that because the load-settlement curve for shaft friction is not scaled with pile dimensions, the shaft resistance prediction for these piles is less reliable than those in full-sized pile tests.

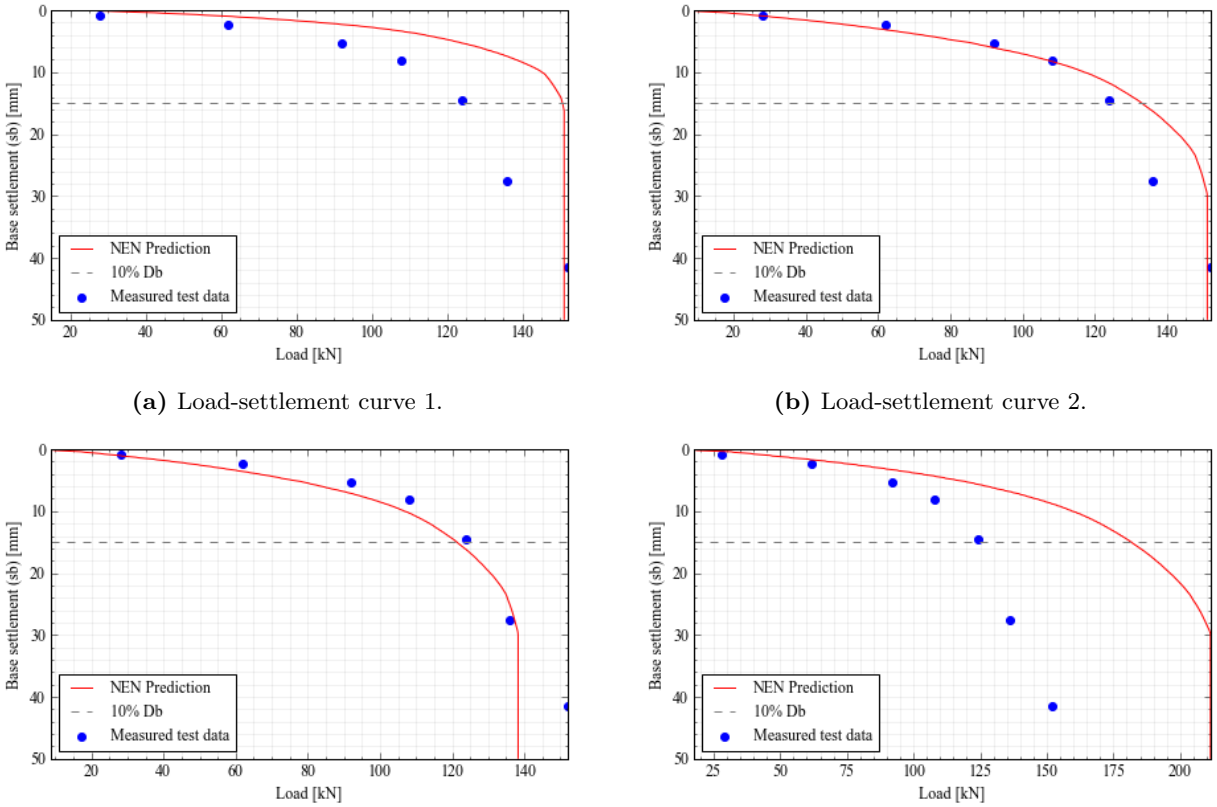

(a) Load-settlement curve 1.

(b) Load-settlement curve 2.

(c) Load-settlement curve 2, with q_c limiting.

(d) Curve 2 with NEN $\alpha_p = 0.63$ and $\alpha_s = 0.009$.

Figure 4.40: Presentation of different load-settlement curves, effect of limiting q_c, and NEN9997-1 prescribed α_p and α_s. Based on data from pile P2.

In addition to the detailed load-displacement graphs shown in Figure 4.39, and to quantify the influence of q_c limits, four options are displayed in Figure 4.40. For these and the final results, an α_p of 0.27 is applied with an α_s of 0.012, in accordance with the findings from the strain readings. The findings from Figures 4.40a to c are similar to those described previously.

Figure 4.40a shows the application of load-settlement curve 1. The mobilisation of clearly too stiff, and the pile is fully mobilised at 10% D_b. Curve 1 does not realistically approach the test data.

Figure 4.40b shows load-settlement curve 2. Compared to curve 1, curve 2 agrees more with the test data. This is indicated by the softer response of the shaft friction and the continuation of mobilisation

after 10% D_b.

Figure 4.40c demonstrates the effect of q_c limiting with LS curve 2. It is interesting to see that even though the q_c values in the sand only reach above 12 MPa for a small portion (reaching 15 MPa only at two peaks), the limiting method described in NEN9997-1 has a noticeable influence on the capacity calculations for the Beemster scale piles.

Figure 4.40d applies the currently prescribed pile factors from the NEN. Clearly, these do not approach the test data at all. This is mostly caused by the much higher α_p.

Based on these findings, the most accurate option is load-settlement curve 2 and no limiting. Figure 4.40a to d shows the best fitting load-settlement behaviour predictions for the piles tested at Beemster. Based on the analysis performed on the Beemster scale test, the following can be noted:

- The dislocation of the cone tip of pile 6 adds an uncertainty to the analysis, although the findings presented are in agreement with the other three piles.
- The NEN load-settlement curve for shaft mobilisation is not corrected for pile size, which casts doubt on calculations performed on piles with unusual dimensions.
- Load-settlement curve 2 without q_c limiting provides the best fitting prediction.
- An α_p of 0.27 and α_s is sand of 0.012 are found. These are appropriate to predict the load-settlement response.
- Load-settlement curve 2 predicts the overall pile behaviour quite well. The behaviour of the pile response resembles that seen in (partly) soil replacing piles.

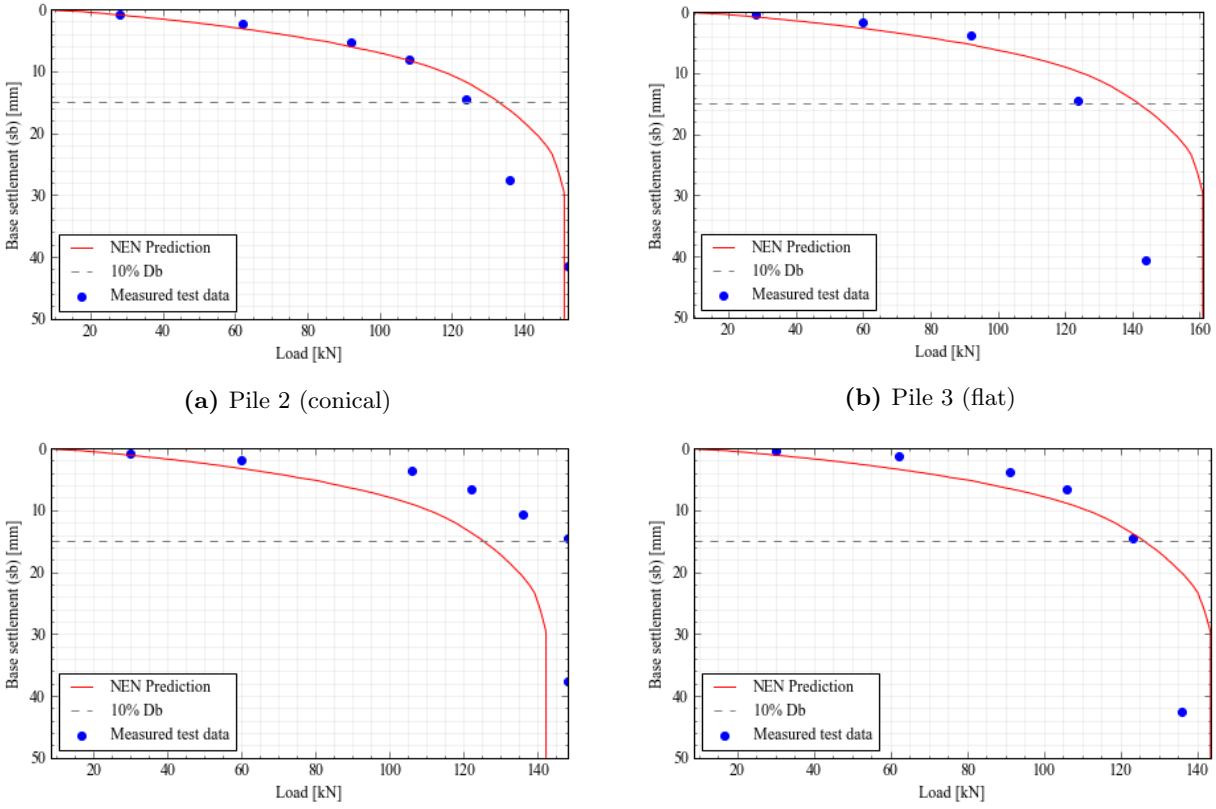

(a) Pile 2 (conical)

(b) Pile 3 (flat)

(c) Pile 6 (conical)

(d) Pile 7 (flat)

Figure 4.41: Load settlement predictions for Beemster scale piles, with α_p 0.27, α_s 0.012.

4.2.5 Beemster - Conclusions

After the analysis performed on the Beemster test, the following may be concluded:

- The load-settlement curve from NEN 9997-1 which predicts shaft mobilisation is not corrected by pile dimensions. Therefore, the approximated shaft friction response for the Beemster piles is softer than in reality.
- The strain data analysis finds a peak α_p of 0.27 and a peak α_s in sand of 0.012.
- A prediction with load-settlement curve 2 and the aforementioned α factors is in agreement with the measured load response.
- Limiting q_c values during calculation as prescribed by NEN9997-1 slightly underestimates the shaft friction.
- No noticeable difference in capacity and behaviour between a flat and cone shaped pile tip is found.
- The mobilisation of the screw piles at the Beemster test site more closely resembles load-settlement curve 2, meaning that these piles behave like (partly) soil replacing piles.

4.3 Rosmalen

In 1991, tests on 5 screw-injection piles were performed near Rosmalen. These tests were carried out in order to investigate the behaviour of the then relatively new pile type. The aim of the research (Geerling et al. 1992) was to get insight into the α_p and α_s factors for these piles, and to find out whether a difference in pile tip shape - pyramid instead of flat - had significant effect on the overall capacity.

4.3.1 Rosmalen - Overview

Ground investigation

The piles were all installed in medium dense sand, with q_c values ranging from around 6 to 20 MPa. Although a clay layer is encountered in the CPT profile, this is outside of the area of influence of the piles. The CPT profile and schematic overview of the layers is shown in Figure 4.42a. An overview of the most important pile parameters is presented in Table 4.7.

The depths are measured in m, compared to a reference level (REF). Ground level is at -0.3 m REF (Geerling et al. 1992).

- -0.3 m to -12.2 m: medium dense sand
- -12.2 m to -12.8 m: sandy clay
- -13.5 m to -16.5 m: dense sand

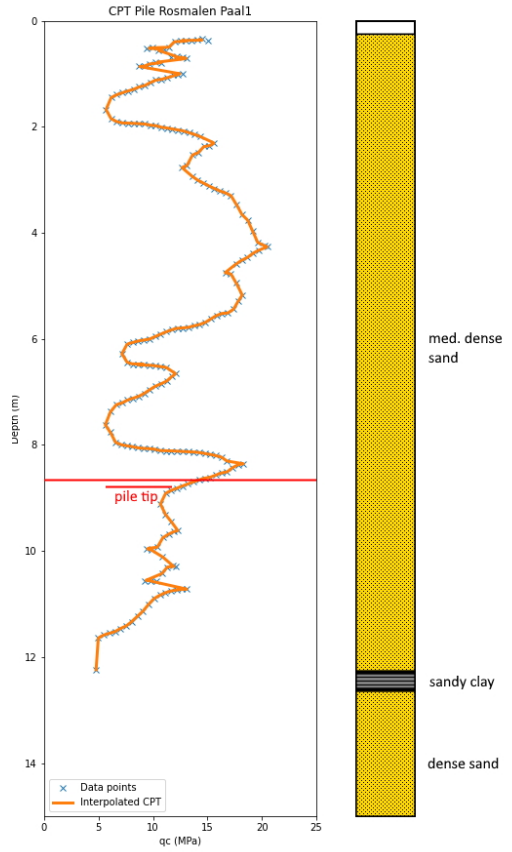

(a) CPT data and soil classification for Rosmalen test.

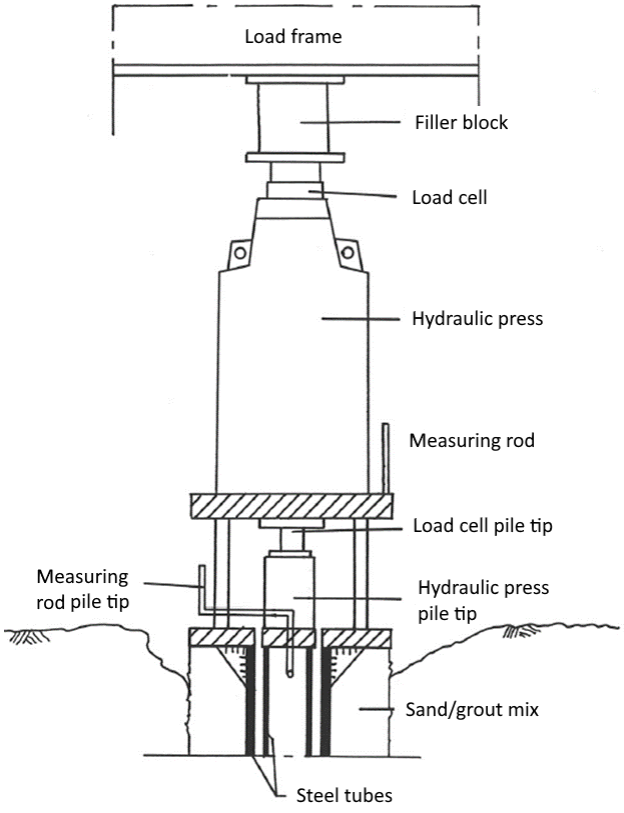

(b) Load test setup for Pile 3, allowing for separate measurement of load on pile base (Geerling et al. 1992).

Figure 4.42

Pile specifications

All piles were installed with steel tubes, which were left in situ, similar to the piles at Maasvlakte 2. The specific pile type is not mentioned in the report by Geerling et al. (1992), but they are classified as a Type 3 screw-injection pile. Grout was injected throughout the installation process, with outlets located above the pile tip, which mixed with the sand and formed a grout body surrounding the steel tube. Pile dimensions are presented in Table 4.7and cross-sectional drawings are shown in Figure 4.43.

One of the aims of this test was to gain more understanding on the effect of pile tip shape. Therefore, two types of shapes were used. The tip on piles 1/2 is essentially a flat tip, whilst the tip on piles 3, 4 and 5 is a pyramid shaped tip. The sides of the tips were flat, without steps or teeth. Schematic drawings and dimensions are depicted in Figure 4.43.

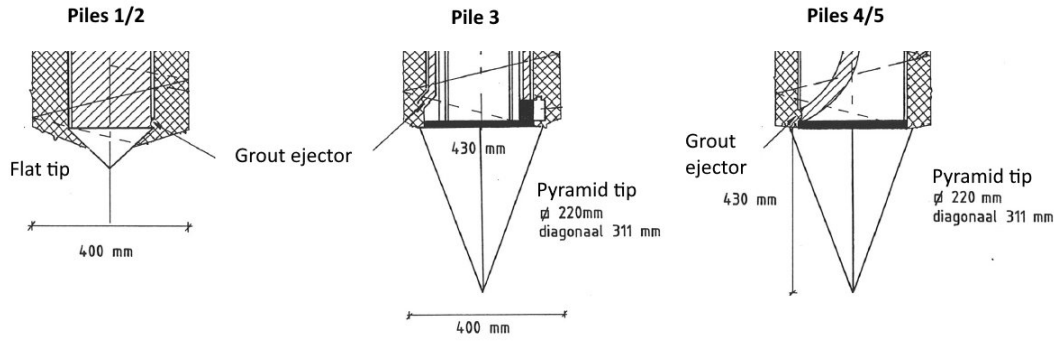

Figure 4.43: Comparison between used pile tips. Edited from Geerling et al. (1992).

Pile no	D_s **calc. [m]**	D_s **meas. [m]**	D_b **[m]**	**Pile bottom [m]**	**Tip shape**
1	0.4	-	0.4	-8.75	Flat
2	0.4	0.53	0.4	-8.5	Flat
3	0.4	0.53	0.4	-8	Pyramid
4	0.4	0.45	0.4	-8.5	Pyramid
5	0.4	0.44	0.4	-7.75	Pyramid

Table 4.7: Overview of pile data for Rosmalen test.

Pile testing

What makes this test interesting for the purposes of this research is that, although the piles were not installed with strain gauges, an original idea was executed that allowed for the separation of shaft friction and base resistance. This unusual load setup was used on one of the five piles, Pile 3. The setup for Pile 3 is drawn in Figure 4.42b. Essentially, the pile tip is connected via a freestanding tube inside the main tube. This freestanding tube is in turn connected to a separate hydraulic press, load cell and measuring rod. The system for the pile tip is in its entirety attached to the main hydraulic press and load cell, which measures the total load and settlement over both the base and shaft. Due to the separate pile tip measurement system, the total load and settlement can be easily split between shaft friction and base resistance. The pile tip settlement s_b is in turn calculated using the stiffness of the freestanding tube. To reiterate, the special load setup does not contain strain gauges but measures the actual load over the whole pile tip.

The **load scheme** for the piles at Rosmalen differs significantly from the NPR7201: between each load step, 3 unload/reload cycles were performed. This can be seen in Figure 4.44. This was done

to mobilise as much base capacity as possible, but will have caused significant friction fatigue. This softens the load-settlement behaviour. Although, because all piles have undergone this treatment, it is difficult to ascertain the true effect of friction fatigue.

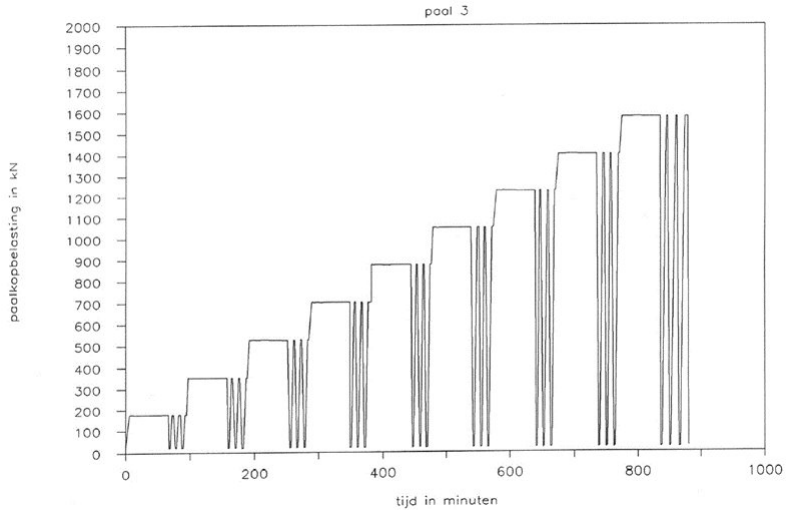

Figure 4.44: Load scheme used in Rosmalen tests, depicted here for Pile 3 (Geerling et al. 1992).

4.3.2 Rosmalen - Test notes

- Test on Pile 5 shows a much lower capacity compared to other piles. It may possibly be caused by a weak layer underneath the pile tip, though no explanation is given in the report by Geerling et al. (1992).
- Pile 1 not extracted due to it being in the vicinity of the foundation for a nearby billboard.
- The high number of unload/reload cycles will have had a significant effect on the load-settlement behaviour of the piles, softening the overall response.
- The force on the base of Pile 3 is measured directly at the bottom via a tube connected to the pile tip. No strain measurements were performed at all. This means that the force is measured over the area of the cone. When converting this force to stress, to calculate α_p, usage of the cross-sectional area of the tip will provide a correct result.

4.3.3 Rosmalen - Pile factor determination

Due to the special load test setup on Pile 3, it is possible to determine the α factors. These factors can then be verified by utilising the load-settlement prediction on the other piles and evaluating the results.

Figure 4.45a shows that the total load on the pile head at the last load step is 1575 kN. From Figure 4.45b, the load on the pile tip can be extracted. For the final load step, F_b is 200 kN. Then, the load taken up by shaft friction δF is 1375 kN.

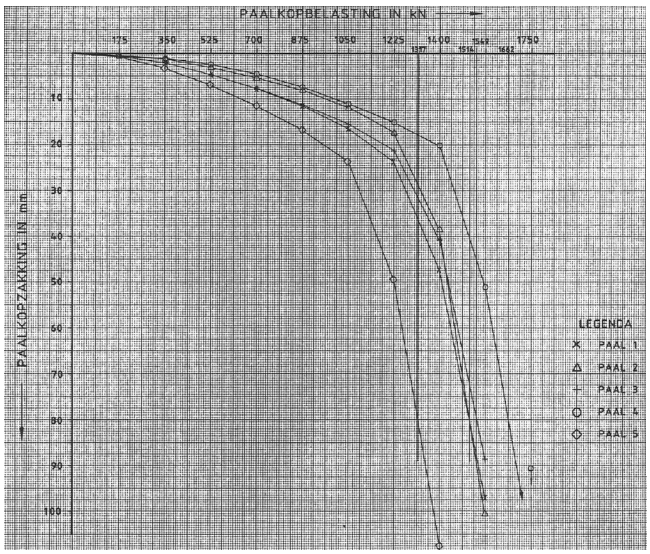

(a) Load-settlement data for piles tested at Rosmalen (Geerling et al. 1992).

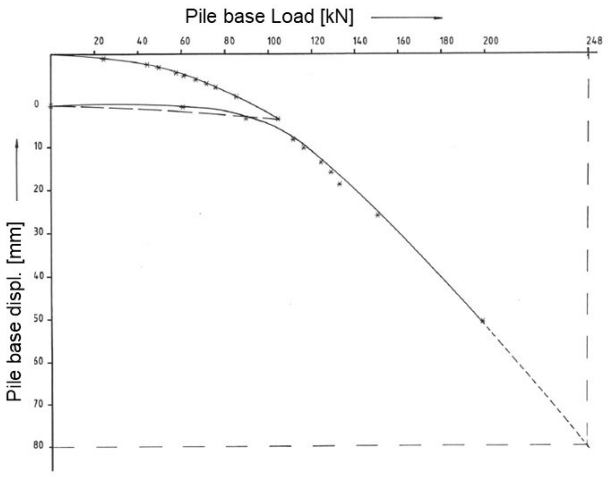

(b) Load on pile tip against base settlement. Each load step indicated with asterisk. Note that the pile tip was preloaded to 15 mm s_b before the test, to mobilise the base capacity. The data is zeroed when the test on the whole pile started (Geerling et al. 1992).

Figure 4.45

α_s The base diameter of 400 mm is also used as diameter of the pile shaft, as is prototypical for screw-injection piles. This means the circumference of the shaft C is 1.257 m. The length of the pile L is 7.7 m. The average q_c along the shaft is found to be 12.6 MPa, which is in agreement with the findings of Geerling et al. (1992). Knowing the load attributed to shaft friction δF (1350 kN), the α_s can now be calculated. This gives 0.011:

$$\alpha_s = \frac{1375kN}{7.7m * 1.257m} \Big/ 12600kPa = 0.011 \tag{4.2}$$

α_p With the base diameter of 400 mm, one can calculate the circular area A_{tip}, which is 0.126 m^2. The $q_{c,avg}$ using the Koppejan method is 7.93 MPa. With the load on the pile base F_b known as 200 kN, the α_p factor may now be calculated. The result is 0.20:

$$\alpha_p = \frac{200kN}{0.1257m^2} \Big/ 7.93MPa = 0.20 \tag{4.3}$$

The relatively low α_p is caused by the base resistance not being fully mobilised at the final load step (seen in Figure 4.45b). Additionally, the numerous unload/reload cycles (which are normally not applied when following NPR guidelines) may cause grain crushing, which can reduce the resistance from the soil at the pile base. Due to the possibility of plotting load-settlement data for only the pile tip, the value of α_p is investigated further in the next section.

4.3.4 Rosmalen - Analysis and results

Due to the load setup used for Pile 3, Figure 4.46a is able to show a prediction of only the base mobilisation, compared to the measured data. The measurement points above a s_b of 0 are because the tip was preloaded to 15 mm s_b before the start of the test.

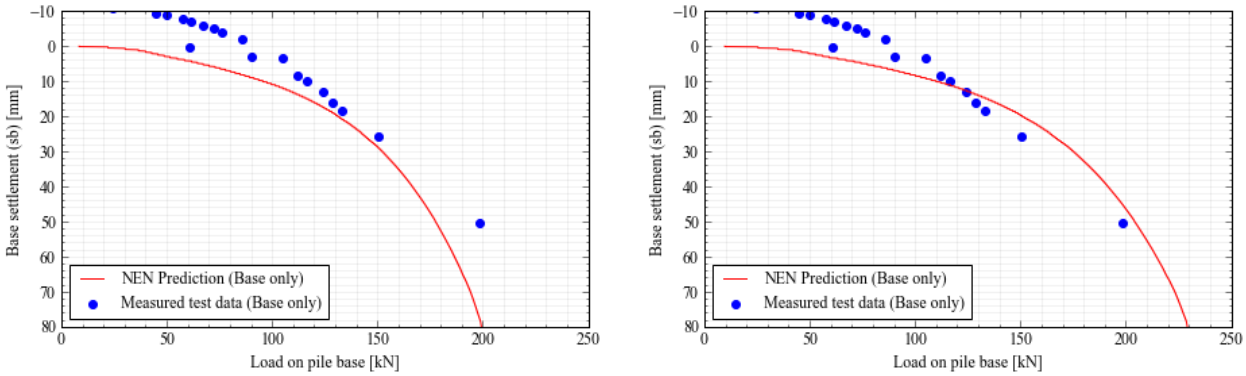

(a) Pile 3 base mobilisation, α_p 0.20.

(b) Pile 3 base mobilisation, α_p 0.23.

Figure 4.46

Figure 4.46a shows the projected behaviour with the calculated factor of 0.20. Although it fits the initial data points well, it underpredicts the base resistance quite significantly at larger settlements, as indicated by the data point at 200 kN.

In order to find a representative α_p for Pile 3, small adjustments the calculated value were considered. Figure 4.46b shows the closest fit, with an α_p of 0.23. This enables a correct prediction of settlements at larger loads. Therefore, an α_p of 0.23 is the best possible approximation for the peak α_p of Pile 3.

Based on the above findings and earlier calculations, the factors determined for the Rosmalen piles are an α_p of 0.23 and an α_s in sand of 0.011.

In order to investigate the influence of different load-settlement curves, q_c limiting along the shaft, and the currently proposed α factors by the NEN, several plots are displayed in Figure 4.47.

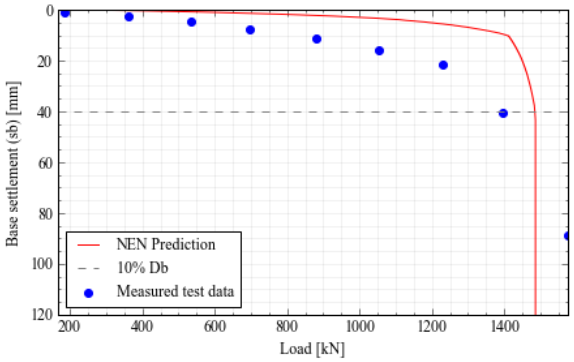

(a) Load-settlement curve 1.

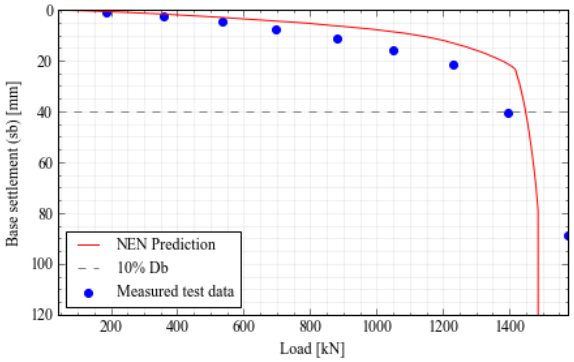

(b) Load-settlement curve 2.

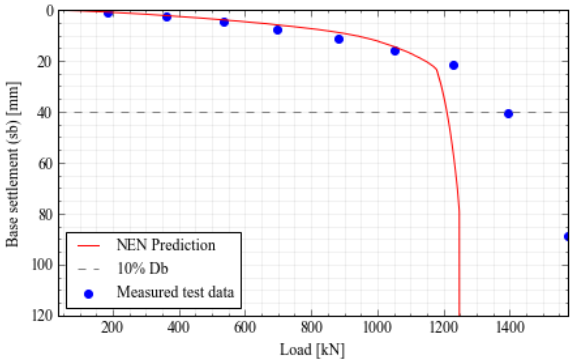

(c) Load-settlement curve 2, with q_c limiting

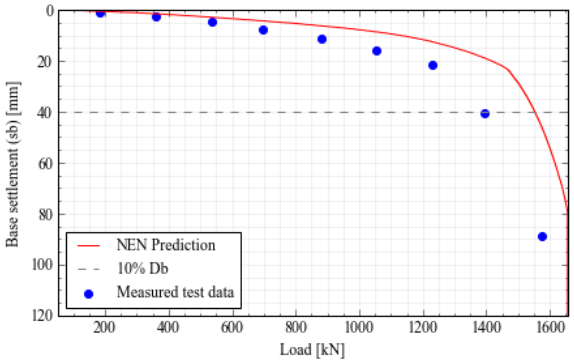

(d) Curve 2 with NEN $\alpha_p = 0.63$ and $\alpha_s = 0.009$.

Figure 4.47: Presentation of the effect of different load-settlement curves, q_c limiting and NEN prescribed α factors. Based on data from Pile 3.

Figure 4.47a shows the prediction with LS curve 1. Very clearly, the shaft mobilisation is too stiff. Additionally, the measured data shows that the base resistance is not fully mobilised at 10% D_b. Therefore, load-settlement curve 1 is no representative fit.

Load-settlement curve 2 is shown in Figure 4.47b. The general behaviour of the measured data is simulated well, especially the shaft mobilisation, when compared to 4.47a. Also note the continued base mobilisation after 10% D_b.

The effects of limiting q_c to a maximum of 15 MPa are shown in Figure 4.47c. Compared to the previous graphs, it is clear to see that the prediction with q_c does not accurately simulate the actual pile behaviour.

Figure 4.47d shows the load-settlement prediction with the current α factors prescribed by the NEN, α_p 0.63 and α_s 0.009. Although the prediction is quite close to the data points, these factors are very different to those supported by the data presented by the load setup of Pile 3 in the previous section.

From the investigation depicted in Figure 4.47, the best option is load-settlement curve 2 with no q_c limiting. Figure 4.48a to e presents the prediction results for the Rosmalen screw-injection piles. Factors α_p 0.23 and α_s in sand 0.011 are applied.

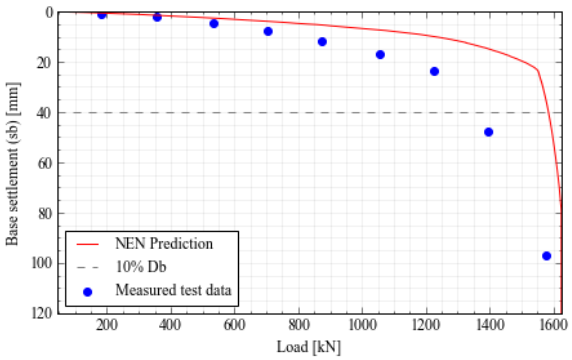

(a) Pile 1 (flat tip)

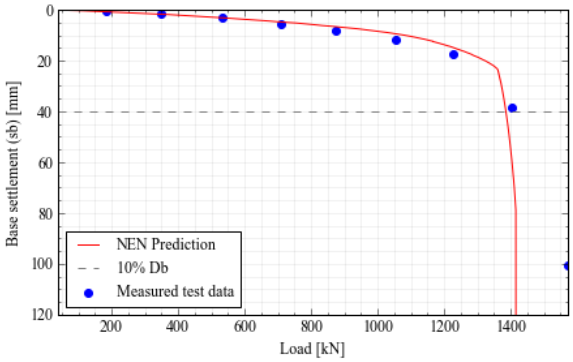

(b) Pile 2 (flat tip)

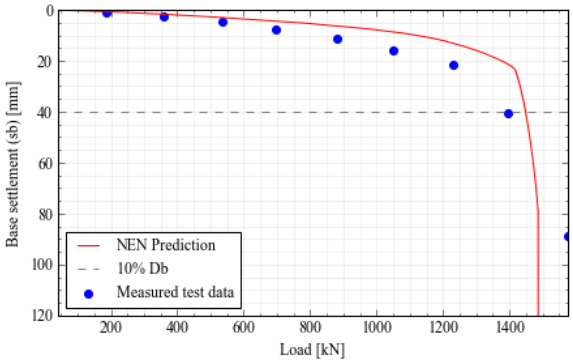

(c) Pile 3 (pyramid tip)

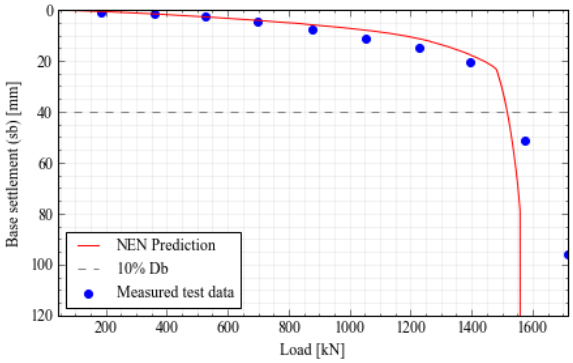

(d) Pile 4 (pyramid tip)

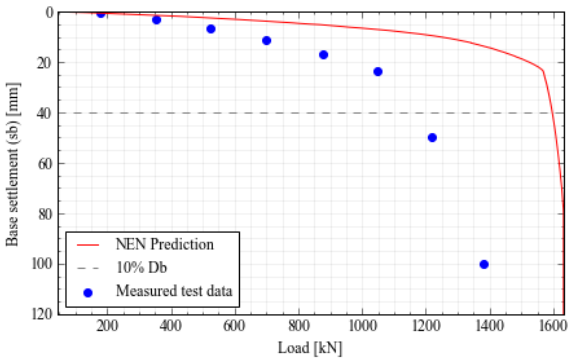

(e) Pile 5 (pyramid tip)

Figure 4.48: Load settlement predictions for Rosmalen piles, with α_p 0.23 and α_s 0.011.

After the end of the test campaign, all piles except Pile 1 were extracted and investigated. This was done to document the shaft diameter over the whole length of the piles. The results of this are presented in Figure 4.49.

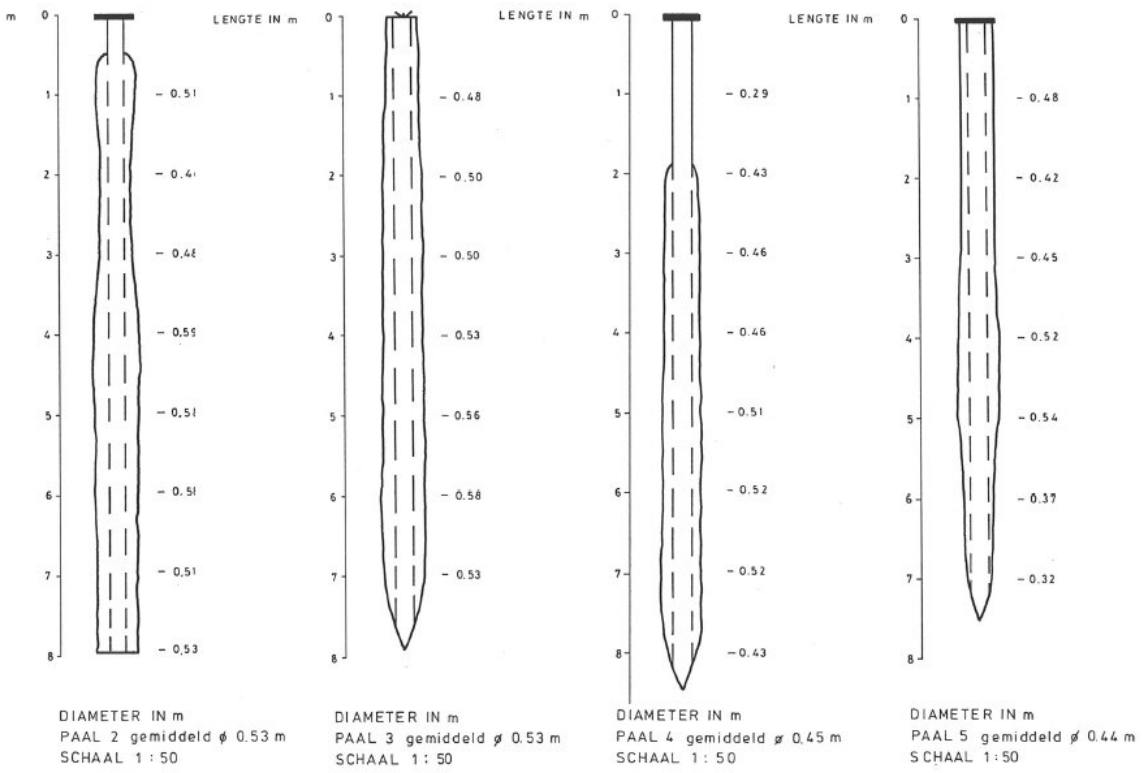

Figure 4.49: Observed pile diameters after excavation. Left to right: pile 2, 3, 4 and 5. Pile 1 was not extracted as it was in vicinity of another foundation (Geerling et al. 1992).

Clearly, there is a lot of variance between the shaft diameter of the extracted piles. Note especially the local fluctuations of piles 2 and 5. On average, the shaft diameters range from 0.44 m to 0.53 m, compared to a predicted shaft diameter of 0.4 m (which is the base diameter). Therefore, using the shaft base diameter to predict the diameter of the grout body is not very accurate. However, due to the large fluctuations of the actual shaft size of the extracted piles, it is impossible to make an accurate guess.

To make predictions, one has to use known parameters, and thus, using D_b for D_s is the best option available. Besides, the results of the load-settlement predictions shown in Figure 4.48 demonstrate that this assumption provides realistic and consistent results. Thus, whilst the true value of D_s for screw-injection piles will vary from the assumed D_b, load-settlement predictions made for screw-injection piles with the assumption $D_s = D_s$ are reliable.

4.3.5 Rosmalen - Conclusions

- Analysis of the load-settlement data from Pile 3 leads to an α_p of 0.23 and α_s in sand of 0.11.
- Load-settlement predictions with curve 2 and aforementioned α factors produce results that compare favourably to the measured pile test data.
- Limiting q_c values along the shaft, as prescribed by NEN9997-1, does not produce realistic load-settlement graphs.
- The results do not indicate any difference in capacity and behaviour between the flat and pyramid shaped pile tips.

- Assuming the base diameter D_b to approximate the shaft diameter D_s of the grout body, provides reliable capacity and load-settlement predictions.
- The behaviour of the screw-injection piles at the Rosmalen test site more closely resembles load-settlement curve 2, indicating that these piles behave akin to (partly) soil replacing piles.

4.4 Limelette

Maertens and Huybrechts (2003) provide an overview of the results of an extended test campaign on screw piles in Limelette, Belgium, between 2000 and 2002. In this campaign, 10 static load tests were performed on 5 different types of screw piles: De Waal, Atlas, Fundex, Olivier and Omega. The pile tips were installed in very dense sand layer, while most of the shaft is surrounded by clay and overconsolidated clay.

4.4.1 Limelette - Overview

Ground investigation

The piles in the Limelette test field are mostly located in clay layers, with the pile tips founded in a dense sand layer. Before the final soil investigation, the upper terrain was reinforced with a 40 cm layer of rubble in order to provide a working platform for the access of heavy machinery. The level of 0 m is at that ground level. The most important data from the CPT investigation is shown in Figure 4.50a. Classification of the layers is as follows:

- -2.2 to -6.2 m: silty clay
- -6.2 to -8.2 m: heavily overconsolidated clay
- <-8.2 m: dense sand

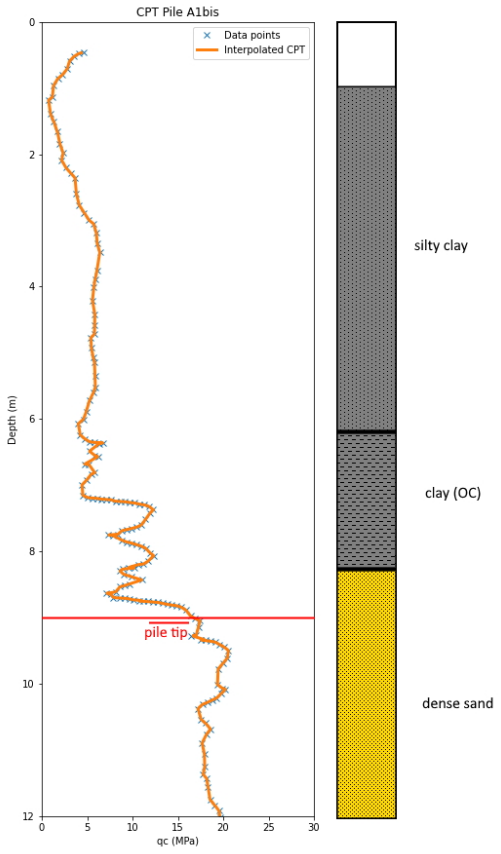

(a) CPT data and soil classification for Limelette.

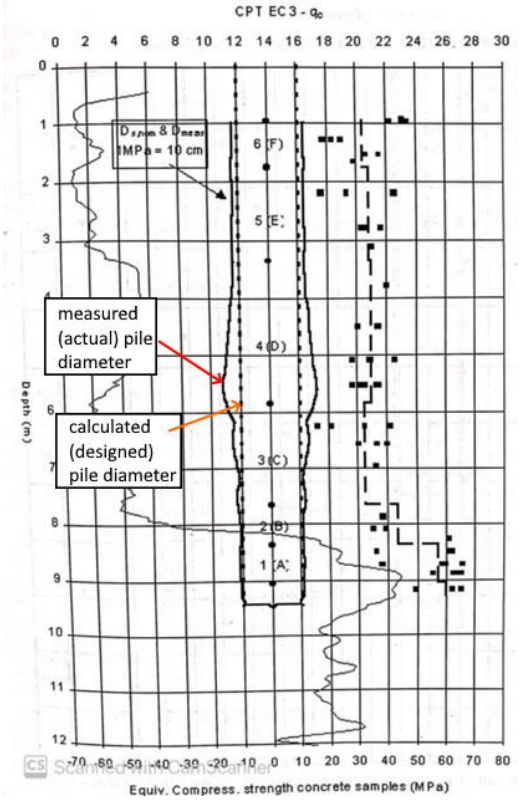

(b) CPT data overlain by calculated and measured pile shaft diameter for Omega pile C3, edited from Maertens and Huybrechts (2003).

Figure 4.50

Pile specifications

A selection of 10 piles were statically loaded. An overview is presented in Table 4.8. No grout injection was used for any of the piles. The following types were installed at the test site:

- Fundex 38/45 screw piles
- Atlas 36/51 screw piles
- Olivier 36/51 screw piles
- De Waal 41/41 screw piles
- Omega 41/41 screw piles

Due to each contractor having a slightly different approach to installing these piles, only the most relevant differences will be described in this section. Refer to Chapter 2 for more detail on the various installation procedures and concrete pouring methods used.

Pile type classification: Olivier and Atlas piles are classified as Type 2 (helical shaft), whereas the other pile types at Limelette are classified as Type 1 (smooth shaft).

Concreting method: For the Fundex piles, the auger was first extracted, and then concrete was poured in the drilling tube. All other pile types started concreting when the auger reached target depth, injecting concrete into the tube with a pump whilst simultaneously extracting the rotating auger out of the drilling tube.

Pile no	Pile type	Ds [m]	Db [m]	Pile bottom [m]	Test moment
A1	Fundex	0.39	0.45	-9.59	151 days after
A2	Fundex	0.55	0.55	-9.2	151 days after
A3	Omega	0.41	0.41	-945	115 days after
A4	De Waal	0.41	0.41	-9.53	115 days after
B3	Atlas	0.51	0.51	-9.43	90 days after
B4	Atlas	0.51	0.51	-9.43	90 days after
C1	Fundex	0.39	0.45	-9.65	87 days after
C2	Olivier	0.55	0.55	-9.13	86 days after
C3	Omega	0.41	0.51	-9.45	79 days after
C4	De Waal	0.41	0.51	-9.52	72 days after

Table 4.8: Overview of static test piles Limelette.

Pile testing

The static load tests were performed 2.5 to 5 months after installation of the piles. As a reaction force, a rolling 4200 kN dead load system was used. This enabled the load tests in 3 rows of 4 piles, ensuring a minimum amount of time required to move the setup. Steel slabs of Sidmar were used as ballast. A schematic overview of the load frame is given in Figure 4.51.

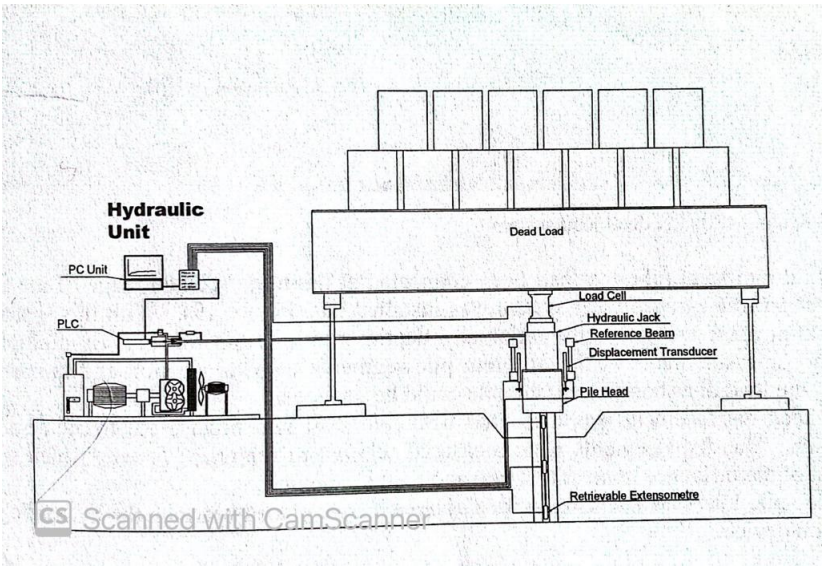

Figure 4.51: Static load test setup (Maertens and Huybrechts 2003).

A hydraulic jack was placed between the pile head and reaction frame to load the piles. The jack was regulated by a high precision hydraulic unit designed by the BBRI. One of the pumps was connected to a computer which also collected all other measurements, so that the load could be applied in a consistent manner. Therefore, the load could be kept constant without a 5 kN precision during a load step.

The head displacement of the piles was measured with four electronic displacement transducers, each with a precision of 0.01 mm. The measurements were referenced relative to reference beams that had been placed outside of the zone of influence of the piles. The applied load at the pile head was measured with a dynamometer, situated between the hydraulic jack and the reaction frame.

The **pile load scheme** was performed according to the Belgian national advisory committee. The maximum test load Q_{max} was determined before the test in order to induce pile failure (Maertens and Huybrechts 2003).

- Enforcing 10 constant load steps with ΔQ until Q_{max} is achieved;
- Holding each load step constant for 60 minutes;
- No intermediate unloading cycles during the static load test;
- Carrying out the load test until a pile head settlement $s_0 \geq 15\%$ of D_b is reached
- Unloading in 4 steps of 10 minutes each, except for total unloading.

When the pile head settlement has reached 25 mm and the pile head penetration rate is smaller than 0.6 to 0.8 mm/min, the next load step is halved. A graphical representation of the loading scheme is shown in Figure 4.52. After the loading tests were completed, the piles were excavated and studied. This included documenting the actual pile diameters, as shown in Figure 4.50b.

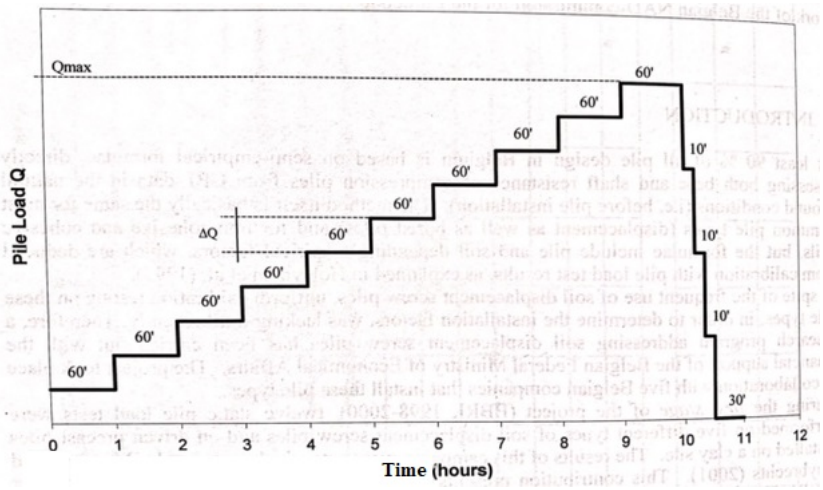

Figure 4.52: Loading scheme for static test piles Limelette (Maertens and Huybrechts 2003)

At the end of the pile tests, the piles were extracted and examined. This included measurements on the shaft diameter, concrete quality and structural integrity of the piles. An example presented by the book is shown in Figure 4.50b.

Pile instrumentation

A retrievable extensometer system was installed in a 50 mm diameter steel tube, connected at the reinforcement cage of the piles. This system enabled the measurement of pile deformations at 6 levels between the pile head and tip. However, the strain measurements are not presented in the book by Maertens and Huybrechts (2003) and can therefore not be analysed. Detailed information on the type of gauges is also missing. Though, the book does present the base settlement s_b in its load settlement graphs, which are used in coming analysis of the pile tests at Limelette.

4.4.2 Limelette - Test notes

Several important factors influenced the outcome of the pile tests and must be noted and discussed. The ones relevant are (Maertens and Huybrechts 2003):

- Due to the 60 minutes of constant load steps employed in the procedure, loaded piles were able to creep during the test. This softened the load-settlement response, of which data was only recorded at the end of each load step. Therefore, it is not possible to quantify the amount of creep.
- For Olivier pile A2, the load frame reached its maximum load before the pile reached a settlement of 10% D_b.
- Olivier pile C2 reached structural pile rupture before the conventional failure load was attained.
- Problems with concrete fluidity for the Fundex piles (A1 and C1) resulted in the segregation of concrete in pile C1 (Maertens and Huybrechts 2003), causing an early structural failure. Therefore, the test results of pile C1 (Figure 4.56g) will be disregarded.
- The measured pile volumes for Omega piles A3 and C3 were 14% and 43% higher, respectively, compared to the nominal pile volumes (Maertens and Huybrechts 2003). This is higher than for all other piles, especially for pile C3. This may be caused by the high-pressure concrete injection method used in soft soil, or upwards soil transportation caused by the auger during installation. The latter is suggested by Maertens and Huybrechts (2003) to be the cause of the large local

variation seen in pile C3 (Figure 4.50b). During the installation of pile C3, the auger was moved upward several times, likely creating the void which was later filled with concrete.

4.4.3 Limelette - Pile factor determination

Due to the unavailability of the strain measurements in the book by Maertens and Huybrechts (2003), it was impossible to accurately determine the α_p and α_s factors for these piles. For the load-settlement analysis, it was decided to use the pile factors determined from the tests at Maasvlakte 2 (Section 4.1.3). The factors found at Maasvlakte 2 are the most reliable in the database due to the number of measurements and thorough analysis performed by Duffy et al. (2021). Applying this to the piles at Limelette provides an opportunity to see how these factors perform when used on different pile types at a different location.

α_p The peak α_p value found at the Maasvlakte 2 tests (Section 4.1.3) is used: 0.35.

α_s **sand** As above, an α_s in sand of 0.011 is used, found at the Maasvlakte 2 test (Section 4.1.3).

α_s **clay** The α_s values provided in the NEN9997-1 range from 0.2 to 0.3 for clay. However, load-settlement predictions with these numbers indicated that the calculated capacity was consistently too low (shown in Figure 4.53a. With the choice of α_p and α_s in sand considered reliable, it was suspected that the NEN values in clay are not realistic for the stiff clay found at the Limelette site. This is likely because the values in the NEN are based on the softer and weaker clays commonly encountered in the Netherlands.

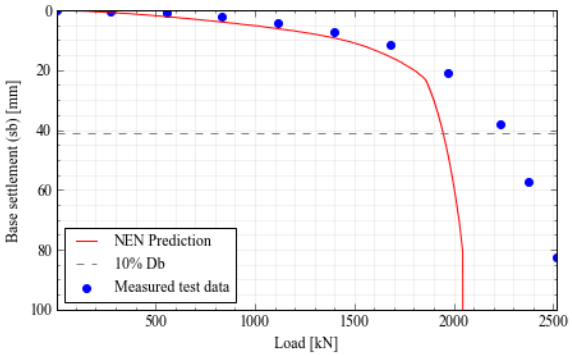

(a) NEN prescribed α_s in clay, between 0.02-0.03.

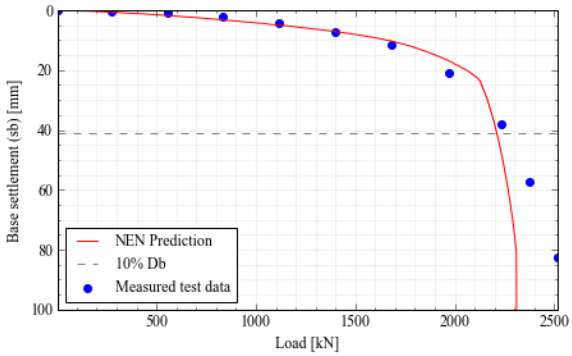

(b) Adjusted α_s in clay, between 0.025-0.0375.

A recent paper by Doan and Lehane (2021) provides an alternative view on appropriate α_s factors. Using the graph and formula shown in Figure 4.54, one will find β_c values between 25 and 40 for clay. This corresponds to α_s values between 0.025 and 0.040. Therefore, it was decided to allocate α_s factors following the protocol as described in NEN9997-1, but multiplying them with a factor 1.25. This brings the values in line with the findings of Doan and Lehane (2021) and are representative for the stiff clay found at Limelette. Load-settlement predictions made with these adjusted α_s factors in clay between 0.025 and 0.0375 provide results much closer to the measured data, shown by Figure 4.53b.

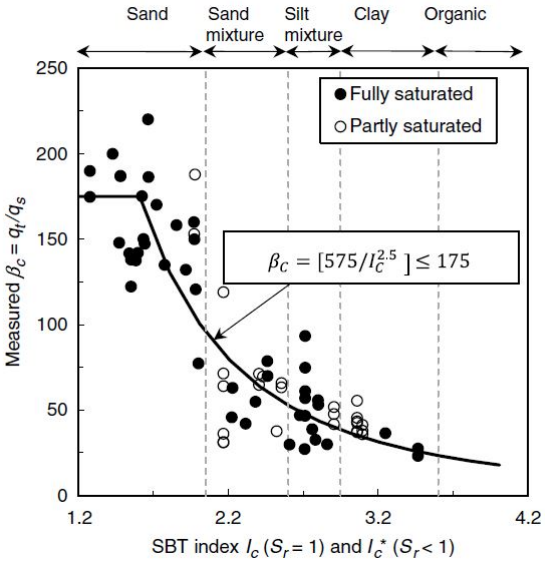

Figure 4.54: Comparison of β_c values in partly and fully saturated soils (Doan and Lehane 2021)

4.4.4 Limelette - Analysis and results

In order to find the influence of q_c limiting, different load-settlement curves and the pile factors described in NEN9997-1, several variations are presented in Figure 4.55.

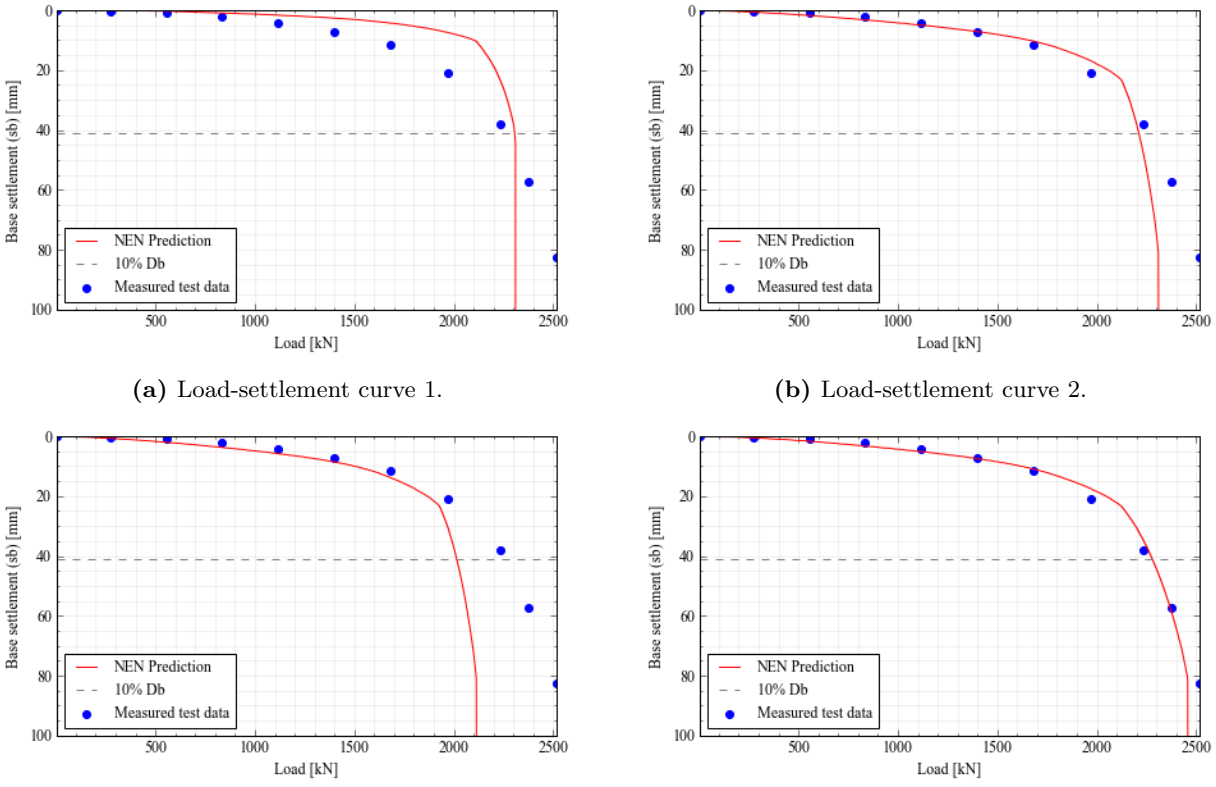

(a) Load-settlement curve 1.

(b) Load-settlement curve 2.

(c) Load-settlement curve 2, with q_c limiting.

(d) Curve 2; NEN α_p 0.63, α_s 0.009, α_s clay 0.02-0.03.

Figure 4.55: Presentation of the effects different load-settlement curves, q_c limiting and NEN prescribed α factors. Based on data from Pile C4.

Figure 4.55a shows the prediction with load-settlement curve 1. This option differs significantly from

the measured data on two aspects. First, the predicted shaft mobilisation is much stiffer than measured. Second, the predicted pile base capacity is fully mobilised after 10% D_b, where the measured data clearly shows that the base continues to mobilise after this point.

Figure 4.55b presents the option with load-settlement curve 2. The predicted shaft mobilisation follows the measured data well. In addition to this, the use of curve 2 also shows the predicted base mobilisation increasing after 10% D_b, as the measured data indicates.

The effect of limiting q_c along the shaft is indicated in Figure 4.55c. Due to large parts of the pile being situated in clay, the effect of limiting q_c to a maximum of 15 MPa is relatively small. However, the difference between Figures 4.55b and 4.55c clearly shows that the overall capacity and behaviour of the pile is less accurate with limiting applied. Values of q_b at the base do not reach over 15 MPa with the suggested α_p values and are thus unaffected by limiting rules.

Figure 4.55d shows a load-settlement prediction with the currently prescribed pile factors in the NEN. The predicted behaviour is closest to the measured data out of all presented options. However, due to the lack of strain data for the Limelette site, the validity of these values cannot be confirmed by measurements. Therefore, the possibility remains that this combination of factors simply coincidentally happens to produce a good prediction.

The behaviour of the piles is best approached by load-settlement curve 2 with no q_c limiting along the shaft. Figures 4.56 and 4.57 show the best fitting load-settlement behaviour predictions for the piles tested at Limelette. Whilst the prediction is off for some of the piles, it simulates the general behaviour of the piles well, especially the that the piles are still significantly mobilising base capacity after 10% D_b. Based on the results shown in Figure 4.55 and 4.56, the following findings can be noted:

- The problems described in 4.4.2 during load testing for Olivier piles A2 and C2 (Figure 4.56b and h) impaired the base resistance to fully mobilise. Therefore, even though the prediction curves fit well, there remains a significant uncertainty in the behaviour of the base mobilisation of the Olivier piles.
- Fundex pile C1 (Figure 4.56g) is disregarded as structural failure of the pile occurred due to improper concrete fluidity (described in 4.4.2).
- Omega piles A3 and C3 attain higher capacities than predicted, especially Pile C3 (Figure 4.56i). This is caused by the larger pile diameters as explained in 4.4.2. Essentially, that means that the input parameters for the model are too small, and thus the capacity of these piles is underestimated.
- Load-settlement curve 2, without limiting q_c values, provides the most realistic pile response predictions.
- An α_p of 0.35, α_s in sand of 0.011, and NEN values of α_s in clay with factor 1.25× produce realistic capacity and load-settlement predictions.
- Load-settlement curve 2 predicts the overall pile response best, which highlights the less stiff shaft and base mobilisation of the screw piles, which resembles behaviour found on (partly) soil replacing piles.

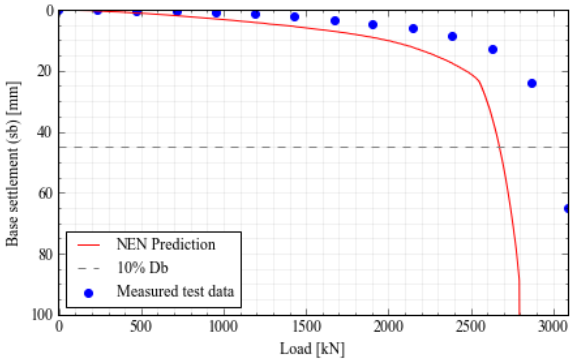

(a) Pile A1

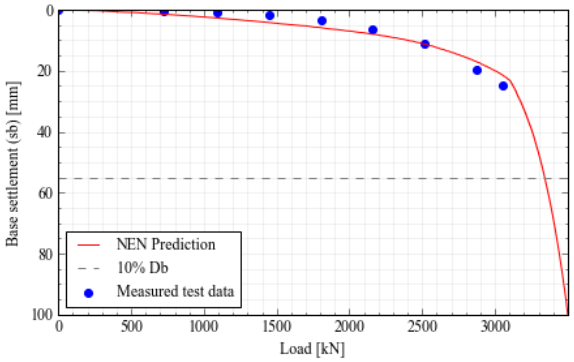

(b) Pile A2

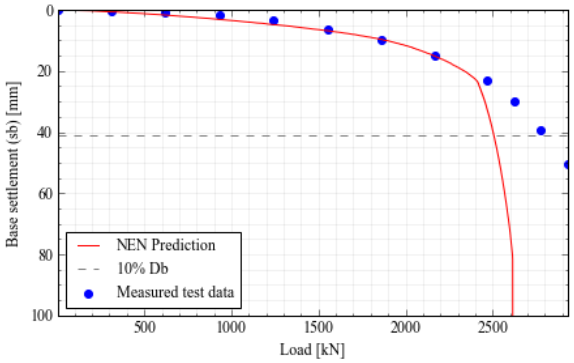

(c) Pile A3

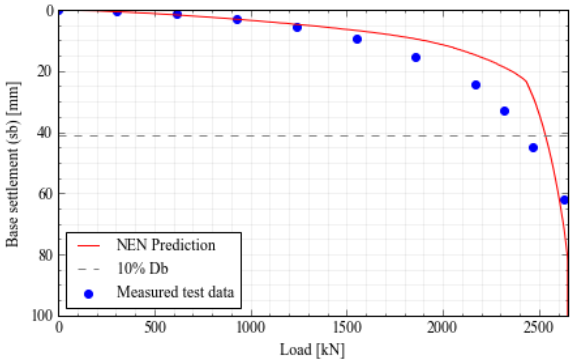

(d) Pile A4

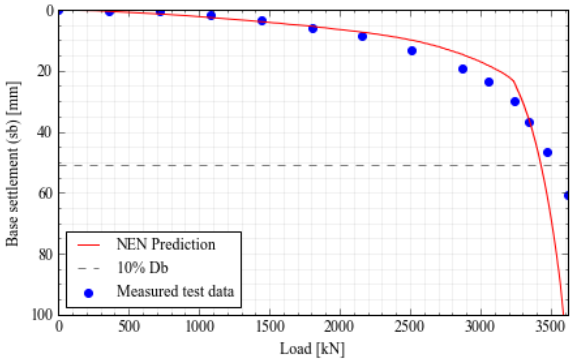

(e) Pile B3

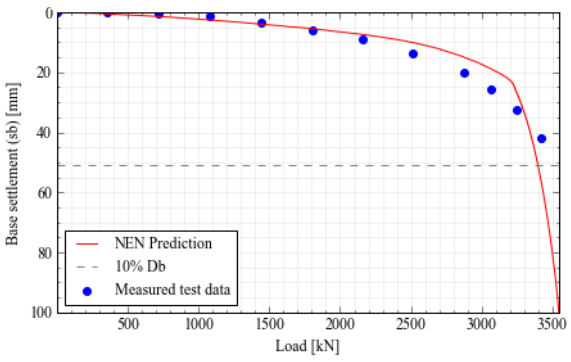

(f) Pile B4

Figure 4.56: Load settlement predictions for Limelette piles, with α_p 0.35, α_s in sand 0.011, α_s in clay 1.25x the values prescribed by the NEN.

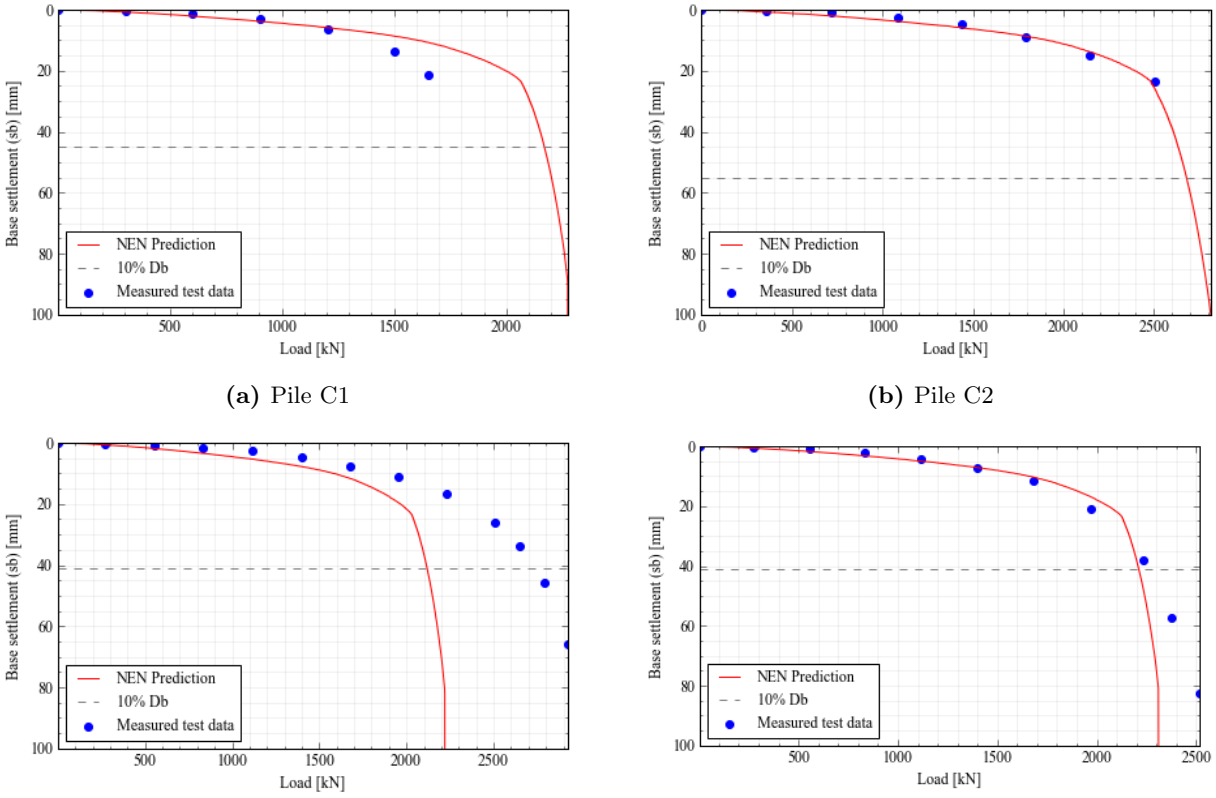

(a) Pile C1

(b) Pile C2

(c) Pile C3

(d) Pile C4

Figure 4.57: Continued: load settlement predictions for Limelette piles, with α_p 0.35, α_s in sand 0.011, α_s in clay 1.25x the values prescribed by the NEN.

4.4.5 Limelette - Conclusions

Based on the findings and analysis performed on the Limelette test, it may be concluded that:

- The significant influence of installation effects on overall pile capacity is exemplified by the overexcavation of the Omega piles, and insufficient concrete fluidity of the Fundex piles.
- The use of an α_p factor of 0.35 and α_s in sand of 0.011 provides predictions in agreement with the load test data.
- Multiplying the NEN α_s factors in clay with factor 1.25× provides results closer to the measured data. These increased values, between 0.025 and 0.0375, are supported by recent literature; and provide realistic predictions in combination with α_p 0.35 and α_s in sand 0.011.
- Limiting q_c values along the shaft as prescribed by NEN9997-1 reduces the accuracy of capacity and load-settlement predictions.
- The behaviour of the screw piles at the Limelette test site more closely resembles load-settlement curve 2, indicating that these piles behave like (partly) soil replacing piles.

4.5 Sonate

A rapid load test (RLT) performed at Sonate, Den Haag is described in the article by IJnsen et al. (2020). Three screw injection piles were installed and tested, founded mostly in sand. Grout injection took place during the screwing process.

4.5.1 Sonate - Overview

Ground investigation

The soil encountered is mainly sand, with a thin layer of clay. The soil investigation until -2.75 m NAP is inconclusive, and therefore q_c values until this depth will not be taken into account. A CPT profile and soil classification is given in Figure 4.58a. The soil layers (depth in m NAP) can be classified as:

- $>$ -2.75 m: mix of clayey sand, peat and clay (q_c values disregarded in calculations)
- -2.75 to -15.75 m: medium dense to dense sand (some local clay lenses)
- -15.75 m to -16.25 m: clay
- -16.25 m to 31.0 m: dense sand

Pile specifications

The screw-injection piles used were of type HEKbuispaal. This is a Type 3 (permanent steel casing) pile, very similar to the piles used at the Maasvlakte 2 tests. The piles have a base diameter of 850 mm and a shaft diameter of 710 mm. Due to the grout injection, the nominal shaft diameter D_s is considered 0.85 m. The piles were founded at level -18 m NAP.

In order to mobilise as much base resistance as possible, it was decided to flush the pile shaft until a level of -13 m with a Dämmer (bentonite) mix after the installation of the pile. The aim of this was to reduce the positive skin friction as much as possible, thus transferring as much load as possible towards to lower part of the pile. Special injection tubes were installed along the pile to enable the flushing. However, it is noted by IJnsen et al. (2020) that the effect of the bentonite flush was less than expected.

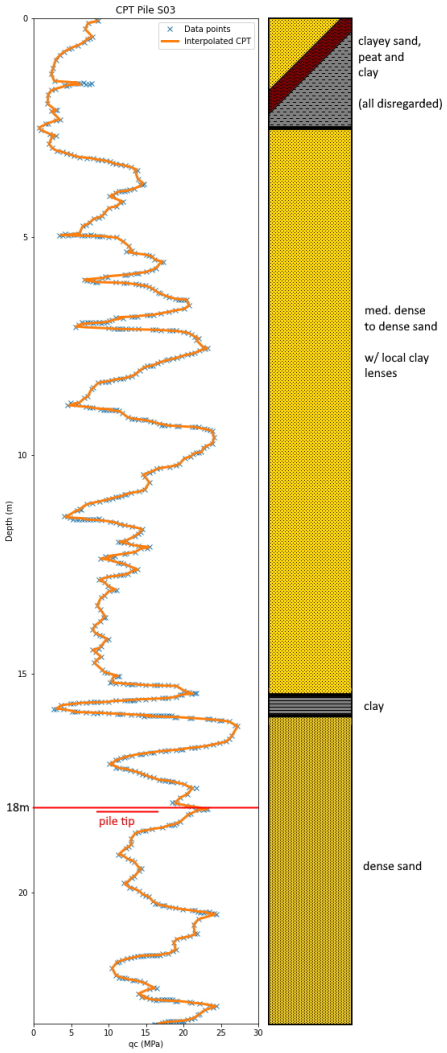

(a) CPT data and soil classification for Sonate test.

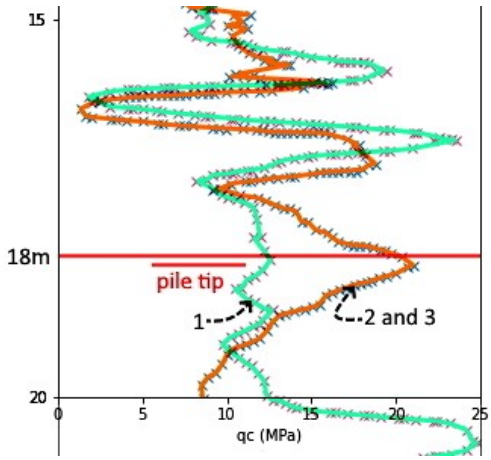

(b) Indication of CPT q_c difference around pile tip between 1 and 2 & 3 (edited from (IJnsen et al. 2020)).

Figure 4.58

Pile testing

The rapid load test was performed as a class A2 test (NPR 2017). The firm Allnamics supplied the machinery and interpretation of the measurements. A StatRapid test was used, with a mass of 40 tonne. This enabled a rapid load of 12 MN.

Pile instrumentation

Strain gauges were installed at two levels of the pile, at -13 m NAP and 0.5 m above the pile tip. Further specifications of the gauge type and their raw measurements are not supplied in the article.

A noticeable quirk from the CPT readings is that the q_c found at the pile base level for pile P1 is significantly lower than encountered at piles P2 and P3. This has a large influence on the calculated $q_{c,avg}$ which mainly determines the predicted base capacity of the pile. Figure 4.58b illustrates the different readings around the pile tips.

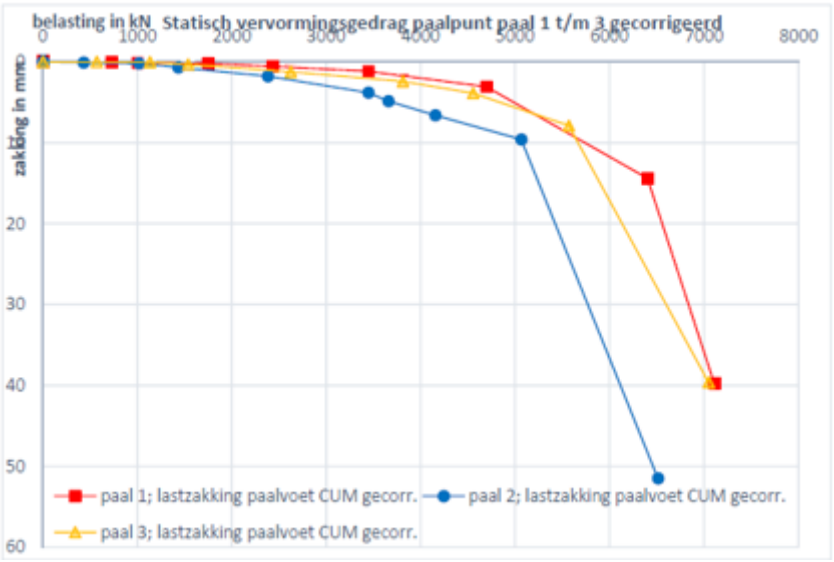

Figure 4.59: "Corrected" load-settlement data for piles 1-3 (IJnsen et al. 2020).

The load-settlement data recorded by the RLT is shown in Figure 4.59. The data points have been corrected, so that the shaft friction for each load step can never be higher than that recorded during the final cycle. There are no data points available for larger settlements: Figure 4.59 shows that not even 10% D_b is reached. This complicates the comparison of load-settlement predictions, especially at larger settlements.

4.5.2 Sonate - Test notes

- The discrepancy between the CPT profile of Pile 1 and P2/3 means that the predicted base capacity of Pile 1 will be noticeably lower.
- The load-settlement measurements are generated by a rapid load test, thereby reducing the reliability of the data.
- No measurement data is available after 10% D_b. This will complicate the judgement of different load-settlement prediction curves.

4.5.3 Sonate - Pile factor determination

Pile factors could not be determined from a strain data analysis. Therefore, the α factors found from the measurements at Maasvlakte 2 (Section 4.1.3) are applied.

α_s **clay** Being only a thin layer, the influence of the clay on the whole pile capacity is limited. A factor of 0.03 is applied to the clay layer, in accordance with NEN9997-1.

α_s **sand** An α_s of 0.011 is applied to the sand, determined from the Maasvlakte 2 tests (Section 4.1.3).

α_p The selected α_p is 0.35, based on Section 4.1.3.

4.5.4 Sonate - Analysis and results

The influence of different load-settlement curves and q_c limiting is investigated in Figure 4.60.

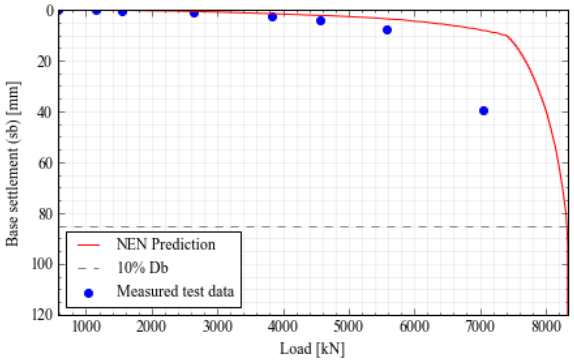

(a) Load-settlement curve 1.

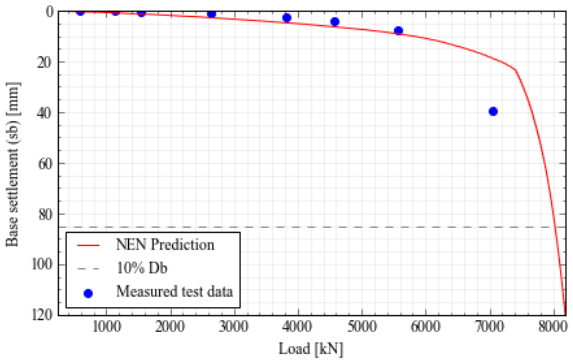

(b) Load-settlement curve 2.

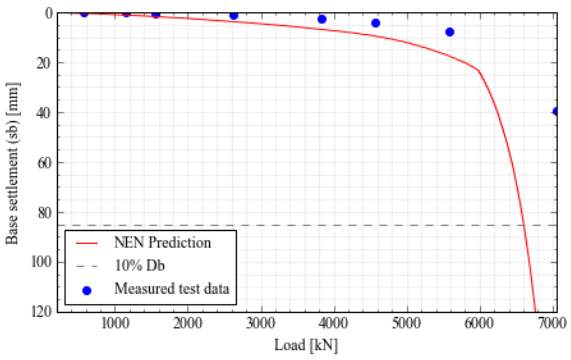

(c) Load-settlement curve 2; with q_c limiting along shaft.

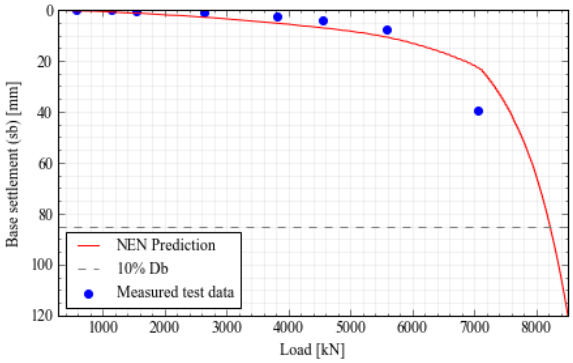

(d) Curve 2; with NEN α_p 0.63 and α_s sand 0.009.

Figure 4.60: Presentation of the effects of different load-settlement curves, q_c limiting along the shaft and the currently prescribed NEN pile factors. Based on data from Pile 3.

Figure 4.60a shows the load-settlement prediction using curve 1. The initial mobilisation, especially along the shaft, is stiffer compared to the measured data.

Load-settlement curve 2 is depicted in Figure 4.60b. The softer response agrees more with the measured data points, and also shows the base continuing to mobilise after 10% D_b.
Figure 4.60c shows the effect of limiting q_c along the shaft. The total capacity of the pile is reduced by more than 1000 kN and producing a load-settlement prediction which does not agree well with the data points. With $q_{c,avg}$ values well below 15 MPa, the maximum base resistance q_b is unaffected by any limiting.

Application of the currently applied NEN α factors is shown in Figure 4.60d. The predicted line agrees well with the measured data points. The decrease in shaft friction is compensated by the significant increase of α_p. However, due the unavailability of strain measurements, these values cannot be verified.

Based on the above described analysis, the best fit is selected to be load-settlement curve 2 and no q_c limiting along the shaft. The prediction results with these options are shown in Figure 4.61. Note that due to the discrepancy in CPT readings, a prediction for Pile 1 with the CPT profile of Pile 3 is shown in Figure 4.61b. This provides an accurate simulation of the actual behaviour of Pile 1.

The following findings can be noted based on the performed analysis:

- Due to the data stemming from a rapid load test and being limited to around 10%D_b, the reliability of the analysis is comparatively lower than the other discussed tests.
- The difference in results for Pile 1 with a different profile clearly demonstrate this. The largest

influence on pile capacity prediction remains the CPT profile the calculations are based on.

- Load-settlement curve 2 without q_c limiting provides the best prediction.
- The application of factors α_p 0.35 and α_s sand 0.011 provide appropriate capacity and response predictions.
- The general behaviour of the piles is best approximated by load-settlement curve 2. This indicates that these screw-injection piles resemble behaviour found on (partly) soil replacing piles.

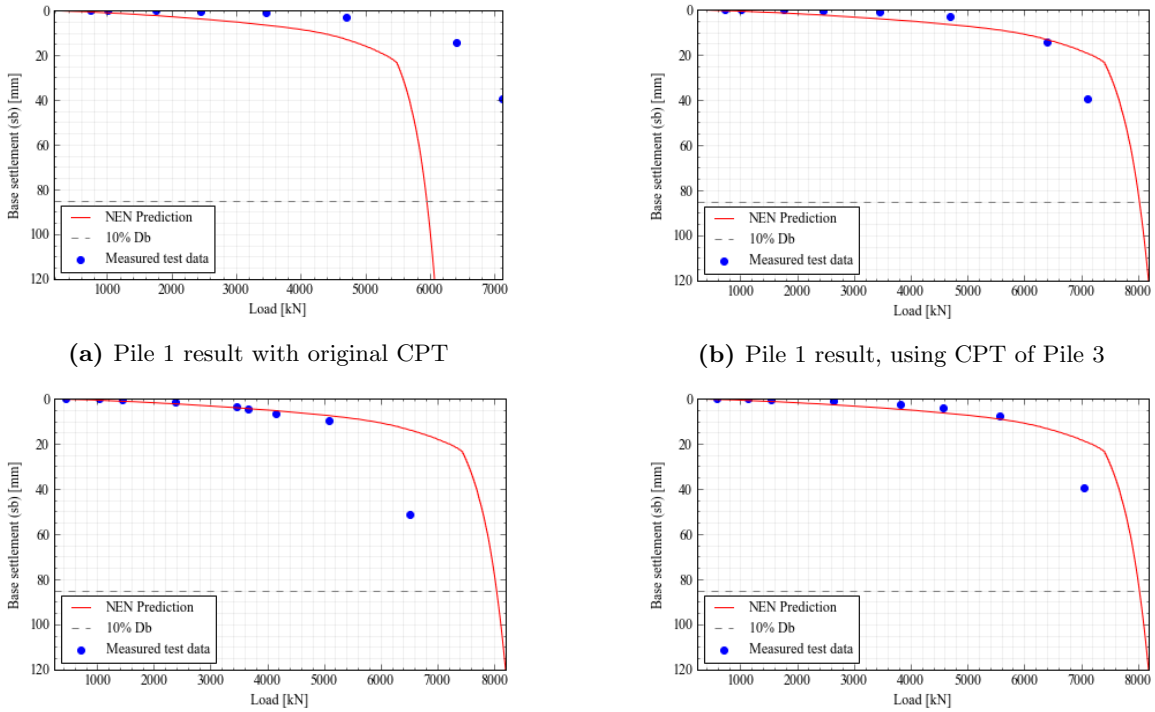

(a) Pile 1 result with original CPT

(b) Pile 1 result, using CPT of Pile 3

(c) Pile 2 result

(d) Pile 3 result

Figure 4.61: Results of load-settlement prediction for Sonate piles, with α_p 0.35, α_s in sand 0.011 and α_s in clay 0.03. Note the more accurate prediction for Pile 1 using the CPT profile of Pile 3 in Figure 4.61b.

4.5.5 Sonate - Conclusions

The analysis performed on the test leads to the following conclusions:

- Application of α_p 0.35 and α_s in sand 0.11 produces realistic results.
- Limiting q_c values along the shaft as prescribed by NEN9997-1 results in less realistic capacity and response predictions.
- The load-settlement behaviour of the screw-injection piles most closely resembles curve 2, which suggests that the piles behave akin to (partly) soil replacing piles.

4.6 Grout sand content: Thijsseweg Delft

Fundex and Tubex screw-injection piles were installed at a site along the Thijsseweg in Delft on 31 January and 1 February 2022. Due to the timing of this report, the testing campaign is not included. However, findings on the grout composition during the installation are relevant to the research and therefore included. Besides the location of each pile, a ditch was dug as to collect the outflowing grout from the borehole. This could then be collected using a pitcher, after which the grout was poured in a container so its volume and unit weight could be measured. The samples were then sieved to weigh the amount of sand in the mix, whereafter the sand content in the grout could be determined. Figure 4.62 shows the method used to collect outcoming grout. As mentioned previously, this analysis contains a lot of assumptions. Sand from the topsoil could have intermixed slightly with the outcoming grout, and it proved difficult to separate the sand from the mix, even with sieving.

Figure 4.62: Grout collection during the installation of one of the Tubex piles at Thijsseweg. Outcoming grout would flow into the ditch, allowing for safe collection.

Not for every pile installed could outcoming samples be taken. Only during the third pile installed on 31 January did grout actually flow out of the borehole. Opinion is site was that most of the excess grout had likely flown into a thick, porous peat layer. After that layer was saturated, grout started flowing upwards. However, outcoming samples could be taken on a constant basis during installation of the third Tubex piles and all three Fundex piles. Provisional findings (as of 21/02/22) indicate that the sand content in the outcoming samples reached values between 20 and 30%, compared to 0% in the incoming grout.

These findings compare well to those made during the Maasvlakte 2 test campaign, where similar observations were made. Therefore, although it is difficult to ascertain the exact amount of soil transported out of the borehole, the findings support the claim that screw-injection piles are not fully soil-displacing, exemplified by the significant amount of sand in the outcoming grout.

4.7 Summarised conclusions from database analysis

The most important findings from this chapter are shown in Table 4.9 and summarised in the conclusions below:

- **Load-settlement behaviour:** In general, the behaviour of screw and screw-injection piles is best represented by load-settlement curve 2. This resembles behaviour like that seen in (partly) soil replacing piles. Sand content between 20 and 40% found in outcoming grout samples support the claim that screw-injection piles are not fully soil displacing. This does not apply to screw piles installed without grout injection, so it is likely that the softer load-settlement response is partly caused by installation effects. Decidedly, the load-settlement behaviour of screw and screw-injection piles is softer than is currently prescribed in the Dutch design method.

- α_p **factor:** Values found for α_p ranged from 0.23 to 0.35 for the instrumented tests. The uninstrumented tests provided convincing load-settlement predictions with an α_p factors of 0.35. Overall, the α_p factors in this thesis range from 0.23 to 0.35. This is significantly lower than the currently prescribed value of 0.63 in the Dutch design method.

- α_s **in sand:** the value of α_s deduced from Maasvlakte 2 and Rosmalen indicate 0.011. The analysis of Beemster found a value of 0.012. The application of 0.011 on the uninstrumented tests provided realistic results. The range of α_s found in the thesis of 0.011-0.012 is significantly higher than the prescribed 0.009 in the Dutch design method.

- α_s **in clay:** Although the investigation of α_s in clay remained limited in this thesis, the factors (between 0.02 and 0.03) as prescribed in the Dutch design method provided an accurate prediction in soft and weak clays commonly found in the Netherlands. In the case of Limelette, where most of the shaft was enclosed by heavily consolidated clay, the current factors did not accurately predict the capacity and behaviour of the piles. To correct these values for the stiff clay it was suggested, supported by recent literature, to apply a multiplication factor of 1.25 to increase the α_s in clay to between 0.025 and 0.0375.

- **Pile tip shape:** The tests at Rosmalen and Beemster indicated that there was no noticeable difference in capacity and load-settlement response between piles with flat tips and conical or pyramid tips. No evidence was found that the shape of the pile tip affects the capacity or response of the pile.

- **Shaft diameter assumption screw-injection piles:** The excavation of the screw-injection piles at Rosmalen proved that using the base diameter D_b to approximate the actual diameter of the grout body D_s was not accurate. The average measured shaft diameters ranged from 0.44 m to 0.53 m, compared to an assumed value of 0.40 m. Clearly, the actual in-situ pile shaft diameter was not assumed correctly. However, when predicting the pile capacity, the input variables must be based on known data. Assuming D_b as D_s for screw-injection piles during design calculations was shown to realistically predict pile capacity and load response.

- **Influence of CPT profile:** The largest source of information for determining the overall pile capacity is the CPT profile. As revealed by the results of Pile 1 of the Sonate test, significantly lower q_c values in the CPT profile around the pile tip caused the load-settlement prediction to be inaccurate, though this may also be related to the choice of averaging method used.

- **Installation effects:** The pile testing campaign at Limelette illustrated the consequences of several installation effects. Overexcavation of the Omega piles caused significant local increases in the pile diameter, which in the case of type 1 piles does not necessarily decrease pile capacity, but did substantially increase concrete consumption. Furthermore, problems with concrete fluidity of the Fundex piles caused these piles to reach structural failure long before the designed capacity

was reached. In general, the screwing motion during installation can reduce the adhesive force of clays and may cause overexcavation of the soil directly surrounding the pile. These negatively affect the radial stresses acting on the pile. Moreover, lateral soil transport and grain crushing under the pile tip can cause a reduction in stiffness of the base resistance. The consequences of the screwing motion during installation likely contribute to the softer load-settlement response seen in test results, when compared to fully displacing piles. Evidently, these installation effects may strongly influence the overall capacity of a pile. However, they cannot always be controlled: if a pile gets stuck during installation, overexcavation might be the only way to continue.

Pile test	**Maasvlakte 2**	**Beemster Scale**	**Rosmalen**	**Limelette**	**Sonate**
Test type	Static	Static	Static	Static	Rapid
No. of piles	4	4	5	10	3
Pile type(s), Brand name	Type 3, Terr-Econ	Type 1, unspecified	Type 3, unspecified	Type 1+2, Fundex, Atlas, Olivier, De Waal, Omega	Type 3, HEKbuispaal
Screw or screw-injection	Screw-injection	Screw	Screw-injection	Screw	Screw-injection
Soil along shaft	Sand	Sand	Sand	Clay	Sand
Soil around base	Sand	Sand	Sand	Sand	Sand
Shaft/base load splitting	Yes	Yes	Yes	No	No
Method load splitting	Fibre optic	Fibre optic	Separate load cell for pile tip	-	-
Strain gauge method(s)	FBG, BOFDA	FBG	-	-	-
Investigation on pile tips	-	Yes, flat and conical	Yes, flat and pyramid	-	-
Piles excavated?	No	Yes	Yes	Yes	No
Shaft diameter [m]	0.61	0.12	0.4	0.36-0.41	0.71
Measured shaft diameter [m]	-	0.12	0.44-0.54	0.39-0.55	-
Base diameter [m]	0.85	0.15	0.4	0.41-0.55	0.85
Load-settlement curve best fit	2	2	2	2	2
Determined α_p	0.35	0.27	0.23	-	-
Determined α_s, sand	0.011	0.012	0.011	-	-
Fitted α_p	0.35	0.27	0.23	0.35	0.35
Fitted α_s, sand	0.011	0.011	0.011	0.011	0.011
Fitted α_s, clay	0.02-0.03	-	-	0.025-0.0375	0.02-0.03
Difference between pile tip shapes?	-	No	No	-	-
q_c limiting along shaft?	No, limiting produces less accurate results	No, limiting produces less accurate results	No, limiting produces less accurate results	No, limiting produces less accurate results	No, limiting produces less accurate results
q_b limited to 15 MPa?	Not affected with stated pile factors	Not affected with stated pile factors	Not affected with stated pile factors	Not affected with stated pile factors	Not affected with stated pile factors

Table 4.9: Overview of pile test database results.

Chapter 5

Conclusion and recommendations

The thesis aims to answer the following research question: *Should screw and screw-injection piles be classified as fully displacing piles, and how can the design process be improved through the interpretation of existing load tests?* Aiding the main question, the following sub-questions are defined:

How do the measurements of screw and screw-injection pile load tests compare to the load-settlement behaviour of fully displacing and (partly) soil replacing piles?

The investigation of existing load tests shows that the measured load test data more closely resembles that of load-settlement curve 2, instead of the currently by NEN9997-1 prescribed curve 1. This implies that the load-settlement response of screw and screw injection piles compares best to (partly) soil replacing piles rather than fully displacing piles. The discussed tests in the database present a softer, slower mobilisation of the shaft friction and indicate a continued base mobilisation after 10% D_b. Both of these aspects are not expressed by load-settlement curve 1, but are correctly modelled with load-settlement curve 2.
Furthermore, analysis of incoming and outcoming grout samples of screw-injection piles indicated a sand content between 20% and 40% in the outcoming grout. Though only directly applicable to screw-injection piles, it supports the notion that these piles are not fully displacing.

Does limiting the cone resistance values q_c and maximum tip resistance q_b as prescribed in NEN9997-1 provide realistic estimates of the pile capacity?

The results from the load test analysis show that none of the piles reach a value of q_b above 15 MPa with the applied α_p factors. Therefore, no observations on the effect of limiting q_b can be made.
However, the results demonstrate that limiting q_c values along the shaft to a maximum of 15 MPa, as prescribed in NEN9997-1, does not provide realistic results. It has been shown that when applying this limit on q_c values, the predicted pile capacity and load-settlement response deviate from the measured data. Although this is more prevalent in tests with dense sands, even results from tests in softer soils produce less favourable results with q_c limiting.

How do the currently prescribed α_p and α_s factors in NEN9997-1 compare to real pile tests?

The currently prescribed α_p factor for screw and screw-injection piles is 0.63. The load tests of Maasvlakte 2 and Beemster, instrumented with strain gauges, have indicated α_p factors of 0.35 and 0.27, respectively. The Rosmalen load test, which separately measured the load at the pile tip,

demonstrates an α_p of 0.23. Load-settlement predictions for the uninstrumented tests have shown that realistic results have been attained using α_p 0.35. The currently prescribed α_p value of 0.63 is significantly higher than the α_p factors found in existing load tests, in the range of 0.23-0.35.

The α_s factor is sand is currently prescribed as 0.009. The tests of Maasvlakte 2 and Rosmalen indicate α_s factor of 0.011. The Beemster test shows a value of 0.012. Application of an α_s of 0.011 in the uninstrumented tests provided results close to the measured test data. The overall results indicate an α_s in sand of in the range of 0.011-0.012, which is noticeably higher than the currently prescribed 0.009.

During the Maasvlakte 2 pile load tests, strain-softening behaviour has been measured. It has been theorised that this behaviour is caused by the debonding between the steel shaft and the grout body surrounding it. A laboratory experiment has been performed to investigate the behaviour of the steel/grout interface. The roughness of the steel, and the water cement factor (WCF) of the grout mix have been varied. The results show that shear stress under which adhesive failure occurs is mostly dependent on the roughness of the steel. Variations of the WCF do not show differences in adhesive failure. Furthermore, no difference between the results is seen between a normal force of 912 and 1459 kPa. The experiment shows that, under normal stresses generated by very dense soils, adhesive failure between steel and grout can occur. Therefore, the debonding between the steel tube and surrounding grout body is a plausible explanation for the strain softening seen at Maasvlakte 2.

In clay, the prescribed α_s factors range from 0.02 to 0.03, depending on the value of q_c. In all but the Limelette pile test, only thin clay layers have been encountered. In these tests with limited clay, the influence of α_s cannot accurately be investigated, although the use of the prescribed values provides reliable results. At Limelette, where most of the pile shaft is founded in stiff overconsolidated clay, it is found that the prescribed α_s factors for clay underestimate the capacity along the shaft. Recent literature recommends values for clays in the range of 0.025 to 0.04. Therefore, the prescribed values have been multiplied with factor 1.25 for the considered test, to values of 0.025 to 0.0375. Results from the Limelette test show that these values provide realistic predictions in stiff clay.

During the investigation into the α_s factor of the Rosmalen test, attention was drawn to an assumption made when designing screw-injection piles. This assumption is that the diameter of the grout body surrounding the pile may be approximated by using the diameter of the pile base, i.e. $D_s = D_b$. However, excavation of the screw-injection piles shows that the true shaft diameters range from 0.44 m to 0.53 m, compared to an assumed 0.40 m. Clearly, the actual in-situ pile shaft diameter of screw-injection piles is not well approximated by this assumption. However, during pile design, calculation variables must be based on known dimensions. The results of the load-settlement tests show that predictions made with the assumption $D_s = D_b$ produce realistic predictions of the pile capacity and behaviour.

Furthermore, the influence of the pile tip shape on α_p and pile response is analysed in the load tests of Beemster and Rosmalen. In both cases, the pile capacity and load-settlement behaviour indicate no discernible difference between flat, cone and pyramid shaped pile tips. Therefore, it may be stated that the shape of the pile tip does not noticeably influence the capacity and load-settlement response of screw and screw-injection piles.

What influence do the installation effects of screw and screw-injection piles have on the load-settlement behaviour?

Although the installation effects of screw piles remain difficult to determine, the screwing motion during installation can reduce the adhesive force of clays, and cause overexcavation of the soil immediately

surrounding the pile. These both result in a reduction of radial stresses acting on the pile. Moreover, lateral soil transport and grain crushing under the pile tip can cause a reduction in stiffness of the base resistance. The aforementioned effects of screwing likely contribute to the softer load-settlement behaviour in screw and screw-injection piles, when compared to driven piles. Collection of incoming and outcoming grout samples has shown that grout injection can cause upwards soil transportation out of the borehole. It is further demonstrated in one of the tests that overexcavation due to excessive rotations can cause significant local increases in pile diameter. In the described case, the cavity could be filled at the cost of extra concrete. However, depending on the pile type, this may also cause a severe reduction in radial stresses acting on the pile shaft, lowering the overall capacity. Furthermore, it has also been found that an inadequate concrete fluidity allowed air pockets to form in the drilling tube, which leads to structural failure of the pile long before the designed capacity is reached.
Evidently, installation effects can have a noteworthy impact on the capacity of a pile. However, their consequences remain difficult to ascertain and cannot always be controlled during pile installation.

Should screw and screw-injection piles be classified as fully displacing piles, and how can the design process be improved through the interpretation of existing load tests?

The interpretation of existing load tests has produced results which strongly signify that the load-settlement behaviour of screw and screw-injection piles does not resemble that of fully displacing piles. The results indicate a response similar to load-settlement curve 2 as described in NEN9997-1, which is currently prescribed for (partly) soil replacing piles, such as Continuous Flight Auger and anchor piles. Thus, this thesis suggests that the load-settlement behaviour of screw and screw-injection piles should be classified as (partly) soil replacing piles, prescribed in NEN9997-1 as load-settlement curve 2.

Investigation into the α_p factor, through strain data and separate pile tip load measurements, has shown that this lies within a range of 0.23 to 0.35 for all piles in the database. Based on the same instrumented tests, an α_s between 0.011 and 0.012 in sand has been determined. The limiting of cone resistance q_c along the shaft, as prescribed in NEN9997-1, has been shown to provide a consistent underestimation of pile capacity and load-settlement behaviour. It is suggested that the design process of screw and screw-injection piles can be improved by further investigation and revaluation of the current α factors and q_c limiting.

Bibliography

Allnamics. (2021, May 13). *Rapid Load Testing*. https://allnamics.com/en/portfolio-posts/rapid-load-testing/

APTS. (2021a, May 13). *Dynamic Load Testing*. https://allnamics.com/en/portfolio-posts/dynamic-load-testing/

APTS. (2021b, May 13). *Static pile load test*. https://www.aptsbv.nl/en/pile-tests/static-pile-load-test

Basu, P., & Prezzi, M. (2009). *Design and applications of drilled displacement (screw) piles*. Purdue University, West Lafayette, Indiana.

Bolton, M. D. (1987). Strength and dilatancy of sands. *Géotechnique*, *37(4)*, 517.

de Boorder, M. (2019). *Development of a new CPT averaging technique and review of existing CPT based methods for the calculation of total pile capacity* (Master's thesis). Delft University of Technology.

Doan, L., & Lehane, B. M. (2021). CPT-Based Design Method for Axial Capacities of Drilled Shafts and Auger Cast-in-Place Piles. *Journal of Geotechnical and Geoenvironmental Engineering*, *148*. https://doi.org/10.1061/(ASCE)GT.1943-5606.0002542.

Doherty, P., & Gavin, K. G. (2011). The shaft capacity of displacement piles in clay: a state of the art view. *Geotechnical and Geological Engineering, 29(4): 389-410*.

Duffy, K., de Lange, D., & Gavin, K. G. (2021). *Report on pile test results at Maasvlakte II*. Delft University of Technology.

Federal Highway Administration. (2021, May 14). *Design and Construction of Driven Pile Foundations - Lessons Learned on the Central Artery/Tunnel Project*. https://www.fhwa.dot.gov/publications/research/infrastructure/geotechnical/05159/chapter4.cfm

Fellenius, B. (1990). Static or Dynamic Test - Which To Trust? *Geotechnical News Magazine*, *8*, 28–32.

Fellenius, B. (2015). Static tests on instrumented piles affected by residual load. *Journal of the Deep Foundation Institute*, *9*, 11–20.

Flynn, K. N., & McCabe, B. A. (2021). Instrumented concrete pile tests - part 1: A review of instrumentation and procedures. *Proceedings of the Institution of Civil Engineers - Geotechnical Engineering*. https://doi.org/https://doi.org/10.1680/jgeen.21.00126

Franki Foundations. (2021a, April 5). *Atlas screw pile*. https://www.ffgb.be/en/techniques/piles/vibration-free-soil-displacement-piles/atlas-screw-pile

Franki Foundations. (2021b, April 5). *Omega screw pile with grout injection*. https://www.frankifoundations.co.uk/en/techniques/piles/vibration-free-soil-displacement-piles/omega-screw-pile-with-grout-injection

Funderingstechniek.com. (2021, May 15). *Screw injection pile*. funderingstechniek.com/g-grouts.html

Fundex. (2021a, April 5). *Fundex paal met groutinjectie*. http://www.fundexgroup.com/nl/expertise/23-fundex-paal-met-groutinjectie/default.html

Fundex. (2021b, April 5). *Tubex paal met groutinjectie*. http://www.fundexgroup.com/nl/expertise/26-tubex-paal-met-groutinjectie/default.html

Gavin, K. G., Kovacevic, M. S., & Igoe, D. (2021). A review of CPT based axial pile design in the Netherlands. *Underground Space*, *6*. https://doi.org/https://doi.org/10.1016/j.undsp.2019.09.004

Gavin, K. G., & O'Kelly, B. C. (2007). Effect of Friction Fatigue on Pile Capacity in Dense Sand. *Journal of Geotechnical and Geoenvironmental Engineering, 133.* https://doi.org/https://doi.org/10.1061/(ASCE)1090-0241(2007)133:1(63)

Geerling, J., Janse, E., & Kruizinge, J. (1992). *Proefbelastingen schroefinjectiepalen Rosmalen* (tech. rep. CO-329720/48). Grondmechanica Delft. Oudekerk a/d IJssel.

Heidarie Golofzani, S., Eslami, A., & Jamshidi Chenari, R. (2020). Probabilistic Assessment of Model Uncertainty for Prediction of Pile Foundation Bearing Capacity; Static Analysis, SPT and CPT-Based Methods. *Geotechnical and Geological Engineering, 38*, 5023–5041. https://doi.org/https://doi.org/10.1007/s10706-020-01346-x

Holeyman, A. E. (2001). *Screw Piles - Installation and Design in Stiff Clay.* A.A. Balkema Publishers.

Hossain, M. A., & Yin, J. H. (2004). Behaviour of a Pressure-Grouted Soil-Cement Interface in Direct Shear Tests. *International Journal of Geomechanics, 14(1), 101-109.*

IJnsen, P., Meinhardt, G., van der Sluis, A., & van Delft, M. (2020). Bepaling van projectspecifieke paalklassefactoren met een snelle paaltest. *Journal of Geotechnical and Geoenvironmental Engineering, 24-1*, 18–24.

Kaddouri, N. (2020). *The De-bonding effect on screw injection piles.* Delft University of Technology.

Karlsrud, K. (2014). Ultimate shaft friction and load-displacement response of axially loaded piles in clay based on instrumented pile tests. *Journal of Geotechnical and Geoenvironmental Engineering, 140(12): 04014074.*

Korff, M. (2020). CIE4363 Lecture 3.2: Installation of sheet piles, diaphragm walls and piled walls (chapter 6 of the reader).

Krasinski, A., & Wisniewski, M. (2018). *The mechanism of grouting action under the base of bored pile.* Gdansk University of Technology, Faculty of Civil; Environmental Engineering, Poland.

Lam, C., & Jefferis, S. (2014). Ultimate shaft friction and load-displacement response of axially loaded piles in clay based on instrumented pile tests. *Journal of Geotechnical and Geoenvironmental Engineering, 140(12): 04014074.*

Larisch, M. (2014). *Behaviour of stiff, fine-grained soil during the installation of screw auger displacement piles* (Doctoral dissertation). The University of Queensland, School of Civil Engineering, Geotechnical Engineering Centre.

Li, Z., Zhang, L., Chu, Y., & Zhang, Q. (2020). *Research on Influence of Water-Cement Ratio on Reinforcement Effect for Permeation Grouting in Sand layer.* Hindawi.

Maertens, J., & Huybrechts, N. (2003). *Belgian Screw Pile Technology - design and recent developments.* Swets & Zeitlinger B.V.

NEN. (2017). *NEN 9997-1+C2:2017 nl, Geotechnical design of structures - Part 1: General rules.* Stichting Koninklijk Nederlands Normalisatie Instituut.

NeSmith, W. M. (2003). Installation Effort as an Indicator of Displacement Screw Pile Capacity.

NPR. (2017). *NPR 7201, Geotechnics - Determination of the axial bearing capacity of foundation piles by pile load testing.* Stichting Koninklijk Nederlands Normalisatie Instituut.

NVAF. (2019). *Eindrapportage Schaalproeven Hei- en Schroefpalen.* https://www.nvaf.nl/wp-content/uploads/2020/08/PR-17.0483-2-Eindrapportage-Schaalproeven-20190717_DEF.pdf

Olivier Industrie. (2021, April 5). *Olivier pile.* https://www.olivierindustrie.be/foundation-tools/olivier-pile/?lang=en#

Rajapakse, R. (2016). *Pile Design and Construction Rules of Thumb, Second Edition.* Elsevier.

Randolph, M. F. (2003). Science and empiricism in pile foundation design. *Géotechnique, 53(10)*, 847–875.

Robertson, P. K. (2016). Soil Behaviour Type from the CPT: an update. *Canadian Geotechnical Journal, 00:1-18.* https://doi.org/dx.doi.org/10.1139/cgj-2016-0044

Rohatgi, A. (2021). WebPlotDigitizer. https://automeris.io/WebPlotDigitizer/

Tang, C., & Phoon, K. (2018). Characterization of model uncertainty in predicting axial resistance of piles driven into clay. *Canadian Geotechnical Journal, 56: 1098-1118.*

Transportation Research Board. (1977). *Design Of Pile Foundations* (tech. rep.). National Research Council, Washington D.C.

van der Geest, A. J., Admiraal, B. J., & IJnsen, P. (2019). Schaalproeven op draagvermogen grondverdingende (schroef)palen. *Geotechniek*, 7–16.

Van Impe, W. (Ed.). (1988). *Proceedings of the 1st International Geotechnical Seminar on Deep Foundations on Augered and Bored Piles*. A. A. Balkema.

Van 't Hek. (2021, April 5). *HEKpile*. https://www.vanthek.com/techniques/hekpile

van Mierlo, W., & Koppejan, A. (1952). Lengte en draagvermogen van heipalen, vaststelling hiervan en enige daarbij verkregen ervaringen. *Bouw 1952, no 3.*

Vroom. (2021a, April 5). *HEK schroefpalen*. https://www.vroom.nl/nl/products/26-hek-schroefpalen

Vroom. (2021b, April 5). *Stalenbuis schroefpalen*. https://www.vroom.nl/nl/products/3-stalenbuis-schroefpalen

Xu, X. (2007). *Investigation of the end bearing performance of displacement piles in sand* (Master's thesis). Perth: University of Western Australia, School of Civil; Resource Engineering.